NASA CONTRACTOR
REPORT

NASA CR-120890

NASA CR-120890

FATIGUE CRACK TIP DEFORMATION AND FATIGUE CRACK PROPAGATION

by

Tai Shan Kang

and

H. W. Liu

Syracuse University
Syracuse, New York 13210

for

NATIONAL AERONAUTICS AND SPACE ADMINISTRATION, WASHINGTON, D. C. February 1972

NASA CR-120890

CONTRACT REPORT

FATIGUE CRACK TIP DEFORMATION AND FATIGUE CRACK PROPAGATION

by

Tai Shan Kang

and

H. W. Liu

Syracuse University
Syracuse, N. Y. 13210

prepared for

NATIONAL AERONAUTICS AND SPACE ADMINISTRATION

February 1972
GRANT NGR-33-022-105
NASA Lewis Research Center
Cleveland, Ohio

NOTICE

This report was prepared as an account of Government sponsored work. Neither the United States, nor the National Aeronautics and Space Administration (NASA), nor any person acting on behalf of NASA:

A) Makes any warranty or representation, expressed or implied, with respect to the accuracy, completeness, or usefulness of the information contained in this report, or that the use of any information, apparatus, method, or process disclosed in this report may not infringe privately-owned rights; or

B) Assumes any liabilities with respect to the use of, or for damages resulting from the use of,any information, apparatus, method or process disclosed in this report.

As used above,"person acting on behalf of NASA" includes any employee or contractor of NASA, or employee of such contractor, to the extent that such employee or contractor of NASA or employee of such contractor prepares, disseminates, or provides access to any information pursuant to his employment or contract with NASA, or his employment with such contractor.

FOREWARD

The work described herein was done at the George Sachs Fracture Research Laboratory, Syracuse University, under NASA Grant NGR-33-022-105 with Mr. Marvin Hirschberg, Materials and Structure Division, NASA-Lewis Research Center, as technical officer. The sustained support and interest of Mr. S. S. Manson and Mr. Marvin Hirschberg are appreciated.

ABSTRACT

The effects of stress ratio, prestress cycling and plate thickness on the fatigue crack propagation rate are studied on 2024-T351 aluminum alloy. Fatigue crack propagation rate increases with the plate thickness and the stress ratio. Prestress cycling below the static yield strength has no noticeable effect on the fatigue crack propagation rate. However, prestress cycling above the static yield strength causes the material to strain harden and increases the fatigue crack propagation rate.

Crack tip deformation is used to study the fatigue crack propagation. The crack tip strains and the crack opening displacements were measured from moire fringe patterns. The moire fringe patterns were obtained by a double exposure technique, using a very high density master grille (13,400 lines per inch).

The cyclic strain range, $\Delta\varepsilon$, was found to be proportional to $r^{-1/2}$. At intermediate ΔK values, i.e. region II, the measured $\Delta\varepsilon$ values are very close to those obtained by theoretical elastic calculations. At the high ΔK values, region III, due to the crack tip necking, the measured $\Delta\varepsilon$ is larger than that obtained by elastic calculation: the higher the ΔK value, the larger the difference between the measured and the calculated values.

Plastic zone size, r_p, was found to be proportional to ΔK^2 in region II and proportional to ΔK^4 in region III. If da/dN is proportional to ΔK^2 in region II and proportional to ΔK^4 in region III, then da/dN is proportional to r_p, i.e. $da/dN = r_p/N_r$, where N_r, a constant, is the number of cycles to propagate a crack through r_p.

The measured crack opening displacement range, $\Delta\delta$, was found to be proportional to $r^{1/2}$. In the range of measurements, $\Delta\delta$ is proportional to ΔK in region II, and proportional to ΔK^2 in region III. The data of $\Delta\delta$ were compared with those predicted by the Dugdale model and the elastic calculations. The differences in $\Delta\delta$, obtained by these two calculations, are small in the range of the measurements. However, the data seem to agree better with the elastic calculations because there was no tendency for the plot of $\Delta\delta$ versus r to level off as r approaches the crack tip, as predicted by the Dugdale model.

TABLE OF CONTENTS

I. INTRODUCTION

A. Fatigue Crack Propagation

Fatigue crack propagation has been studied quite extensively both from the crack length measurements on specimen surfaces and from striation spacings on fracture surfaces. The first fatigue crack propagation law which drew wide attention was the one derived by Head in 1953[1]. After substantial calculations and deductions, the law was given[2] as

$$\frac{da}{dN} = \frac{C_1(\Delta\sigma\sqrt{a})^3}{(\sigma_Y-\Delta\sigma)r_p^{1/2}} \tag{1}$$

where C_1 is a constant, which depends on the strain-hardening modulus, Young's modulus, the yield stress σ_Y and fracture stress of a material; $\Delta\sigma$ is the applied stress range; a is the half crack length and r_p is the plastic zone size ahead of the crack tip, which was assumed to be constant during crack propagation. However, in 1958, Frost and Dugdale[3] noticed that the plastic zone size increases with crack length.

Based on dimensional analysis, both Frost and Dugdale[3] and Liu[4] concluded that crack propagation rate should be directly proportional to the crack length, if crack length was the only pertinent length parameter. Their equation was given as

$$\frac{da}{dN} = f(\Delta\sigma)a \tag{2}$$

Frost and Dugdale[3] observed empirically that $f(\Delta\sigma) = C_2(\Delta\sigma)^3$, therefore their equation becomes

$$\frac{da}{dN} = C_2(\Delta\sigma)^3 a \qquad (3).$$

On the other hand, Liu[5] used the concept of total hysteresis energy absorption to failure and emphasized the damage caused by cumulative cyclic strain at a crack tip[6]. He found that $f(\Delta\sigma) = C_3(\Delta\sigma)^2$, which led to

$$\frac{da}{dN} = C_3(\Delta\sigma)^2 a \qquad (4).$$

The quantity $(\Delta\sigma)^2 a$ is the square of the stress intensity factor range, ΔK^2, for a centrally cracked infinite plate.

Paris[7] noted that the stress intensity factor at a crack tip should be the factor controlling the rate of crack extension. Crack tip stress and strain will be reviewed later in this section. Later on, Paris, Gomez and Anderson[8] proposed that crack propagation rate should be determined by the maximum stress intensity factor, K_{max}. Subsequently, Paris and Erdogan[2] used the stress intensity factor range, rather than maximum stress intensity factor, to correlate data on fatigue crack propagation rate.

Since then, the concept of crack tip stress intensity factor has been used to analyze the experimental data and a large amount of data have been collected on the correlation between fatigue crack propagation rate and stress intensity factor range. Based on experimental data, Paris and Erdogan[2] proposed that fatigue crack propagation rate should be proportional to the fourth power of ΔK. Their equation was therefore given as

$$\frac{da}{dN} = C_4 \Delta K^4 \tag{5}$$

Ever since, the fourth power relation has been observed by a number of investigators. However, other values of the exponents, from 2 to 7 have also been observed.

McClintock[9] used Manson-Coffin's low cycle fatigue equation and derived the fourth power relation by a model including a material structural size ρ. His equation is

$$\frac{da}{dN} = \frac{7.5}{\rho} \left(\frac{\varepsilon_Y}{\varepsilon_F}\right)^2 r_p^2 \tag{6a}$$

By replacing $r_p = (1/2\pi)(\Delta K/\sigma_Y)^2$ and $\varepsilon_Y = \sigma_Y/E$ one obtains

$$\frac{da}{dN} = C_5 \frac{\Delta K^4}{\varepsilon_F^2 (E\sigma_Y)^2 \rho} \tag{6b}$$

where ε_F is the true fracture strain for monotonic fracture; ε_Y is the yield strain and E is Young's modulus.

Rice[10,11] also derived the fourth power relation from a rigid plastic strip model, which assumed that plastic deformation is limited to a strip of material ahead of a crack tip. His equation is

$$\frac{da}{dN} = \frac{5\pi(1-\nu^2)\varepsilon_Y\sigma_Y}{96U^*}\left(\frac{\Delta K}{\sigma_Y}\right)^4 \qquad (7)$$

where ν is the Poisson's ratio and U* is the postulated critical energy to create a new surface. A realistic physical explanation of Rice's rigid plastic strip model was the model of localized necking at a crack tip as suggested by Liu[6].

Krafft[12] assumed that fatigue crack propagation rate has a fourth power dependence on ΔK. On the basis of an empirical correlation between the plane strain fracture toughness and the plastic flow property of a material, he proposed an equation for fatigue crack propagation rate

$$\frac{da}{dN} = \frac{16\times10^6 f(\gamma)}{7E^3K_{IC}^2\, n} K_{max}^4 = C_6K_{max}^4 \qquad (8a)$$

where $f(\gamma) = (1+\gamma)^4\,[1-(1-\gamma)^2]$, $\gamma = 1-(K_{min}/K_{max})$ and n = strain hardening exponent. Later on the equation was modified[13]

$$\frac{da}{dN} = \left[10^8\,\frac{n}{E}\right]\gamma^2\left(\frac{K_{max}}{K_{IC}}\right)^4 d_T \qquad (8b)$$

where $d_T = (K_{IC}/En)^2/2\pi$, which is the process zone size.

Frost and Dixon[14] assumed that crack propagation rate is equal to the increase in crack length of the ellipse perimeter between the loading and the unloading conditions. They gave the equation as

$$\frac{da}{dN} = \frac{(\Delta\sigma)^2 a}{E^2}\left(\ell n \frac{4E}{\Delta\sigma} - 1\right) \qquad (9).$$

Bibly, Cottrell and Swinden[15] used a continuous dislocation model to calculate the crack tip plastic displacement, δ_o. In their model, flow occurs only in a narrow strip ahead of a crack tip. The crack tip opening displacement was given as

$$\delta_o = \frac{4\sigma_Y a}{\pi\mu} \ell n\left(\frac{\ell}{a}\right) \qquad (10)$$

where μ is the shear modulus and ℓ is the sum of the crack length and the length of the plastic zone. This dislocation model is equivalent to the Dugdale's strip necking model. The equations for crack opening displacement, δ were given by Goodier and Field[17], using the Dugdale's strip necking model:

$$\delta = 2V(x,a) = \frac{2\sigma_Y \ell}{\pi E}\left[\cos\theta \log \frac{\sin^2(\theta_2-\theta)}{\sin^2(\theta_2+\theta)} + \cos\theta_2 \log \frac{(\sin\theta_2+\sin\theta)^2}{(\sin\theta_2-\sin\theta)^2}\right] \qquad (11a)$$

where $\cos \theta_2 = a/\ell$

$\cos \theta = x/\ell$ for $|x| < \ell$, $-\pi < \theta < \pi$

$\theta_2 = \pi\Delta\sigma/2\sigma_Y$

and by Rice[11] as

$$\delta = 2V(x,0) = \frac{(\kappa+1)\sigma_Y r_p}{\pi\mu}\{(1-\frac{x}{r_p})^{1/2} - \frac{1}{2}\frac{x}{r_p}\log[\frac{1+(1-\frac{x}{r_p})^{1/2}}{1-(1-\frac{x}{r_p})^{1/2}}]\}$$

where $0 < x < r_p$ and $r_p = (\pi/8)(K_I/\sigma_Y)^2$ (11b)

the crack tip opening displacement, δ_o is given as

$$\delta_o = 2V(0,0) = \frac{(\kappa+1)\sigma_Y r_p}{\pi\mu} = (\frac{1}{E\sigma_Y})K_I^2 \quad \text{for plane stress (11c).}$$

Weertman[18] applied the Bibly, Cottrell and Swinden's crack tip plastic displacement to the problem of fatigue crack propagation. He adopted a fracture criterion which stated that a crack will grow whenever the sum of all the cyclic plastic displacements at the crack tip exceed the critical value δ^*, and a growing crack will stop at a point where the total plastic displacement at the crack tip is less than δ^*. The equation was given as

$$\frac{da}{dN} = \frac{0.4(\Delta\sigma\sqrt{a})^4}{(\sigma_Y\delta^*)\mu\sigma_Y^2} \tag{12}$$

McEvily and Johnston[19] also proposed the following empirical equation, which is similar to Equation (12),

$$\frac{da}{dN} = \frac{\Delta K^4}{E\left(\frac{\sigma_Y+\sigma_u}{2}\,\varepsilon_m\right)\sigma_u^2} \tag{13}$$

where σ_Y is the 0.2 percent offset yield strength, σ_u is the ultimate tensile strength and ε_m is the engineering strain at maximum load.

Lardner[20] also applied the theory of Bibly, Cottrell and Swinden's to derive a fatigue crack propagation law. He assumed that a crack can propagate during the unloading and the equation was given as

$$\frac{da}{dN} = \frac{(1-\nu)}{4\mu\sigma_Y}\,\Delta K^2 \tag{14}.$$

McClintock[21] suggested that if the fatigue crack propagation rate is related to the crack opening displacement by a proportionality constant C_7, one can write

$$\frac{da}{dN} = C_7\,\delta = \frac{4C_7(\Delta\sigma)^2 a}{E\sigma_Y} \tag{15}.$$

Tomkins[22] assumed that during the tensile half of the cycle, plastic flow occurred in two narrow shear bands of length D, radiating at $\pm$ 45° from the crack plane at the crack tip. Because of the shear

strain concentrated in these two narrow bands, the Dugdale model of plastic cohesive forces can be applied to the fatigue problem. He further assumed that the rate of fatigue crack propagation is equal to the crack tip opening displacement, i.e.

$$\frac{da}{dN} = \delta_o = D\Delta\varepsilon_p \tag{16a}$$

where $\Delta\varepsilon_p$ is the applied plastic strain range, which is related to the cyclic stress by a power relationship. Using the plastic zone size equation for D[23], Tomkins derived a fatigue crack propagation equation for low stress region,

$$\frac{da}{dN} = C_8(\Delta\sigma)^3\sigma_m\, a \tag{16b}$$

where σ_m is the applied mean stress.

Analyzing the effect of stress ratio, R, to the fatigue crack propagation rate, Broek and Schijve[24] proposed an exponential equation for the case of a centrally cracked aluminum plate. Their equation has the form of

$$\frac{da}{dN} = C_9(K'_{max})^3 \exp(-C_{10}R) \tag{17a}$$

where $K'_{max} = \sigma_{max}\sqrt{a}[1+40(\frac{a}{W})^2]^{1/3}$, and W is the width of the specimen.

Equation (17a) can also be written in terms of the stress intensity factor range as

$$\frac{da}{dN} = C_9\left(\frac{\Delta K'}{1-R}\right)^3 \exp\left(-C_{10}R\right) \qquad (17b).$$

Forman, Kearney and Engle[25], considering the instability of the crack growth when the stress intensity factor approaches the fracture toughness, K_c, proposed an equation for fatigue crack propagation rate as

$$\frac{da}{dN} = \frac{C_{11}(\Delta K)^n}{(1-R)K_c - \Delta K} \qquad (18).$$

Hudson and Scardina[26] also studied the effect of stress ratio on fatigue crack propagation in 7075-T6 aluminum alloy sheet. They found that all the data from tests at negative R values fell into a relatively narrow scatter band with the data from the R = 0 tests, which indicates that the compression portion of the loading cycle did not significantly affect the crack propagation rate. On the other hand, for a positive R, they found the higher the stress ratio at a given value of ΔK, the higher the fatigue-crack-propagation rate. This spread in rates was small at the lower ΔK value, but became progressively larger as the ΔK value was increased. They also concluded that the equation of Forman et al.[25] gave the best fit to their data.

Both striation spacings and specimen surface crack propagation rates have been studied on the same specimens by Pelloux[27], Hertzberg

and Paris[28] and Kershaw and Liu[29]. Pelloux[27] and Kershaw and Liu[29] found that the fatigue crack propagation rates observed on the specimen surface was faster than the fatigue crack propagation rates measured from the striation spacings. Pelloux has attributed this difference to the extensive cracking of brittle second phase particles ahead of the main crack. The effect of these brittle second phase particles has been analyzed by McClintock[9,20]. On the other hand, Hertzberg and Paris[28] have not found a significant difference between propagation rates based upon striation spacing and those based upon surface measurements.

Applying notch fracture analysis to a sharp crack and considering that cyclic process of a fatigue crack as a continuing re-initiation of fracture, Weiss[30] derived a crack propagation equation for strain controlled fatigue as

$$\frac{da}{dN} = a\left(\frac{\varepsilon_N}{\varepsilon_{FF}}\right)^{(n+1)} - \frac{\eta}{2} \qquad (19)$$

where ε_N is nominal net section strain; ε_{FF} is equal to σ_{FF}/E. σ_{FF} is equal to or at least related to the endurance limit. η is Neuber's equivalent particle size for sharp notches and n is strain hardening exponent.

This equation was obtained, based on the assumption that da/dN was equal to the distance beyond the crack tip, over which the stress exceeded σ_{FF}.

Typical fatigue crack propagation data which correlate da/dN with ΔK can be divided into three regions as shown by Liu and Iino[31]. In region I, the low ΔK region, the slope of the curve is around 4 and the crack propagation rate is usually less than a few micro-inches per cycle. In region III, the high ΔK region, the slope of the curve is greater than 4. The fracture mode in this region has been changed from normal flat mode to shear mode. Therefore the fatigue crack propagation rate is strongly affected by specimen thickness and necking process. Region III is a region close to the final failure of the specimen. As a consequence, it is less important than other regions.

In region II, the intermediate ΔK region, the slope of the curve is close to 2. Crack propagation in this region is under the normal fracture mode and is not complicated by a shear or necking process. Most of the investigation in this report concerns this region. Only part of the investigations are extended to region III or region I.

B. Stresses and Strains Near a Crack Tip

In the paper of "Analysis of Stresses and Strains Near the End of a Crack Traversing a Plate," Irwin[32] derived a group of equations which were identical to those of Williams[33], except that he emphasized only the first term of an infinite series. The equations were given as

$$\sigma_y = \left(\frac{E\mathcal{G}}{2\pi r}\right)^{1/2} \cos\frac{\theta}{2}\left(1+\sin\frac{\theta}{2}\sin\frac{3\theta}{2}\right)$$

$$\sigma_x = \left(\frac{E\mathcal{G}}{2\pi r}\right)^{1/2} \cos\frac{\theta}{2}\left(1-\sin\frac{\theta}{2}\sin\frac{3\theta}{2}\right) \qquad (20a)$$

$$\tau_{xy} = \left(\frac{E\mathcal{G}}{2\pi r}\right)^{1/2} \cos\frac{\theta}{2}\sin\frac{\theta}{2}\cos\frac{3\theta}{2}$$

$$\delta = \frac{8}{E}\left(\frac{E\mathcal{G}r}{2\pi}\right)^{1/2} \qquad \text{for plane stress,} \qquad (20b)$$

where r is the distance from crack tip, θ is the angle from x axis, δ is the crack opening displacement and $\mathcal{G}$ is the strain energy release rate. The coordinates of the crack tip are shown in Figure (1a). Equation (20a) shows that the stresses ahead of a crack tip are inversely proportional to the square root of the distance from the crack tip, while the crack opening displacement is proportional to the square root of r.

By defining $(E\mathcal{G})^{1/2} = K$ as the stress intensity factor, Equation (20) becomes

$$\sigma_y = \frac{K}{\sqrt{2\pi r}} \cos\frac{\theta}{2}\left(1+\sin\frac{\theta}{2}\sin\frac{3\theta}{2}\right)$$

$$\sigma_x = \frac{K}{\sqrt{2\pi r}} \cos\frac{\theta}{2}\left(1-\sin\frac{\theta}{2}\sin\frac{3\theta}{2}\right) \qquad (21a)$$

$$\tau_{xy} = \frac{K}{\sqrt{2\pi\theta}} \cos\frac{\theta}{2}\sin\frac{\theta}{2}\cos\frac{3\theta}{2}$$

$$\delta = \frac{8K_I}{E}\left(\frac{r}{2\pi}\right)^{1/2} \qquad (21b).$$

Thus the stress distribution at the vicinity of a crack tip are completely described by the new term K, the stress intensity factor. The stress intensity factor, which describes the stress fields near the crack tip, is a function of applied stress, crack length and overall specimen geometry. The general formula for the stress intensity factor range can be written as

$$\Delta K = \Delta\sigma(\pi a)^{1/2} f(\alpha) \qquad (22)$$

where $\Delta\sigma$ is the applied stress range, a is the half crack length and $f(\alpha)$ is the dimensionless function of geometry, which is a stress field correction factor for the finite geometry. In the literature[34], one can easily find various formulas for K for various specimen geometry and loading conditions.

A number of analytical solutions to the problems of crack tip plasticity have been given in the past years. Some of these results will be compared and discussed with the moire strain measurements in a subsequent section of this investigation.

Hult and McClintock[35] introduced the mode III plasticity analysis. They calculated the strain distribution around a crack tip for the anti-plane shear loading. For non-strain hardening materials, they found that plastic strain was inversely proportional to the distance, r, from a crack tip. The relation was given as

$$\varepsilon_{yz} = \left(\frac{\tau_Y}{\mu}\right) \frac{R_a}{r} \tag{23}$$

where τ_Y is the yield stress in shear, μ is the shear modulus of elasticity and R_a is the size of plastic zone.

Equation (23) showed that strain singularity within plastic region was inversely proportional to the distance from crack tip. Throughout the whole plastic region, τ_{yz} was taken to be equal to the shear yeild stress.

The material of the above analysis is perfectly plastic. The strain distribution ahead of a crack tip was proportional to r^{-1} instead of $r^{-1/2}$ which was derived from the linear elastic model. Most of the metallic materials behaved neither perfectly plastic nor perfectly elastic. They exhibit a certain degree of strain hardening. If the stress-strain relationship in the plastic region follows the well known power law as

$$\sigma = C_{12}\, \varepsilon^n \tag{24}$$

and applying Neuber's notch stress analysis to analyze the plastic flow, Weiss[36] obtained stress and strain distributions in front of a sharp notch

$$\frac{\varepsilon_Y}{\varepsilon_N} = C_{13}\, (x)^{-1/n+1}$$

$$\frac{\sigma_y}{\sigma_N} = C_{14}\, (x)^{-n/n+1} \tag{25}$$

where x is the distance from notch root, σ_y and ε_y are the stress and strain at x respectively, and σ_N and ε_N are the net section stress and net section strain respectively.

Hutchinson[37] studied the tensile crack in a hardening material under both plane strain and plane stress conditions. He found that the magnitude of the tensile stress ahead of the crack in plane strain is larger than the magnitude of that in plane stress. Using a stress-strain relation as $\varepsilon = \sigma + C_{15}\,\sigma^{n}$, suggested by Ramberg and Osgood to describe the plastic flow around a crack tip, Hutchinson also obtained two equations for stress and strain similar to those of Weiss.

Almost at the same time, Rice and Rosengren[38] investigated the plane strain deformation near a crack tip in a power law hardening material. They also found the same crack tip strain singularity as that of Weiss and Hutchinson. The product of stress and strain exhibits a singularity of 1/r for all materials.

Swedlow[39] and Swedlow, Williams and Yang[40] used the finite element method to analyze the stress-strain distributions around a crack tip in a plate under plane stress condition. They observed that, in the early stage of loading, both stress and strain are proportional to the same singularity of $r^{-1/2}$ as predicted by the linear elastic analysis. However, the stress and strain singularities changed their character and deviated from the value of $r^{-1/2}$ as loading progressed. At a later stage of loading, the strain singularity gradually levels off toward some stable value of $r^{-1/n+1}$ as predicted by Weiss[36], Hutchinson[37] and Rice and Rosengren[38] while the stress singularity becomes less severe and levels off toward some stable value which is slighlty above the value of $r^{-n/n+1}$.

On examining the stress and strain singularity results presented above, one finds that within a plastic zone, strain is a more meaningful and easily measurable quantity; and the strain singularity at a crack tip depends strongly on the stress-strain relation. An elastic model gives the strain singularity of $r^{-1/2}$, a perfectly plastic model gives the strain singularity of r^{-1}, while a strain hardening model gives the strain singularity of $r^{-1/n+1}$. To verify these analytical models, strain measurements ahead of but close to a crack tip are needed. Moire strain measurements with very high density grille seem capable to provide such information.

In this investigation, the effects of stress ratio, plate thickness and prestress on the fatigue crack propagation rate in 2024-T351 aluminum alloys were studied. Here the effect of stress ratio on the fatigue crack propagation rate,as well as the low cycle fatigue data and the cyclic stress-strain curve for 7075-T6 aluminum alloy are also reported. The data on 7075-T6 aluminum alloy were analyzed in terms of the cyclic fracture ductility. On the other hand, based on the results of prestress effect on the fatigue crack propagation rate for 2024-T351 aluminum alloy, a simple equation for fatigue crack propagation rate expressed in terms of plastic zone size is formulated. The validity of this equation was substantitated by the plastic zone size obtained from the moire strain measurements at the tip of a fatigue crack.

Moire strain measurements were made on the plates of 2024-T351 aluminum alloy. Moire fringes were obtained by double exposure

technique. Strain distribution ahead of a crack tip as well as crack opening displacements behind a crack tip were measured from these fringe patterns. Plastic zone size, r_p, and crack opening displacements, δ, were determined for each stress intensity factor K. The data of r_p and δ were correlated with fatigue crack propagation rate.

II. FATIGUE CRACK PROPAGATION

Fatigue crack propagation has been studied on 2024-T351 and 7075-T6 aluminum alloys. Centrally cracked plate specimens either 4 inches or 6 inches wide were tested. A jeweler's saw cut of 0.25 to 0.50 inches long served as a crack starter. The specimen geometry is shown in Figure (1b). For 2024-T351 aluminum alloy, the effects of stress ratio, plate thickness and prestress-cycling on fatigue crack propagation rate were investigated. The results will be compared and correlated with the crack tip plastic zone size, r_p, which was measured from the moire fringe patterns. For 7075-T6 aluminum alloy, the effect of stress ratio on the rate of fatigue crack propagation, as well as the low cycle fatigue data and cyclic stress-strain curve are reported. The data will be analyzed in terms of the cyclic fracture ductility.

It has been shown[31] that fatigue crack propagation rate data can be correlated by three line segments. In the low ΔK region, i.e. region I, the slope of the line is approximately 4 to 5 ; in the intermediate ΔK region, i.e. region II, the slope is close to 2; and in the high ΔK region, i.e. region III, the slope is equal to or larger than 4. Figure (2a) shows the plot of da/dN versus ΔK for 7075-T6 aluminum alloy in region I and region II. The data were collected from five specimens. The applied stress ranges and specimen dimensions are indicated in the figure. All the specimens were tested under an applied stress ration, R = 1/10. The slopes are 5 and 2.1 in region I and region II, respectively. The transition from region I to region II takes place at $\Delta K = 6 \text{ksi } \sqrt{\text{in}}$, where da/dN is equal to 4 micro-inches per cycle.

A. The Effect of Stress Ratio on Fatigue Crack Propagation

A study of stress ratio effect on fatigue crack propagation was conducted on both 2024-T351 and 7075-T6 aluminum alloys. Two stress ratios,

R = 1/10 and 1/3, were tested on 2024-T351 aluminum alloy; and three stress ratios, 1/10, 1/3 and 1/2, were tested on 7075-T6 aluminum alloy. Two specimen thicknesses, 0.050 inches and 0.25 inches of 2024-T351 aluminum alloy were used,while only one specimen thickness, 0.125 inches, was used for 7075-T6 aluminum alloy. In Figures (2b), (2c) and (2d), fatigue crack propagation rate, da/dN versus stress intensity factor range, ΔK, were plotted. The applied stress ratios and applied stress ranges were all indicated in the figures. Figures (2b) and (2c) are the plots of 2024-T351 aluminum alloy for 0.050 inches thick and 0.25 inches thick specimens respectively. Figure (2d) is the plot of 7075-T6 aluminum alloy. The data shown in the figure fall in region II and region III. They indicate the following:

(a) The slopes of the lines, which correlated da/dN with ΔK, increase with stress ratios. In region II, the values of the slopes are 2.0 and 2.7 for R = 1/10 and 1/3 respectively for both 2024-T351 and 7075-T6 aluminum alloys; and 3.4 for R = 1/2 for 7075-T6 aluminum alloy. In region III, the slopes of the 2024-T351 aluminum alloy data are 4 and 5.4 for R = 1/10 and 1/3 respectively; they are twice the values of the slopes in region II.

(b) The higher the stress ratio at a given value of ΔK, the higher the rate of fatigue crack propagation. This spread in rates is smaller at lower ΔK values but it becomes progressively larger as the ΔK value increases. For instance, at ΔK = 7.3 ksi $\sqrt{in}$ in Figure (2c), da/dN is 5.4 micro-inches per cycle for all three values of R. However, at ΔK = 15 ksi $\sqrt{in}$, the da/dN values are 25, 40 and 72 micro-inches per cycle for R = 1/10, 1/3 and 1/2, repectively. This phenomenon was also observed by Hudson and

Scardina[26]. The increase in da/dN as R increases is caused by the increase in K_{max}. At the same value of ΔK, K_{max} at R = 1/3 is 1.35 times the value at R = 1/10, and K_{max} at R = 1/2 is 1.8 times the value at R = 1/10.

(c) All the lines for region II converge at $\Delta K \simeq 7.3$ ksi $\sqrt{in.}$ Therefore, one can write an empirical equation that correlates the data as

$$\frac{da}{dN} = C_{16} \left(\frac{\Delta K}{7,300}\right)^n \qquad (26)$$

where n are the values of slopes, which depend on the stress ratio R, i.e. 2.0, 2.7 and 3.4 for R = 1/10, 1/3 and 1/2 respectively. C_{16} is the value of da/dN at $\Delta K = 7.3$ ksi $\sqrt{in.}$ The values of C_{16} are 2.8 and 4.6 micro-inches per cycle for 0.050 inches and 0.25 inches thick 2024-T351 aluminum alloy, respectively; and 5.4 micro-inches per cycle for the 0.125" thick 7075-T6 aluminum alloy.

(d) Comparing the data of 2024-T351 aluminum alloy of Figures (2b) and (2c) for the same stress ratio, one found that the thicker the specimen is, the faster a crack will propagate. This was also observed by Broek and Schijve[24] and Barsom[41]. At the same ΔK value and the same R value, the da/dN value of the thicker 2024-T351 aluminum specimen is 1.64 times that of the thinner specimen. The value of 1.64 is the ratio of the C_{16} values for thick and thin specimens in the Equation (26). This is explained by the fact that the stresses and strains near a crack tip in the thick specimen are closer to the plane strain condition than in the thin one. As pointed out by Hutchinson[37], the magnitude of the tensile stress at a crack tip is higher in the plane strain case than in the plane stress case. This high tensile

stress in a thick specimen enhances crack propagation.

(e) The transition point from region II to region III takes place at $\Delta K = 21$ ksi $\sqrt{in}$ for 2024-T351 aluminum alloy. The thickness does not seem to have any significant effect on the transition point. Clark and Wessel[42] found that the transition point for their WOL specimen of 5456-H321 aluminum alloy was $\Delta K = 25$ ksi $\sqrt{in}$.

B. Effect of Prestress-Cycling on Fatigue Crack Propagation

The effects of prestress-cycling on fatigue crack propagation have been studied on 2024-T351 aluminum alloy. Each specimen was cyclically prestressed, at certain stress range for a given number of cycles. After the prestress cycling, a slot was introduced into the specimen and the effect on subsequent fatigue crack propagation rate was investigated. The specimen geometry is shown in Figure (3a). Due to the load limit of our fatigue machine (20,000 lbs), a reduced test section was necessary in order to apply a meaningful prestress range, $\Delta\sigma_p$. Two thicknesses, 0.10 inches and 0.08 inches, were tested. Four prestress ranges were used in this investigation. They were 22,000±18,000 psi, 27,500±22,500 psi, 33,000±27,000 psi and 35,750±29,250. The corresponding fatigue lives at these four prestress ranges were found to be 220,000, 46,000, 12,000 and 5,500 cycles respectively. The first two prestress ranges were below the static yield strength of the materials, while the last two exceeded it. The maximum stress levels and the stress ranges have to be reset frequently, during the process of setting-up the prestress levels, in order to reach the desired levels. This was especially true for the prestress tests above the static yield strength. After the initial setting, the prestress levels were checked and adjusted if necessary. The number of prestress cycles at the prestress level were also shown for each test in the figure. At the two lower prestress levels, both below the static yield strength of the material, very slight plastic

deformation occurred and the material was not hardened. On the other hand, at the two high prestress levels, the static yield strength was exceeded, plastic deformations were accumulated and the material was cyclically strain hardened. Figure (3b) shows the recording of the load-strain curve for prestress at 35,750 ± 29,250 psi. The specimen started to yield and strain hardened at the first cycle, when the stress reached the static yield strength. After the first cycle, the specimen showed no noticeable cyclic deformation up to ten cycles. The specimen was then put into the fatigue machine, and prestressed up to 3,300 cycles. After prestress-cycling, a central slot of $2a \simeq 0.20$ inches was machined into each specimen, and all the specimens were set at the applied stress range of 11,000 ± 9,000 psi. The stress ratios of the prestress cycling and for the fatigue crack propagation tests were all kept at 1/10. Specimens 1, 2 and 3 were 0.100 inches thick and specimens 4, 5, 6 and 7 were 0.080 inches thick.

Fatigue crack propagation in these specimens were measured. Since the specimen thickness affects fatigue crack propagation, the data of these two groups of specimens were plotted in separate figures. In Figures (4a) and (4b), the half crack length, a, was plotted versus the difference of the number of cycles of load and the number of cycles of load at $a \simeq 0.23$ inches, N_i. In this way, the change of crack propagation rates caused by cyclic prestressing can be easily observed.

In Figure (4a) specimen No. 1 was not prestressed. It served as a reference to detect the effect of prestress on fatigue crack propagation rate. Specimens No. 2 and 3 are both prestressed at 22,000 ± 18,000 psi

at 160,000 and 200,000 cycles respectively. This prestress is below the static yield strength. The data of specimens No. 1 and 3 coicide with each other,while the crack in specimen No. 2 propagated more slowly than in specimen No. 1. The irregularity could be caused by the scatter of the material property. The average fatigue crack propagation rate of specimen No. 2 was 10 percent lower than that of specimen No. 1. The deviation is well within the scatter band of fatigue crack propagation data. The effect of a low prestress level, if any, must be small. Figure (4c) shows the data of da/dN versus ΔK of these three specimens. All the data points fall pretty well within a band.

Figure (4b) shows the data of specimens 4, 5, 6 and 7. Specimen 4 was not prestressed. Specimen 5, 6 and 7 were prestressed at $27,500 \pm 22,500$ psi, $33,000 \pm 27,000$ psi and $35,750 \pm 29,250$ psi, respectively. The number of prestress cycles are listed in the figure. The data indicate that the prestress at $27,500 \pm 22,500$ psi has a negligible effect on fatigue crack propagation rate. The prestress at $33,000 \pm 27,000$ psi increases the average fatigue crack propagation rate by one third while prestress at $35,750 \pm 29,250$ psi increases the average fatigue crack propagation rate by one half. In Figure (4d) the data of da/dN versus ΔK were plotted. In region II the data of specimen 4 and 5 shows a slope of 2, but that of specimen 6 has a slope of 2.6. Specimen 7 shows a much steeper slope. The data clearly show that the two lower prestress levels, which are below the static yield strength have negligible effects on the fatigue crack propagation rate. However, prestress above static

yield strength increases fatigue crack propagation rate considerably. These observations lead one to conclude that cyclic deformation at very low levels makes a negligible contribution to fatigue damage of a material element. The high strain cycles, when a material element moves close to a crack tip, cause much severer damage. Therefore, the damage caused strain cycles, when a material element was outside of r_p, can be neglected.

Based on the blunting model for fatigue crack propagation[43] and with the suggestion that the crack opening displacement, δ, given by the Dugdale model[17], is a measure of bluntness, the crack propagation rate was written as[21]

$$\frac{da}{dN} = D_7 \delta = 4C_7 \Delta K^2 / E\sigma_Y \qquad (15)$$

Accordingly, if prestress-cycles increase σ_Y, as in the case of 2024-T351 aluminum alloy, the da/dN should be decreased. But the experimental data shows the contrary. Both da/dN and σ_Y were increased by prestress cycling. This contradiction suggests that blunting mechanism alone cannot be attributed as the only cause of fatigue crack propagation.

C. Low Cycle Fatigue Data for 7075-T6 Aluminum Alloy

Low cycle fatigue data for 4340 fully annealed steel and 2024-T351 aluminum alloy were collected by Liu and Iino[31]. Based on their data, the rate of fatigue crack propagation was given in terms of ductility, M, cyclic yield stress and cyclic yield strain,

$$\frac{da}{dN} = C_{17} \left(\frac{\Delta K}{\Delta\sigma_{Y(c)}}\right)^2 \left(\frac{\Delta\varepsilon_{Y(c)}}{M}\right)^2 \qquad (27)$$

where C_{17} is a proportional constant equal to 1.15.

In this report, the work was extended to 7075-T6 aluminum alloy. Smooth specimens, with a diameter of 0.247 inches, were used. The gauge length was 0.3 inches. Figure (5a) shows the plot of total strain range, $\Delta\varepsilon_T$ versus the number of cycles to fracture, N_f. The slope was found to be - 0.45. The slopes for the curves of 2024-T351 aluminum alloy and 4340 fully annealed steel are - 0.49. By the extrapolation of the line in Figure (5a), the cyclic fracture ductility for 7075-T6 aluminum alloy was found to be 0.25. Figure (5b) shows the curve of total cyclic stress range, $\Delta\sigma_T$, versus total longitudinal cyclic strain range, $\Delta\varepsilon_T$ for both 7075-T6 and 2024-T351 aluminum alloys. The cyclic yield strength range, $\Delta\sigma_{Y(c)}$ and the cyclic yield strain range, $\Delta\varepsilon_{Y(c)}$, for 7075-T6 aluminum alloy were found to be 170,000 psi and 0.015 respectively. By putting all the values of C_{17}, $\Delta\sigma_{Y(c)}$, $\Delta\varepsilon_{Y(c)}$, and M into Equation (27), an empirical equation of fatigue crack propagation rate for 7075-T6 aluminum alloy was obtained.

$$\frac{da}{dN} = 1.15 \left(\frac{\Delta K}{170{,}000}\right)^2 \left(\frac{0.015}{0.250}\right)^2 = 0.143\times10^{-6}\Delta K^2 \text{ micro inch/cycle} \qquad (28)$$

By comparing the values of da/dN, obtained from the substitution of ΔK values into Equation (28), with the experimental values as shown in Figure (2a), the correlation is surprisingly good in the intermediate

ΔK region, region II, where the slope of the line is 2. For instance, at ΔK = 10 ksi $\sqrt{in}$, Equation (28) predicts that da/dN is equal to 14.3 micro-inches per cycle, while the average experimental value is 10.5 micro-inches per cycle. The predicted values fall into the upper band of the measured values.

III. CRACK TIP DEFORMATION

A. Experimental Procedures

Cyclic deformations, both strains ahead of a crack tip and crack opening displacements behind a crack tip were measured. The material used in this investigation was 2024-T351 aluminum alloy. Two stress ratios, R = 1/10 and 1/3, were studied. Four inch wide centrally cracked plate specimens, 0.25 inches or 0.050 inches thick, were tested. The as received plate was 0.25 inches thick. The 0.05 inches thick specimens were thinned down on one side. All the specimens were made from the same plate. The geometry of specimens is shown in Figure (6).

The specimens were carefully polished, cleaned and dried. A coat of photo-resist was sprayed on these cleaned and dried surfaces. A high density master grille of 13,400 lines per inch was used. Moire patterns were obtained by the double exposure technique[44]. Both total maximum strain, ε_{max}, and strain amplitude, $\Delta\varepsilon$, were measured.

As the crack propagated toward a point, the strain at the point increased because of the decrease in r. If plastic deformation took place, a cyclically induced creep strain, ε_{cs} occurred. The total maximum strain ε_{max} is the sum of the cyclically induced creep strain, ε_{cs} and the strain range, $\Delta\varepsilon$. To measure the total maximum strain, the photo-resist coating was first exposed to a grille master at zero load. In order to avoid the residual strains caused by the earlier cycles, the crack was allowed to grow more than five times the plastic zone size estimated by the Irwin's formula, $r_p = (1/2\pi)\ (\Delta K/\sigma_Y)^2$.

Then the second exposure was made at the maximum load. The moire pattern gave the sum of the accumulated strains, as the crack propagated into the region where the measurements were made, as well as the strain caused by the last loading cycle. After the measurements of the total maximum strains were made, the moire pattern was erased. The specimen surface was cleaned, dried and coated with photo-resist again. At the same crack length and at same values of ΔK and K_{max}, the strain ranges were measured. The first exposure was made at σ_{min} and the second one at σ_{max}. Therefore at each set of values of K_{max} and ΔK, the total maximum strains, ε_{max}, and the strain ranges, $\Delta\varepsilon$ were measured. All the measurements were made along the crack line. Figure (7a) shows a set of fringe pictures to measure ε_{max} and $\Delta\varepsilon$.

Figure (7b) shows the definition of the strain quantities. ε_{min} is the difference between ε_{max} and $\Delta\varepsilon$. It corresponds to the strains at K_{min} including the accumulated strains caused by the earlier cycles. When the specimen was completely unloaded, i.e. $K = 0$, the residual strain was the accumulated strain ε_{acc}, caused by all the previous stress cycles. Therefore ε_{min} is the sum of ε_{acc} and the strain cuased by K_{min} of the last cycle alone. ε_{acc} can also be viewed as the cyclically induced creep strain, ε_{cs}.

The basic principle of moire strain analysis can be found elsewhere[45,46]. Knowing the pitch, p, of the master grille and the moire fringe spacing, d_y, in the y-direction (see Figure (1) for reference system), the average tensile strain, ε_y, over the fringe spacing is calculated from

$$\varepsilon_y = \frac{p}{(d_y - p)} \tag{29a}$$

For small strain and high density grille, i.e. $d_y >> p$, Equation (29a) can be simplified as

$$\varepsilon_y = \frac{p}{d_y} \tag{29b}$$

Note that moire strain measurement is basically a displacement measurement method. It measures the average strain over a finite gauge length equal to the inter-fringe spacing. The resolution of the method is directly dependent on the grille density. The high grille density used can easily resolve a strain of 0.1 percent. Because of the small fringe spacing, the gauge lengths are much shorter. Therefore the measurements in an area of high strain gradient are much more accurate.

B. Crack Tip Strain

The cyclic strain ranges, $\Delta\varepsilon$, and the maximum strains ε_{max}, ahead of a crack tip were measured and plotted against the distance from the crack tip on a log-log scale. Figures (8a, 8b) and (9a, 9b) show the strain measurements at stress ratios R = 1/10 and 1/3 respectively. The specimen thickness is 0.05 inches. Figures (10a, 10b) and (11a, 11b) are the ones for a specimen thickness, t = 0.25 inches, and at stress ratios R = 1/10 and 1/3 respectively. Close to a crack tip, the data at a given ΔK or K_{max} value can be correlated by a stright line. All the lines for $\Delta\varepsilon$ have the slope of - 0.5, regardless of the stress ratio and

specimen thickness. The cyclic strain range at a point is the change of the strain at the point, as the applied stress changes from minimum to maximum values. The measurements in Figure (8a) were made on three specimens. The applied maximum stresses are in the neighborhood of 15,000 psi. The stress ratio is 1/10. Since the applied stresses are considerably below the yield strength of the materials, the plastic zone sizes must be quite small in comparison to their corresponding crack lengths. In this case, the deformations are close to the values given by the elastic solution. One can write the strain in y-direction, ε_y along the crack line, for the plane stress model as

$$\begin{aligned} \varepsilon_y &= (\sigma_y - \nu\sigma_x)/E = \sigma_y (1 - \nu)/E \\ &= K (1 - \nu)/E (2\pi r)^{1/2} \end{aligned} \tag{30}$$

where K is the stress intensity factor, E is the elastic modulus, ν is Poisson's ratio and r is the distance from the crack tip. The expression of σ_x and σ_y are given by Equation (21a) with $\theta = 0$. In order to calculate $\Delta\varepsilon$, ΔK instead of K, should be used in Equation (30).

In the lower ΔK range, i.e. below 23 ksi $\sqrt{in}$, the measured strains agree closely with the strains calculated from the elastic solution of Equation (30), with $E = 10.1 \times 10^6$ psi and $\nu = 0.3$. On the average, the measured values are approximately 10 percent higher than the calculated ones. As ΔK increases beyond this value, the deviation of

the measured and the calculated values increases rapidly. At $\Delta K=34.2$ ksi $\sqrt{in}$, the measured values are 1.33 times the calculated elastic strains as shown in Figure (12). The solid lines are the measured strains replotted from Figure (8a). The dashed lines are the calculated ones. These high measured strains are caused by crack tip necking.

Figure (8b) shows the maximum strain, ε_{max}, measured at five K_{max} values. The slopes of the lines decrease as the values of K_{max} increase. They are all less than - 0.5 and vary from - 0.66 to - 0.78, as listed in the figure. The average value is - 0.71. This variation of the slopes of the lines agrees qualitatively with the analysis given by Swedlow, Williams and Yang[40]. However it should be pointed out that the calculation by Swedlow et al. was made for a monotonic loading and the measured strains were the accumulated strains under a cyclic load with a positive mean load.

Figure (13) shows two sets of the measured accumulated maximum strains, ε_{max}, which were replotted from Figure (8b) as the solid lines. The dashed lines are the elastic strains calculated from Equation (30) for the same K_{max} values of the measured lines. For K_{max} = 13.4 ksi $\sqrt{in}$ at r = 0.01 inches, the measured ε_{max} is 1.3 times the calculated value. The deviation decreases as r increases. At r = 0.03 inches, the measured ε_{max} is less than 1.1 times the calculated value. At the higher values of K_{max}, the deviation is much larger. For K_{max} = 25.4 ksi $\sqrt{in}$, at r = 0.01 inches, the ε_{max} is 2.9 times the calculated value.

Figure (14) shows the plot of strain versus the distance from a

crack tip. Two pairs of ε_{max} and $\Delta\varepsilon$ curves were plotted. The data were obtained from Figures (8a) and (8b). For each pair, the values of ΔK and K_{max} are nearly the same. They are approximately 13.4 ksi $\sqrt{in}$ and 20.7 ksi $\sqrt{in}$. The difference is less than 2 percent. The values of ΔK and K_{max} are listed in the figure. The differences between these two curves of each pair are the accumulated residual strains, ε_{acc}, as a specimen is unloaded. It is expected that ε_{acc} will increase as R increases. As r increases and strain decreases, the two curves of each pair converge. Both of these two pairs of curves, converge at $\varepsilon \simeq 0.0021$. At this level of strain, there is no accumulation of plastic deformation, even if the mean load is positive. If the stress-strain characteristics of the material are symmetrical in tension and compression, one can conclude that for a completely reversed stress cycle, if the strain amplitude is less than 0.0021, there is no noticeable cyclic plastic deformation. If fatigue damage nucleation is caused by repeated cyclic plastic deformation, this strain amplitude must correspond to the endurance limit of the material, i.e. 21,000 psi. The measured endurance limit of 2024-T3 aluminum alloy for a completely reversed stress cycle is 20,000 psi, as given in the Alcoa Aluminum Handbook of 1959. If this correspondence is valid, a convenient and quick means to measure endurance limit can be developed. However, additional data are needed to substantiate this conclusion, especially the investigation of effects of the residual stresses near a crack tip on the strain distribution.

For a K value equal to 20.7 ksi $\sqrt{in}$, these two curves converge at r = 0.14 inches. At any point further away, the deformation is elastic. At a point, where r is slightly less than 0.14 inches, plastic deformation takes place, even though the local stress at the point is less than one half of the static yield strength of the material. The deviation of the actual strain from the linear elastic relation is so minute that it is very difficult to detect whether or not the load is monotonic. At r=0.01 inches, ε_{max} is 2.3 times $\Delta\varepsilon$. For the case K = 13.4 ksi $\sqrt{in}$, the difference between ε_{max} and $\Delta\varepsilon$ is much smaller. These two curves converge at a distance r = 0.04 inches. The larger difference in ε_{max} and $\Delta\varepsilon$, at a high K value is caused by crack tip necking.

Figure (15) shows the plot of ε_{max} and $\Delta\varepsilon$ versus r in linear scale. Both were measured at the same crack length. The value of K_{max} is 25.5 ksi $\sqrt{in}$ while ΔK is 22.8 ksi $\sqrt{in}$. The upper solid curve is the measured ε_{max} curve. It is the maximum strain of the cyclic deformation. The dashed curve is $\Delta\varepsilon$. The lower solid curve is the difference between ε_{max} and $\Delta\varepsilon$, therefore it is the minimum strain, ε_{min}, curve. If the crack length is very long in comparison with the distance to a point ahead of a crack tip, the K value does not change much as the crack propagates toward the point. Therefore the decrease in r is linearly proportional to the number of cycles of loading. Consequently, the abscissa axis can be considered as a time scale. For the point at r = 0.1 inches, one can view r = 0.1 inches

as time zero. The time scale moves toward the left of the figure. The figure indicates clearly that as time goes on ε_{max}, $\Delta\varepsilon$ and ε_{min} increase rapidly.

Near a crack tip, both ε_{max} and $\Delta\varepsilon$ curves can be plotted as straight lines on a log-log scale, with different slopes. The data can be fitted by the empirical equations as,

$$\frac{\varepsilon_{max}}{\varepsilon_{Y(s)}} = \left(\frac{r}{r_{max(s)}}\right)^{n_1}$$

$$\frac{\Delta\varepsilon}{\Delta\varepsilon_{Y(c)}} = \left(\frac{r}{r_{p(c)}}\right)^{n_2} \qquad (31)$$

The strain at any time can be written as,

$$\varepsilon = \varepsilon_{mean} + \frac{\Delta\varepsilon}{2} \sin(2\pi N) \qquad (32a)$$

and

$$\varepsilon_{mean} = \varepsilon_{max} - \frac{\Delta\varepsilon}{2} \qquad (32b)$$

After substitution, one obtains

$$\varepsilon = \varepsilon_{Y(s)} \left(\frac{r}{r_{max(s)}}\right)^{n_1} - \frac{1}{2}\Delta\varepsilon_{Y(c)} \left(\frac{r}{r_{p(c)}}\right)^{n_2} [1 - \sin(2\pi N)] \qquad (33)$$

Equation (33) is the cyclic strain history ahead of a crack tip in Figure (15).

Figures (9a) and (9b) show the plots of $\Delta\varepsilon$ and ε_{max} for R = 1/3 and t = 0.05 inches. The slopes of the lines in Figure (9a) for $\Delta\varepsilon$ are all equal to - 0.5. The measured strains in this case are about 20 percent higher than the calculated elastic strains. This increase in the measured strains are much higher than those of R = 1/10, i.e. 10 percent. This increased deviation is caused by crack tip necking enhanced by the high stress ratio. At higher values of R, the ε_{max} is much higher than $\Delta\varepsilon$. In other words, at the same value of ΔK, the ε_{max} for R = 1/3 is much higher than the ε_{max} for R = 1/10. For example, at $\Delta K = 22.8$ ksi $\sqrt{in}$ for R = 1/10, at r = 0.05 inches, ε_{max} is twice $\Delta\varepsilon$, i.e. 0.006 and 0.003 respectively. For the case of R = 1/3, at $\Delta K = 22.5$ ksi $\sqrt{in}$, $\varepsilon_{max} = 0.0135$ and $\Delta\varepsilon = 0.0032$, that is $\varepsilon_{max} = 4.2\ \Delta\varepsilon$. This higher value of ε_{max} enhances necking for the higher value of R. The slopes of the lines in Figure (9b) for ε_{max} vary from - 0.65 to - 0.8. The average slope is - 0.77.

Figure (10a) and (10b) are the plotted data for specimens tested at R = 1/10 and t = 0.25 inches. On the average, the measured values of $\Delta\varepsilon$ are approximately 25 percent higher than the calculated elastic strains. The measured values of $\Delta\varepsilon$ for 0.25 inches thick specimens are 15 percent higher than the 0.050 inches thick specimens at the same corresponding ΔK values. This agrees with the finding that fatigue crack propagation rate is faster in thick specimens than in thin ones.

Figure (16) shows the comparison of ε_{max} for t = 0.25 inches

and 0.050 inches specimens at three K_{max} values, and at R = 1/10. The K_{max} values of each pair of lines are nearly equal to each other. The data are taken from Figures (8b) and (10b). The solid lines represent the thick specimens and the dashed lines represent the thin ones. The values of K_{max} are shown in the figure. At lower K values, the measured strains, ε_{max}, are close to each other. As K_{max} is increased to 20 ksi $\sqrt{in}$ the ε_{max} of thin specimens is nearly 1.2 times that of thick one. The ε_{max} values at K_{max} = 25.5 ksi $\sqrt{in}$ for thin specimens is nearly 1.5 times that of the thick ones at K_{max} = 23.7 ksi $\sqrt{in}$, even though the difference in K_{max} is only 7.6 percent. The data indicate that the ε_{max} values increase much more rapidly for thin specimens as K_{max} values increase. This is another indication of crack tip necking. At high K_{max} value, the thicker specimen, i.e. t = 0.25 inches, has more constraint and less tendency to neck than the thinner one. Therefore it has lower values of ε_{max}.

Figures (11a) and (11b) show $\Delta\varepsilon$ and ε_{max} for specimens tested at R = 1/3 and t = 0.25 inches. In Figure (11a), the slopes of the lines are - 0.5. On the average, the measured values of $\Delta\varepsilon$ are 33 percent higher than the calculated elastic strains. In Figure (11b), the slopes of the lines vary from - 0.5 for the low values of K_{max} to - 0.8 at higher values of K_{max}. The deviation of the measured strains from the calculated elastic strains increases with K_{max}.

C. Plastic Zone Size

As a crack propagates toward a point, the strain at the point

increases. If a point is far away from a crack tip, the deformation is elastic. As a point moves to $r_{p(e)}$, permanent plastic deformation begins to accumulate. Plastic deformation occurs only during the loading half cycle, if the maximum cyclic effective stress exceeds the static yield strength, $\sigma_{Y(s)}$. Plastic deformation will take place during the unloading half cycle, if the cyclic effective stress range, $\Delta\sigma_{eff(c)}$, exceeds the cyclic yield strength range, $\Delta\sigma_{Y(c)}$. The cyclic stress-strain curve of 2024-T351 aluminum alloy is shown in Figure (5b). The cyclic yield strength range, $\Delta\sigma_{Y(c)}$, is 134,000 psi, which is more than two times higher than the static yield strength, $\sigma_{Y(s)}$, i.e. 52,000 psi.

The stress σ_y at a point along a crack line can be calculated from Equation (30) if ε_y is known. Assuming $\sigma_x = \sigma_y$ and $\sigma_Z = 0$, the effective stress is

$$\sigma_{eff} = \{\tfrac{1}{2}[(\sigma_x - \sigma_y)^2 + (\sigma_y - \sigma_z)^2 + (\sigma_z - \sigma_x)^2]\}^{1/2} = \sigma_y \qquad (34)$$

With $\sigma_{Y(s)}$ = 52,000 psi, E = 10.1 x 10^6 psi and ν = 0.3, the static yield strain, $\varepsilon_{Y(s)}$ was calculated from Equation (30) as

$$\varepsilon_{Y(s)} = \frac{(1-\nu)}{E}\sigma_{Y(s)} = \frac{(1-0.3)}{10.1\text{x}10^6} \text{ x } 52{,}000 = 3.6 \text{ x } 10^{-3} \qquad (35a)$$

Similarly, the cyclic yield strain range, $\Delta\varepsilon_{Y(c)}$, was calculated with $\Delta\sigma_{Y(c)}$ = 134,000 psi, E = 10.1 x 10^6 psi and ν = 0.3.

$$\Delta\varepsilon_{Y(c)} = \frac{(1-\nu)}{E}\Delta\sigma_{Y(c)} = 9.3 \times 10^{-3} \qquad (35b)$$

Using $\varepsilon_{Y(s)} = 3.6 \times 10^{-3}$, $\Delta\varepsilon_{Y(c)} = 9.3 \times 10^{-3}$ and the data of strain distribution curves in Figures (8a) to (11b), both static plastic zone size, $r_{p(s)}$ and cyclic plastic zone size, $r_{p(c)}$ can be obtained experimentally for each stress intensity value. Figure (17a) shows the plot of static plastic zone size, $r_{p(s)}$ versus stress intensity range, ΔK for the thin specimen of 0.050 inches thick. The dashed line is the calculated value. For the case of R = 1/10, at ΔK = 11.6 ksi $\sqrt{in}$, the measured $r_{p(s)}$ is equal to 0.0085 inches. At ΔK = 22.8 ksi $\sqrt{in}$, measured $r_{p(s)}$ is equal to 0.037 inches.

Wihtin the range of ΔK = 11.6 ksi $\sqrt{in}$ to 22.8 ksi $\sqrt{in}$, the average value of $r_{p(s)}$ is 12 percent higher than the calculated one. As the value of ΔK becomes larger than 22.8 ksi $\sqrt{in}$, the measured values of $r_{p(s)}$ start to deviate from the line having a slope of 2 to the line with a slope of 4. At ΔK = 34.2 ksi $\sqrt{in}$, the measured $r_{p(s)}$ is about 81 percent higher than the calculated one. The empirical equations for these two line segments can be written as

$$r_{p(s)} = C_{18}\left(\frac{\Delta K}{\sigma_{Y(s)}}\right)^2 = 0.18\left(\frac{\Delta K}{52{,}000}\right)^2 = 66.56 \times 10^{-6}\,\Delta K^2 \text{ micro-inch}$$

for region II (36a)

and

$$r_{p(s)} = C_{19}\left(\frac{\Delta K}{\sigma_{Y(s)}}\right)^4 = 0.8\left(\frac{\Delta K}{52{,}000}\right)^4 = 10.9\times10^{-14}\ \Delta K^4 \text{ micro-inch}$$

for region III (36b).

For the case of R = 1/3, the measured $r_{p(s)}$ is about 38 percent higher than the calculated value. The difference between R = 1/10 and 1/3 is 23 percent.

Figures (17b) shows the plot of cyclic plastic zone size, $r_{p(c)}$ versus stress intensity range, ΔK. The data was obtained from Figures(8a) and (9a). At lower ΔK values, the lines in Figures (8a) and (9a) have to be extrapolated to determine the cyclic plastic zone size. The characteristics of both lines for R = 1/10 and 1/3 are the same as those in Figure (17a) as expected. The slopes of the lines for R = 1/10 also change from 2 to 4 at ΔK = 24 ksi $\sqrt{\text{in.}}$ On the average the values of $r_{p(c)}$ are about 6.7 times lower than those of $r_{p(s)}$. The empirical equations for these two line segments of R = 1/10 can also be written as

$$r_{p(c)} = C_{20}\left(\frac{\Delta K}{\Delta\sigma_{Y(c)}}\right)^2 = 0.12\left(\frac{\Delta K}{134{,}000}\right)^2$$

$$= 6.68\times10^{-6}\ \Delta K^2 \text{ micro-inch}$$

for region II (37a)

$$r_{p(c)} = C_{21}\left(\frac{\Delta K}{\Delta\sigma_{Y(c)}}\right)^4 = 5\left(\frac{\Delta K}{134,000}\right)^4$$

$$= 1.55 \times 10^{-14}\Delta K^4 \quad \text{micro-inch}$$

for region III (37b).

Figure (18) shows the plot of static plastic zone size, $r_{p(s)}$ versus stress intensity range ΔK for 0.25 inches thick specimens. Only the data for region II were shown. The slopes for both lines of R = 1/10 and 1/3, are also 2. For the case of R = 1/10, the measured $r_{p(s)}$ is 1.55 times higher than the calculated one, while the $r_{p(s)}$ for R = 1/3 is also 23 percent higher than that of R = 1/10. Comparing Figure (18) with Figure (17a) for the same stress ratio R, one finds that the values of $r_{p(s)}$ for the thick specimens are 35 percent higher than that of thin ones. However, the differences between the values of $r_{p(s)}$ for R = 1/10 and 1/3 are the same for both thick and thin specimens, i.e. 23 percent. This observation leads one to formulate an empirical equation for r_p as

$$r_{p(s)} = C_{22}\frac{\Delta K^2}{1-R} \tag{38}$$

where C_{22} is a constant dependent on thickness.

Figure (19) shows the maximum static plastic zone size, $r_{max(s)}$ versus the maximum stress intensity factor K_{max}. The data were obtained from the maximum strain distribution in Figures (8b), (9b),

(10b) and (11b) with $\epsilon_{Y(s)} = 3.6 \times 10^{-3}$. The specimen cross-sectional area and the applied stress ratios are all shown in the figure. The overall slope for all of the data is 2.6. However, if one examines more closely, it seems that every individual set of data can be correlated by a line segment with a slope of 2, except the one with the cross sectional area, A = 4" x 0.050" and R = 1/10, which were obtained from three different specimens. In toto,the data indicate that the effects of thickness and stress ratio to the maximum plastic zone size is not severe.

D. Crack Opening Displacement

The relative crack opening displacement between two points, one on the upper and the other on the lower crack surfaces, can be measured from the moire fringe pattern and calculated as

$$\delta = pN_o \tag{39}$$

where p is the pitch of the master grille, which is equal to 1/13,400 inches. N_o is the total number of fringes along the crack surface between these two points.

There are two models to calculate the crack opening displacement i.e. linear elastic model and Dugdale's strip necking model. The linear elastic model gives

$$\delta = 2K\left(\frac{r}{2\pi}\right)^{1/2} \frac{4}{E} \qquad \text{for plane stress.} \tag{21b}$$

On the other hand, Dugdale model predicts that crack tip opening displacement, δ_o, is proportional to the square of the stress intensity factor as shown in Equation (11c). The crack opening displacement, δ, is given by Goodier and Field[17] as

$$\delta = 2V(x,a) = \frac{2\sigma_Y \ell}{\pi E}\left[\cos\theta \log\frac{\sin^2(\theta_2-\theta)}{\sin^2(\theta_2+\theta)} + \cos\theta_2 \log\frac{(\sin\theta_2+\sin\theta)^2}{(\sin\theta_2-\sin\theta)^2}\right] \qquad (11a)$$

Figures (20a) and (20b) show the plots of the crack opening displacement range, $\Delta\delta$, versus the distances from a crack tip for 0.050 inches thick specimen. $\Delta\delta$ was measured as the applied stress was increased from σ_{min} to σ_{max}. Therefore the measured $\Delta\delta$ corresponds to the stress intensity factor range, ΔK. Figure (20a) is for R = 1/10 and Figure (20b) is for R = 1/3. Each line in the figures corresponds to one ΔK value. All the lines have a slope of 0.5. This means that crack opening displacement is proportional to the square root of the distance from a crack tip, which is predicted by the linear elastic model shown in Equation (21b).

Figure (20c) shows the plot of $\Delta\delta$ at r = 0.04 inches versus ΔK for both cases of R = 1/10 and R = 1/3. The data were obtained from Figures (20a) and (20b). With $E = 10.1 \times 10^6$ psi, the dashed line was calculated using the elastic model of Equation (21b). The slope of the dashed line is one. In region II, i.e. the intermediate ΔK

values, the lines, correlating $\Delta\delta$ with ΔK, have a slope of one for both R = 1/10 and R = 1/3. This agrees with the prediction of the linear elastic model. On the average, the measured values of $\Delta\delta$ for R = 1/3 are 6 percent less than the calculated ones; and those for R = 1/10, the measured values of $\Delta\delta$ are 24 percent below the calculated ones. In region III, i.e. high ΔK values, the data of R = 1/10 can be correlated with a straight line having a slope of two.

Figures (20d) and (20e) are another two sets of data of $\Delta\delta$ versus r for 0.25 inches thick specimens. Figure (20d) is for R = 1/10 and Figure (20e) is for R = 1/3. The slopes of the lines in both figures are all 0.5. This indicates that crack opening displacement is proportional to the square root of distance from the crack tip, regardless of the effects of specimen thickness and applied stress ratio. Figure (20f) shows the plot of $\Delta\delta$ at r = 0.04 inches versus their corresponding ΔK values for both R = 1/10 and R = 1/3. the data were obtained from Figures (20d) and (20e). The dashed line in the figure was calculated from the elastic model using Equation (21b). Similar to thin specimens, the lines, correlating $\Delta\delta$ with ΔK in region II, can be correlated with a straight line having a slope equal to one. On the average, the measured $\Delta\delta$ values for R = 1/10 are 10 percent below the calculated ones; and those for R = 1/3 are 8 percent higher than the calculated ones. In toto,the measured $\Delta\delta$ for R = 1/3 is 18 percent higher than those at R = 1/10. This difference is the same as in the case of 0.050 inches thick specimens. Comparing Figures (20c) and (20f) for the effect of thickness on the values of $\Delta\delta$ at the same stress

ratio, one finds that $\Delta\delta$ of the thicker specimens, t = 0.25 inches, is 14 percent higher than that of thinner specimens for both R = 1/10 and R = 1/3.

Figure (21a) shows the relative maximum crack opening displacement, δ_{max}, versus the distance from the crack tip for the specimens 0.050 inches thick at R = 1/10. Figure (21b) are those for R = 1/3. The values of δ_{max} were measured from the same pictures of moire fringe patterns which were used to measure the ε_{max}. The corresponding K_{max} values for each line are indicated in the figures. The slopes of these lines are close to 0.5. They vary from 0.5 to 0.6. Figures (22a) and (22b) are another two sets of data which show δ_{max} versus r for 0.25 inches thick specimens. The values of K_{max} and R are also shown in the figures. For the case of R = 1/10, all the slopes of the lines are equal to or very close to 0.5. While in the case of R = 1/3. the slopes of the lines vary from 0.5 to 0.6.

Figure (22c) is the plot of δ_{max} at r = 0.04 inches versus K_{max} for both thin and thick specimens. The data are obtained from Figures (21a), (21b), (22a), and (22b). The applied stress ratios and specimen thicknesses are shown in the figure. The dashed line is the calculated line using Equation (21b) of elastic model. The data for both thin and thick specimens can be correlated with a straight line having a slope equal to one regardless of the stress ratio.

Figures (22d) and (22e) show the comparison of $\Delta\delta$ predicted by elastic model and Dugdale model with the measured values. Figure

(22d) is for thin specimen and Figure (22e) is for thick one. The measured data for two ΔK values are shown in each figure. The solid and the dashed lines are calculated using Dugdale model and elastic model respectively. The cyclic yield stress range, $\Delta\sigma_{Y(c)}$, is used for Dugdale's model.

The experimental points seem to agree better with the calculated displacements of the elastic crack. However the differences in displacements calculated by these two models are small in the range of the measurements. A straight line correlates well with the measured displacements. There is no tendency to level off as r approaches the crack tip.

IV. DISCUSSION

A. Crack Tip Deformation and Fatigue Crack Propagation

Based on dimensional analysis, Frost and Dugdale[3] and Liu[4] have pointed out that fatigue crack propagation is proportional to the crack length if the crack length is the only pertinent length parameter. Subsequently, Liu[5] has shown that if the plastic zone size is very small or if the ratio $\Delta\sigma/\sigma_Y$ is low, the crack tip stresses and strains can be characterized by ΔK and R. This conclusion is correct, if the crack tip stress and strain distributions are not affected by crack tip necking. In this case, r_p is proportional to ΔK^2, if R remains constant. The crack tip region can be scaled by r_p so that at the homologous points, i.e. at the geometrically similar points, the stresses and strains are identical. If a crack increment is proportional to r_p, the stresses and strains within the area of the crack increment must be the same regardless of the value of ΔK or the size of r_p. If crack propagation is caused by the stresses and strains, da/dN must be proportional to r_p. That is

$$\frac{da}{dN} = C_{23}\, r_p \tag{39a}$$

By applying the cumulative damage rule within the plastic region ahead of a crack tip, Lehr and Liu[47] and Liu and Iino[31] derived a fatigue crack propagation equation for a cracked plate. They showed that fatigue crack propagation rate was proportional to the plastic zone size as

$$\frac{da}{dN} = C_{24}\left(\frac{M}{\varepsilon_{Y(c)}}\right)^{1/Z} r_p \tag{39b}$$

where C_{24} is a proportional constant, M is the strain range corresponding to the fatigue life of one cycle, Z is the slope of log $\Delta\varepsilon_T$ versus log N_f and $\varepsilon_{Y(c)}$ is the cyclic yield strength found from the strain controlled fatigue test.

Assuming that the true mechanical conditions around a crack tip are represented by the plastic deformations, Erdogan and Roberts[48] proposed a model of fatigue crack propagation as

$$\frac{da}{dN} = C_{25}(r_p)^{\alpha} \tag{40a}$$

where C_{25} and α are constants for a given material, and r_p is a characteristic length of the plastic zone at the crack tip.

Later on, Roberts and Erdogan[49], studying the effect of mean stress on fatigue crack propagation, generalized the above equation to

$$\frac{da}{dN} = C_{26}(r_{max})^{\alpha_1}(r_p)^{\alpha_2} \tag{40b}$$

where C_{26}, α_1 and α_2 are constants for a given material and r_{max} and r_p are the maximum and range values of the plastic zone size, respectively, as measured along the prolongation of the crack.

Now, let us assume that fatigue damage occurs only inside of the plastic region. As we have shown prestress cycling below the static yield strength has a negligible effect on the rate of fatigue crack propagation. In other words, fatigue damage occurs mainly after an element enters the plastic zone boundary. Before the elements enter the plastic zone boundary, there is only negligible fatigue damage to the elements. If $r_p << a$, ΔK is essentially constant during the time period after a material element enters r_p and before it arrives the crack tip. Therefore, one can assume da/dN, within r_p, is essentially constant.

If

$$da/dN = C_{23} r_p \tag{39a}$$

then

$$\int_a^{a+r_p} da = C_{23} r_p \int_o^{N_r} dN$$

or

$$C_{23} = 1/N_r$$

therefore

$$\frac{da}{dN} = \frac{r_p}{N_r} \tag{41}$$

where N_r, a constant, is the number of cycles to propagate a crack through the length of r_p. The validity of Equation (41) will be discussed and clarified by r_p values obtained from the moire strain measurements ahead of a crack tip and da/dN, measured on the specimen surfaces.

Figure (23a) shows the plot of da/dN versus ΔK, as well as $r_{p(s)}$ versus ΔK for 0.050 inches thick specimens at R = 1/10. The data were obtained from Figures (2b) and (17a). In the lower ΔK region the data give a slope of two for both lines, while the data in the higher ΔK region give a slope of four. The transitions take place at ΔK equal to

21 ksi $\sqrt{in}$ and 24 ksi $\sqrt{in}$ for da/dN and r_p respectively. The data in Figure (23a) give the empirical constant N_r for region II.

$$N_r = r_{p(s)}/(da/dN) = 1.08 \times 10^3 \text{ cycles}$$

or

$$\frac{da}{dN} = r_{p(s)}/N_r = \frac{C(\frac{\Delta K}{\sigma_K})^2}{N_r} = \frac{0.18}{1.08 \times 10^3} (\frac{\Delta K}{52,000})^2 \qquad (42).$$

$$= 61.6 \times 10^{-9} \Delta K^2 \quad \text{micro-inch/cycle}$$

For the data in region III, the empirical constant N_r is

$$N_r = r_{p(s)}/(da/dN) = 0.75 \times 10^3 \text{ cycles}$$

or

$$\frac{da}{dN} = r_{p(s)}/N_r = \frac{C(\frac{\Delta K}{\sigma_Y})^4}{N_r} = \frac{0.8}{0.75 \times 10^3} (\frac{\Delta K}{52,000})^4 \qquad (43).$$

$$= 14.6 \times 10^{-17} \Delta K^4 \quad \text{micro-inch/cycle}$$

Similar data for 0.25 inches thick specimens at R = 1/10 are shown in Figure (23b). The data give the empirical constant N_r for region II.

$$N_r = r_{p(s)}/(da/dN) = 1.0 \times 10^3 \text{ cycles}$$

or

$$\frac{da}{dN} = r_{p(s)}/N_r = \frac{C(\frac{\Delta K}{\sigma_Y})^2}{N_r} = \frac{0.26}{1.0 \times 10^3} (\frac{\Delta K}{52,000})^2 \qquad (44).$$

$$= 96.2 \times 10^{-9} \Delta K^2 \quad \text{micro-inch/cycle}$$

The values of N_r for thick and thin specimens in region II are found to be 1.0×10^3 cycles and 1.08×10^3 cycles respectively. They have only an 8 percent difference. This amount of difference is well within the experimental error. Therefore, one can conclude that the number of cycles, N_r, to propagate a crack through the plastic zone size, r_p, is a material constant.

The data for R = 1/3 are plotted in Figures (24a) and (24b). The slopes of the line that correlate da/dN with ΔK and the line that correlates $r_{p(s)}$ with ΔK do not agree. The slope of the former line is 2.6 and that of the latter is 2, for both 0.050 inches and 0.25 inches thick specimens.

In Figure (24a) the dashed line is the fatigue crack propagation rate predicted from Equation (42). The measured and predicted lines intersect at $\Delta K = 11.5$ ksi $\sqrt{in}$, where the crack propagation rate is equal to 10 micro-inches per cycle. At $\Delta K = 20$ ksi $\sqrt{in}$, the da/dN are 30 micro-inches per cycle and 40 micro-inches per cycle for predicted and measured values respectively. In Figure (24b), the measured da/dN deviates from that given by Equation (44). At $\Delta K = 7$ ksi $\sqrt{in}$ the predicted value of da/dN is 1.4 times the measured one. While at $\Delta K = 18$ ksi $\sqrt{in}$, the measured value of da/dN is 1.4 times the predicted one.

The correlation of da/dN with r_p will be examined in terms of the characterization of crack tip stresses and strains by ΔK and R. As we have pointed out earlier, the crack tip cyclic deformation is

characterized by ΔK and R, if the deformation is not affected by necking. In this case, the region ahead of a crack tip can be scaled by the characteristic length r_p, so that as a crack grows, the deformation at geometrically similar points is identical.

Cyclic deformation can be specified by $\Delta\varepsilon$ and ε_{max}. In Figures (25a to 25d), both $\Delta\varepsilon$ and ε_{max} are plotted against $r/r_{p(s)}$. The data are obtained from Figures (8a to 11b). The $r_{p(s)}$ is the distance r for $\varepsilon_{Y(s)} = 3.6 \times 10^{-3}$. For each pair of $\Delta\varepsilon$ and ε_{max} curves, the same value of $r_{p(s)}$ is used. Since all the lines for $\Delta\varepsilon$ have the same slope, i.e. - 0.5, all the data are consolidated into a single line. In Figure (25a), the data for 0.050 inches thick specimens at R = 1/10 are shown. The three lines of ε_{max} data at ΔK = 16.2, 13.3 and 11.6 ksi $\sqrt{in}$ fall into a narrow band. This indicates clearly that the region ahead of a crack tip can be scaled by $r_{p(s)}$ so that at geometrically similar points, the cyclic strains, i.e. $\Delta\varepsilon$ as well as ε_{max}, are identical. As discussed earlier, if r_p can be used to scale the region near a crack tip, da/dN should be proportional to r_p and K^2. As indicated by the crack growth data in Figure (2b) all these three values of ΔK are in region II, and da/dN is indeed proportional to ΔK^2. For the line at K_{max} = 25.5 ksi $\sqrt{in}$, the ε_{max} curve is considerably above the other three. This K_{max} value is above the transition point of the da/dN curve in Figure (23a). Because the ε_{max} is higher than the value given by the scaling law, it is reasonable to expect that da/dN is faster than that given by Equation (44), i.e. da/dN proportional to ΔK^2. Figure (25b) shows similar data for 0.25 inches thick specimens

at R = 1/10. All the lines of ε_{max} data fall into a narrow band, too. This is another indication that the region ahead of a crack tip can be scaled by $r_{p(s)}$, so that at geometrically similar points the cyclic strains are identical.

Figures (25c) and (25d) show the data of R = 1/3 for 0.050 inches and 0.25 inches thick specimens, respectively. Unlike the data of R = 1/10, the data of R = 1/3 do not fall into a narrow band. The data indicate that at geometrically similar points ahead of a crack tip, the maximum cyclic strains, ε_{max}, are not identical, due to the effect of higher stress ratios. The higher the value of K_{max}, the higher the value of ε_{max} at geometrically similar points. As a consequence, one would expect that the measured values of da/dN for R = 1/3 would increase more rapidly than those of R = 1/10, and that the slope of da/dN versus ΔK would deviate from two.

This deviation is also illustrated in Figure (25e), which shows the plot of $(da/dN)/r_{p(s)}$ versus $r_{max(s)}$. The values of da/dN are obtained from Figures (2b) and (2c), while the values of $r_{p(s)}$ and $r_{max(s)}$ are obtained from Figures (8a) to (11b), with $\varepsilon_{Y(s)} = 3.6 \times 10^{-3}$. The values of $(da/dN)/r_{p(s)}$ at R = 1/10 are almost constant for both thick and thin specimens. The average values are 1.02×10^{-3} per cycle and 0.85×10^{-3} per cycle for thick and thin specimens respectively. However, at R = 1/3, the values of $(da/dN)/r_{p(s)}$ increase with increasing $r_{max(s)}$. The slopes of the lines, correlating $(da/dN)/r_{p(s)}$ with $r_{max(s)}$, are 0.41 and 0.62 for thick and thin specimens respectively.

Based on these experimental data, one can write an empirical equation as

$$\left(\frac{da}{dN}\right) \frac{1}{r_{p(s)}} = C_{23}\, r_{max(s)}^{\alpha_1} \qquad (45)$$

or

$$\frac{da}{dN} = C_{23}\, r_{p(s)}\, r_{max(s)}^{\alpha_1}$$

where C_{23} is the proportional constant, α_1 is the slope in Figure (25e), which is zero at R = 1/10 and 0.41 and 0.62 for thick and thin specimens respectively, at R = 1/3.

Equation (45) is similar to Equation (40b), which was proposed by Roberts and Erdogan[49].

B. Crack Opening Displacement and Fatigue Crack Propagation

In this investigation, it has been shown that crack opening displacement range, $\Delta\delta$, is proportional to the square root of the distance from a crack tip, and it is linearly proportional to the stress intensity factor range. The measured values agree better with the calculated elastic displacements of the crack surfaces. Schaeffer, Liu and Ke[44] have shown that the crack opening displacements given by the Dugdale model agree well with the measured values in a thin steel specimen. In a thin specimen, necking takes place at a crack tip and the crack tip necking causes a thin narrow strip of extensive plastic

deformation. The strip necking zone agrees with the main feature of the Dugdale model. As specimen thickness increases, the size of the strip necking zone decreases. For a thick specimen, the region of extensive plastic deformation must be diffused rather than a thin narrow strip. Therefore, even if crack opening displacement exists at a crack tip, its value must be much smaller than that given by the Dugdale model.

Laird[21] proposed a crack tip blunting model for fatigue crack propagation. The crack tip opening displacement, δ_o, given by the Dugdale model[11] or by the Wells [50] calculation is often used as a measure of the crack tip "blunting". In either calculation, the crack tip opening displacement is inversely proportional to the yield strength, σ_Y, of a material. According to the model, an increase in σ_Y reduces crack tip opening displacement and da/dN. The study of the effects of pre-stress clearly indicates the contrary. The static yield strength of the 2024-T351 aluminum alloy is 52,000 psi, and the cyclic yield strength range, $\Delta\sigma_{Y(c)}$, is 134,000 psi. The material cyclically strain hardens. As the prestress level increases, $\Delta\sigma_{Y(c)}$ increases. Yet this increase in $\Delta\sigma_{Y(c)}$ causes an increase in da/dN. Furthermore according to the model, the crack tip opening displacement should be less in the interior of a specimen than on the specimen surface. If da/dN is linearly proportional to crack tip opening displacement, the crack should advance faster on the surface than in the interior. All the observations indicate otherwise. This contradiction certainly warrants additional studies in this important area of fatigue crack propagation research.

V. SUMMARY AND CONCLUSIONS

1. Fatigue crack propagation rate is proportional to ΔK^2, if the region ahead of a crack tip can be scaled by the characteristic length, r_p, so that as a crack grows, the deformation at geometrically similar points is identical.

2. Fatigue crack propagation rate is affected by thickness and stress ratio. The larger the plate thickness or stress ratio is, the faster the crack propagation rate will be. This spread in rate, due to the stress ratio effect, is small at lower ΔK values but becomes progressively larger as ΔK is increased. This means that the slopes of the crack propagation rate increase with increasing stress ratio. In these studies, the slopes in region II are found to be 2.0, 2.7 and 3.4 for R = 1/10, 1/3 and 1/2, respectively.

3. For 2024-T351 aluminum alloy, prestress cycling below the static yield strength has no noticeable effect on the fatigue crack propagation rate. However, prestress cycling above the static yield strength causes hardening and increases the fatigue crack propagation rate. This observation leads one to conclude that fatigue damage occurs mainly after the material elements ahead of a crack have entered the plastic region. Before the material elements enter the plastic boundary, there is negligible damage to the elements. Therefore, fatigue crack propagation rate can be written as

$$\frac{da}{dN} = \frac{r_p}{N_r} \tag{41}$$

where N_r is the number of cycles to propagate a crack through r_p.

4. Under the plane stress condition, the cyclic strain distribution ahead of a crack tip, measured by moire method, agrees very well with the calculation from linear elastic theory, when the values of ΔK are small. This indicates that the high density grille moire technique is a very useful tool for the measurements of surface strains around a crack tip.

5. The measured crack tip strains can be correlated with a straight line in a log-log plot. The slopes of these lines for $\Delta\varepsilon$ are all equal to -0.5, while those for ε_{max} are varied from -0.5 to -0.8. The cyclic strain history ahead of a crack tip can be written as

$$\begin{aligned} \varepsilon &= \varepsilon_{mean} + \frac{\Delta\varepsilon}{2} \sin(2\pi N) \\ &= \varepsilon_{Y(s)} \left(\frac{r}{r_{max(s)}}\right)^{n_1} - \frac{1}{2}\Delta\varepsilon_{Y(c)} \left(\frac{r}{r_{p(c)}}\right)^{n_2} [1 - \sin(2\pi N)] \end{aligned} \tag{33}$$

where ε_{mean} is the cyclic mean strain, $\varepsilon_{Y(s)}$ is the static yield strain, $\Delta\varepsilon_{Y(c)}$ is the cyclic yield strain range, $r_{max(s)}$ is the static maximum plastic zone size, $r_{p(c)}$ is the cyclic plastic zone size, n_1 varies from -0.5 to-0.8, and n_2 is -0.5.

6. The plastic zone size, r_p is found to be proportional to ΔK^2 in region II for all the cases investigated. In region III, it is found to be proportional to ΔK^4 for the case of 0.050 inches at R = 1/10.

If da/dN is proportional to r_p, one obtains the following two equations

$$\frac{da}{dN} = \frac{r_p}{N_r} = C_3 \Delta K^2 \qquad \text{for region II} \qquad (4)$$

$$\frac{da}{dN} = \frac{r_p}{N_r} = C_4 \Delta K^4 \qquad \text{for region III} \qquad (5).$$

The last equation is the fourth power law of fatigue crack propagation, proposed by Paris and Erdogan[2].

7. The effect of stress ratio on the fatigue crack propagation rate can also be written as

$$\frac{da}{dN} = C_{23} r_p r_{max}^{\alpha_1} \qquad (45)$$

where α_1 is a constant which is equal to or larger than zero. This is the equation proposed by Roberts and Erdogan[49].

8. The crack opening displacement range, $\Delta\delta$, is found to be proportional to the square root of the distance from a crack tip. At a fixed distance near a crack tip, $\Delta\delta$ is linearly proportional to ΔK in region II for all the cases investigated, and is proportional to ΔK^2 in region III for the case of 0.050 inches thick at R = 1/10.

9. In the region investigated, i.e. between 0.01 inches and 0.1 inches from a crack tip, the predicted $\Delta\delta$ by the Dugdale model and the elastic

model is very close. However, the experimental points seem to agree better with the calculated $\Delta\delta$ by the elastic model because there is no tendency to level off as r approaches the crack tip.

REFERENCES

1. A. K. Head, "On the Growth of Fatigue Cracks," The Phil. Mag., vol. 44, Series 7, p. 925 (1953).

2. P. C. Paris and F. Erdogan, "A Critical Analysis of Crack Propagation Laws," An ASME publication, Paper No. 62-WA-234.

3. N. E. Frost and D. S. Dugdale, "The Propagation of Fatigue Cracks in Sheet Specimens," J. Mech. and Phys. Solids, vol. 6, No. 2, p. 92, (1958).

4. H. W. Liu, "Crack Propagation in Thin Metal Sheets Under Repeated Loading," ASME Trans., J. Basic Eng., vol. 83, Series D, No. 1, p. 23, March (1961).

5. H. W. Liu, "Fatigue Crack Propagation and Applied Stress Range - An Energy Approach," ASME Trans., J. Basic Eng., March (1963).

6. H. W. Liu, "Fatigue Crack Propagation and the Stresses and Strains in the Vicinity of a Crack," Applied Materials Research, p. 229, Oct. (1964).

7. P. C. Paris, "A Note on the Variables Effecting the Rate of Crack Growth Due to Cyclic Loading," The Boeing Company Document No. D-17867, Addendum N., Sept. 12. (1957).

8. P. C. Paris, M. P. Gomez and W. E. Anderson, "A Rational Analytic Theory of Fatigue," The Trend in Engineering, vol. 13, p. 9, Jan. (1961).

9. F. A. McClintock, "On the Plasticity of the Growth of Fatigue Cracks," Fracture of Solids, John Wiley, New York, p. 65 (1965).

10. J. R. Rice, "Plastic Yielding at a Crack Tip," The First International Conference on Fracture, Sendai, Japan, p. 283 (1965).

11. J. R. Rice, "Mechanics of Crack Tip Deformation and Extension by Fatigue," Fatigue Crack Propagation, ASTM STP415, p. 247 (1967).

12. J. M. Krafft, "On Prediction of Fatigue Crack Propagation Rate From Fracture Toughness and Plastic Flow Properties," Trans., ASM, vol. 58, p. 691 (1965)

13. J. M. Krafft, Discussion of a Paper by R. P. Wei, P. M. Talda and Che-Yu Li, "Fatigue-Crack Propagation in Some Ultrahigh-Strength Steels," ASTM STP415, p. 460 (1967).

14. N. E. Frost and J. R. Dixon, "A Theory of Fatigue Crack Growth," Inter. Jour. of Fracture Mechanics, vol. 3, p. 301 (1967).

15. B. A. Bibly, A. H. Cottrell and K. H. Swinden, "The Spread of Plastic Yield From a Notch," Proc. Roy. Soc. Lond., A272, p. 304 (1963).

16. D. S. Dugdale, "Yielding of Steel Sheets Containing Slits," J. Mech. and Physics of Solid., vol. 8, p. 100 (1960).

17. J. N. Goodier and F. A. Field, "Plastic Energy Dissipation in Crack Propagation," Fracture of Solids, John Wiley, New York p. 103 (1963).

18. J. Weertman, "Rate of Growth of Fatigue Cracks Calcualted From the Theory of Infinitesmal Dislocations Distributed on a Plane," The First International Conference on Fracture, Sendai,Japan, p. 153 (1965).

19. A. J. McEvily, Jr. and T. L. Johnston, "On the Role of Cross-Slip in Brittle Fracture and Fatigue," The First International Conference on Fracture, Sendai, Japan, Sept. (1965).

20. R. W. Lardner,"A Dislocation Model for Fatigue Crack Growth in Metals," Phi. Mag., vol. 17, p. 71 (1968).

21. F. A. McClintock, Discussion of a paper by C. Laird, "The Influence of Metallurgical Structure on the Mechanism of Fatigue Crack Propagation," ASTM STP 415, p. 170 (1967).

22. B. Tomkins, "Fatigue Crack Propagation - An Analysis," Phil. Mag. vol. 18, No. 155, p. 1041 (1968).

23. B. A. Bibly and K. H. Swinden, "Representation of Plasticity at Notches by Linear Dislocation Arrays," Proc. Roy. Soc. Lond., A285, p. 22 (1965).

24. D. Broek and J. Schijve, "The Effect of Sheet Thickness on the Fatigue - Crack Propagation in 2024-T3 Alclad Sheet Material," NLR-TR M 2129, April (1963).

25. R. G. Forman, V. E. Kearney and R. M. Engle, "Numerical Analysis of Crack Propagation in Cyclic-Loaded Structures," J. Basic Eng., p. 459, Sept. (1967).

26. C. M. Hudson and J. T. Scardina, "Effect of Stress Ratio on Fatigue-Crack Growth in 7075-T6 Aluminum Alloy Sheet," Eng. Fracture Mech., vol. 1, p. 429 (1969).

27. R. M. N. Pelloux, "Fractographic Analysis of the Influence of Constituent Particles on Fatigue Crack Propagation in Aluminum Alloys," ASM Trans. Quart., vol. 57, No. 2, p. 511, June (1964).

28. R. W. Hertzberg and P. C. Paris, "Application of Electron Fractography and Fracture Mechanics to Fatigue Crack Propagation," First International Conference on Fracture, Sendai, Japan, vol. 1, p. 459 (1965).

29. J. Kershaw and H. W. Liu, "Electron Fractography and Fatigue Crack Propagation in 7075-T6 Aluminum Sheet," Int. Journ. of Fracture Mech., vol. 7, No. 3, p. 269, Sept. (1971).

30. V. Weiss, "Notch Analysis of Fracture," Fracture An Advanced Treatise, Edited by H. Liebowitz, Academic Press, New York, vol. III, p. 228 (1971).

31. H. W. Liu and N. Iino, "A Mechanical Model for Fatigue Crack Propagation," Fracture , Proc. Second Inter. Conf. on Fracture, Brighton, April (1969).

32. G. R. Irwin, "Analysis of Stresses and Strains Near the End of a Crack Traversing a Plate," J. Appl. Mech., p. 361, Sept. (1957).

33. M. L. Williams, "On the Stress Distribution at the Base of a Stationary Crack," J. Applied Mech., p. 109, March (1957).

34. P. C. Paris and G. C. Sih, "Stress Analysis of Cracks," STP381 ASTM-NASA, p. 30 (1965).

35. J. A. H. Hult and F. A. McClintock, "Elastic-Plastic Stress and Strain Distributions Around Sharp Notches Under Repeated Shear," Ninth International Congress for Applied Mechanics, (Brussels), vol. 8, p. 51 (1956)

36. V. Weiss, Fatigue - An Interdisciplinary Approach, Proc. Tenth Sagamore Army Materials Conf., Syracuse Univ. Press., Syracuse (1964).

37. J. W. Hutchinson, "Singular Behavior at the End of a Tensile Crack in a Hardening Materials," J. Mech. and Phys. Solids, vol. 16, p. 13, Jan. (1968).

38. J. R. Rice and G. F. Rosengren, "Plane Strain Deformation Near a Crack Tip in a Power-Law Hardening Material," J. Mech. Phys. Solids, vol. 16, p. 1 (1968).

39. J. L. Swedlow, "The Thickness Effect and Plastic Flow in Cracked Plates," Doctoral Dissertation, California Inst. of Tech. (1965).

40. J. L. Swedlow, M. L. Williams and W. H. Yang, "Elasto-Plastic Stresses and Strains in Cracked Plates," Proc. First International Conf. on Fracture, Sendai, Japan, vol. 1, p. 259 (1965).

41. J. M. Barsom, "Investigation of Subcritical Crack Propagation," Ph.D. Dissertation, Univ. of Pittsburgh (1969).

42. W. G. Clark, Jr. and E. T. Wessel, "Interpretation of the Fracture Behavior of 5456-H321 Aluminum with WOL Toughness Specimens," Westinghouse Research Lab. Scientific Paper 67-1D6-BTLFR-P4, Sept. (1967).

43. C. Laird and G. C. Smith, "Crack Propagation in High Stress Fatigue," Phil. Mag., vol. 7, p. 847 (1962).

44. B. J. Schaeffer, H. W. Liu and J. S. Ke, "Deformation and the Strip Necking Zone in a Cracked Steel Sheet," Exper. Mech., p.175, April (1971).

45. C. A. Sciammavella and A. J. Durelli, "Moire Fringes as a Means of Analysing Strains," J. Eng. Mech. Div., Proc. of ASCE, Feb. (1961).

46. A. J. Durelli and V. J. Parks, Moire Analysis of Strain, Prentice-Hall, Inc.,Englewood Cliffs, N. J. (1970).

47. K. R. Lehr and H. W. Liu, "Fatigue Crack Propagation and Strain Cycling Properties," Inter. Jour. of Fracture Mechanics, March (1969).

48 F. Erdogan and R. Roberts, "A Comparative Study of Crack Propagation in Plates Under Extension and Bending," First International Conference on Fracture, Sendai, Japan,p. 341, September (1965).

49. R. Roberts and F. Erdogan, "The Effect of Mean Stress on Fatigue Crack Propagation in Plates Under Extension and Bending," J. Basic Eng., p. 885, Dec. (1967).

50. A. A. Wells, "Application of Fracture Mechanics at and Beyond General Yielding," British Welding Journal, p. 563, Nov. (1963).

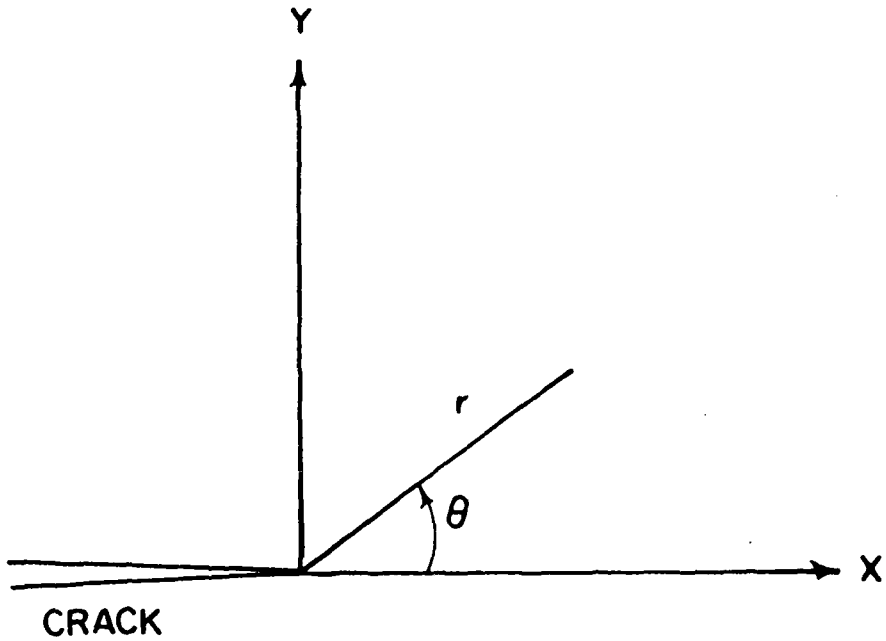

FIGURE 1a. CRACK AND COORDINATES

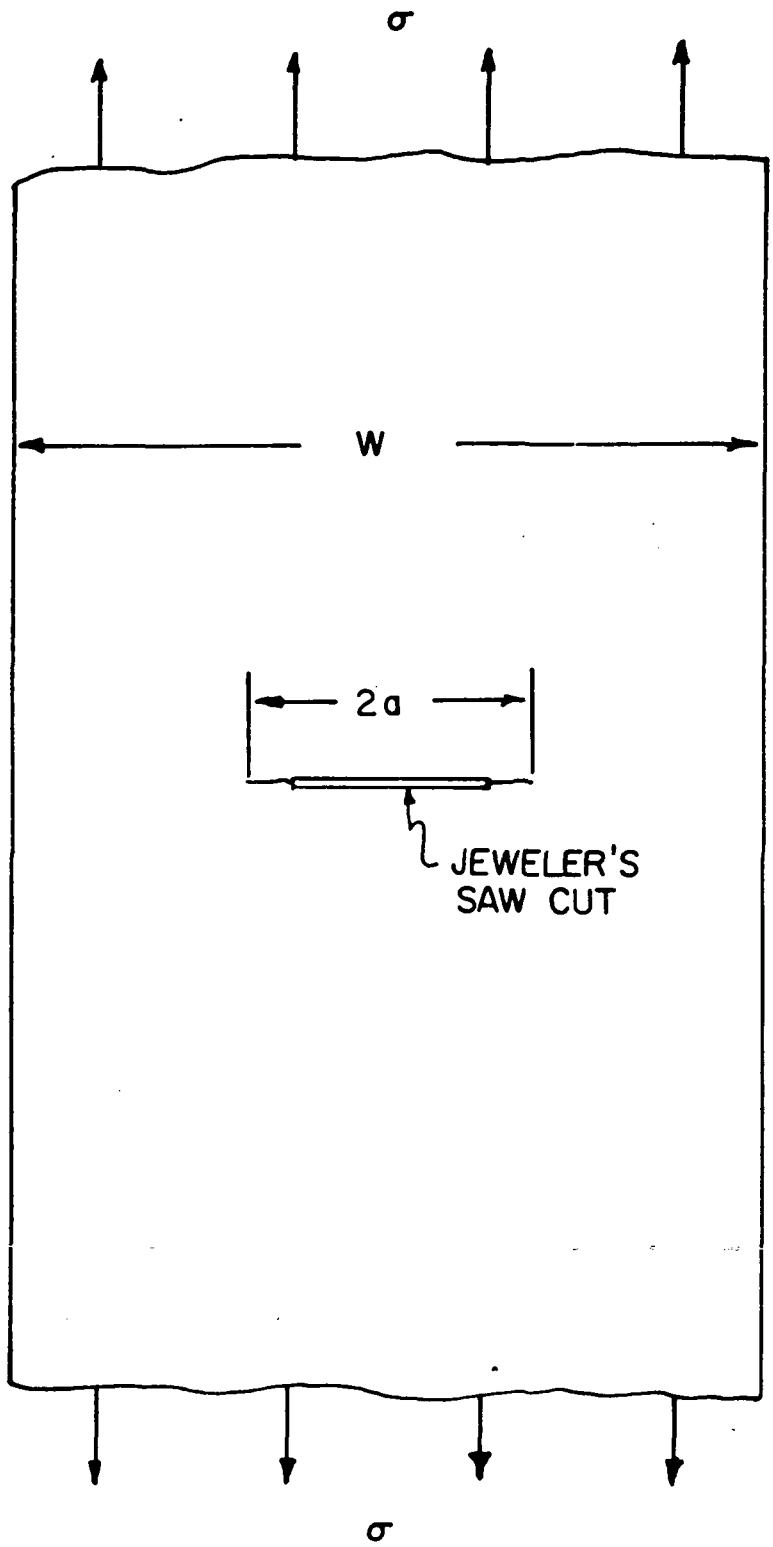

FIGURE 1b. A CENTRALLY CRACKED PLATE SPECIMEN.

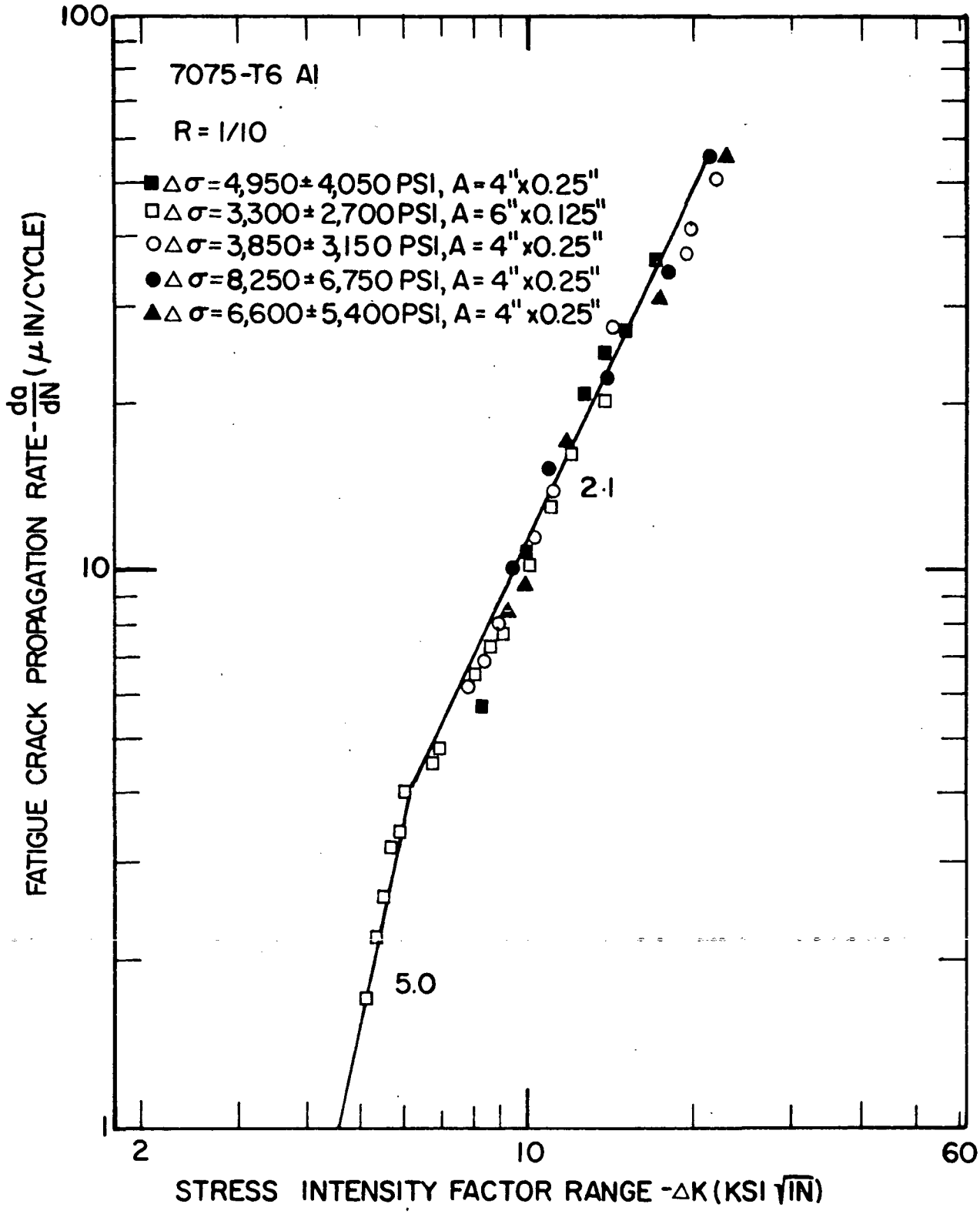

FIGURE 2a. FATIGUE CRACK PROPAGATION RATE FOR 7075-T6 ALUMINUM ALLOY

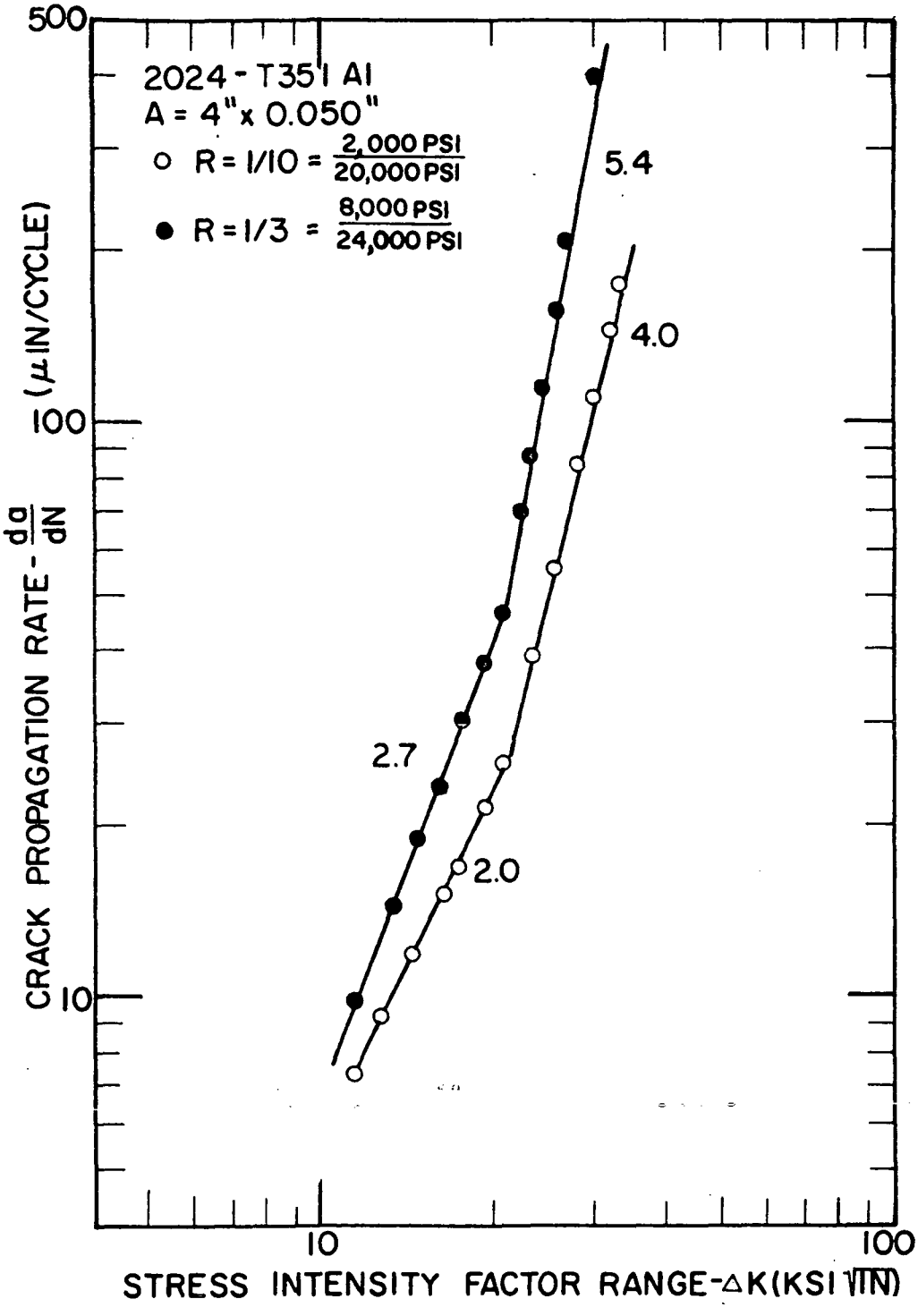

FIGURE 2b. FATIGUE CRACK PROPAGATION RATE FOR 0.050 INCHES THICK 2024-T351 ALUMINUM ALLOY

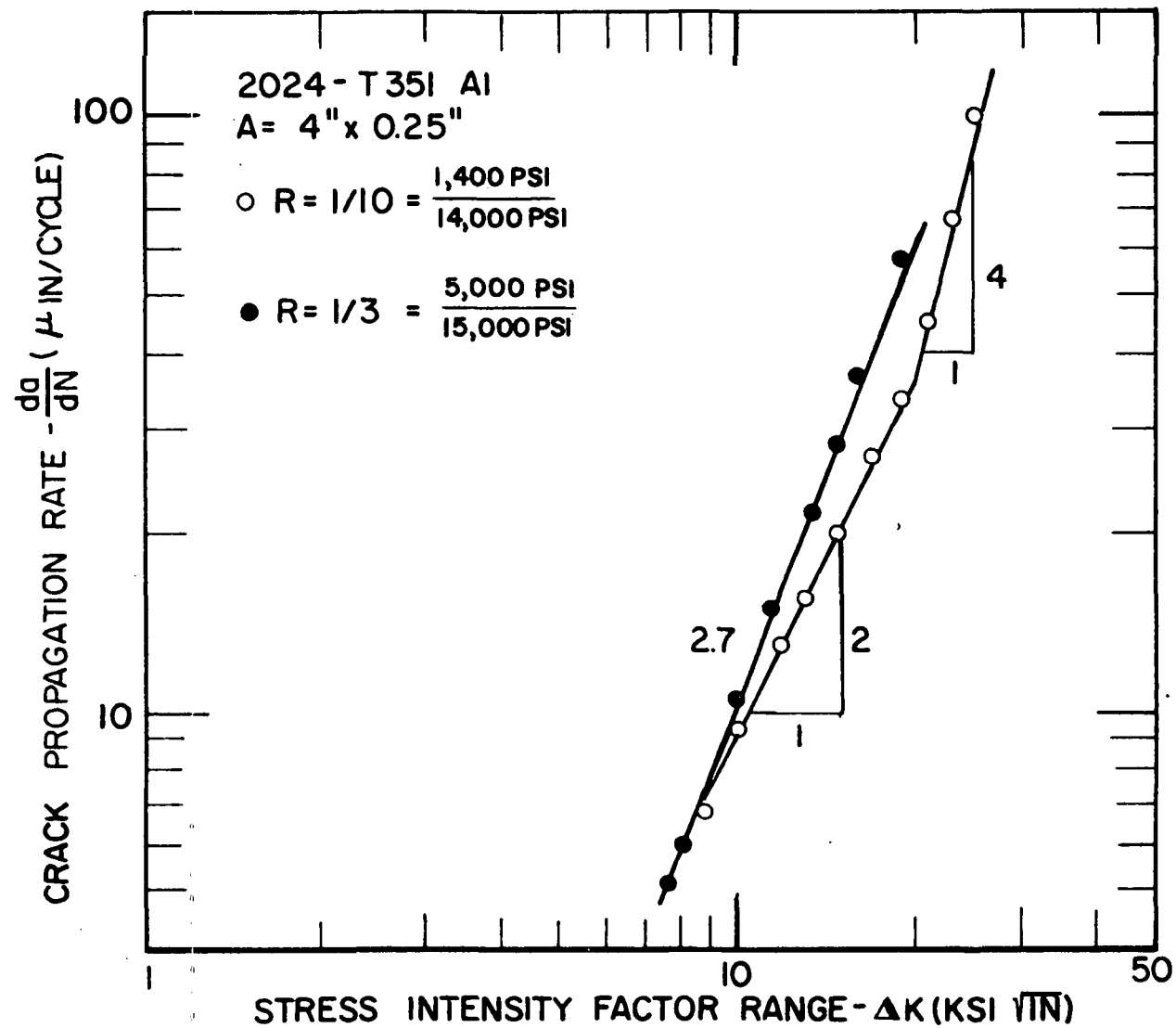

FIGURE 2c. FATIGUE CRACK PROPAGATION RATE FOR 0.25 INCHES THICK 2024-T351 ALUMINUM ALLOY

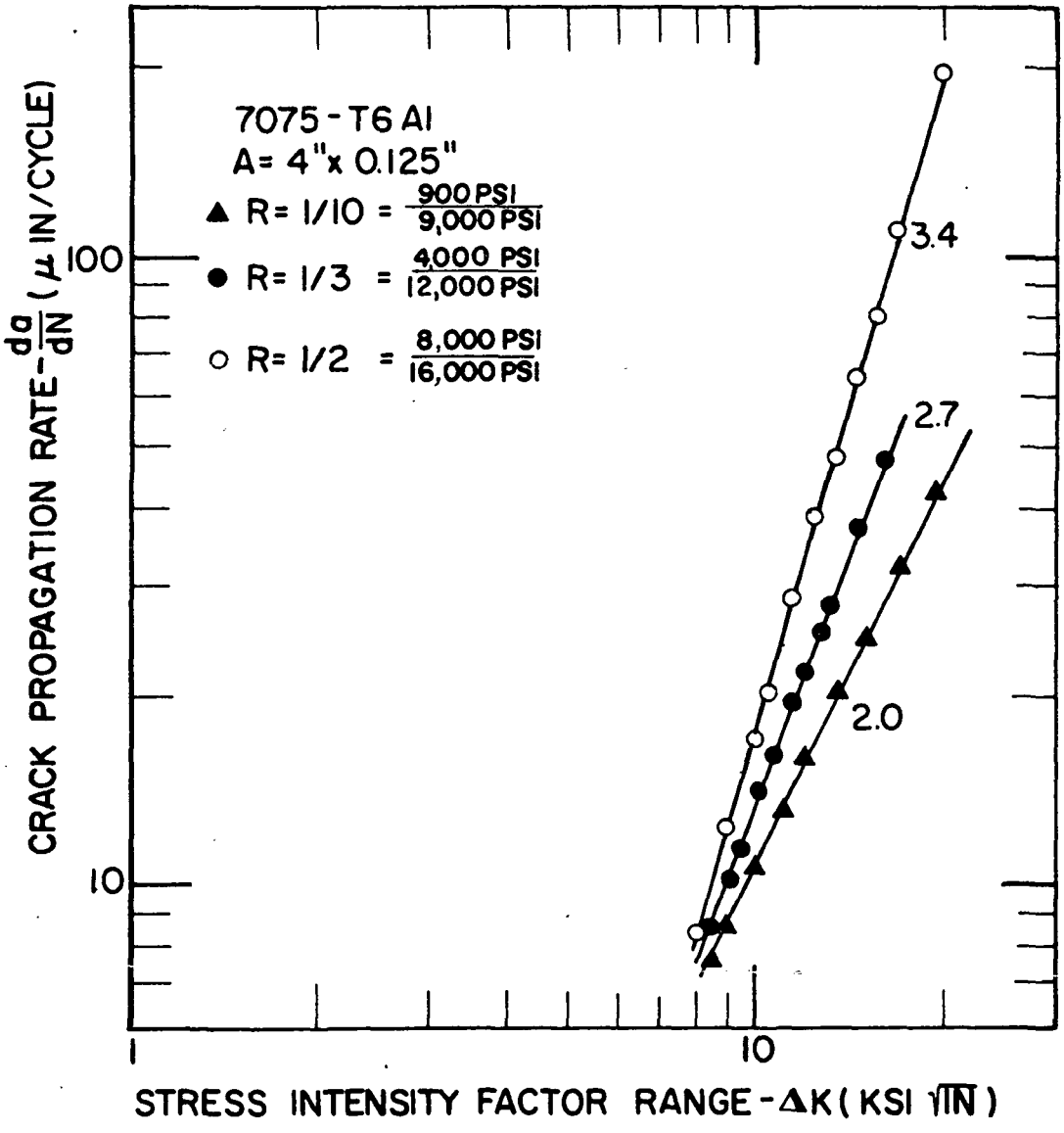

FIGURE 2d. FATIGUE CRACK PROPAGATION RATE FOR 0.125 INCHES THICK 7075-T6 ALUMINUM ALLOY

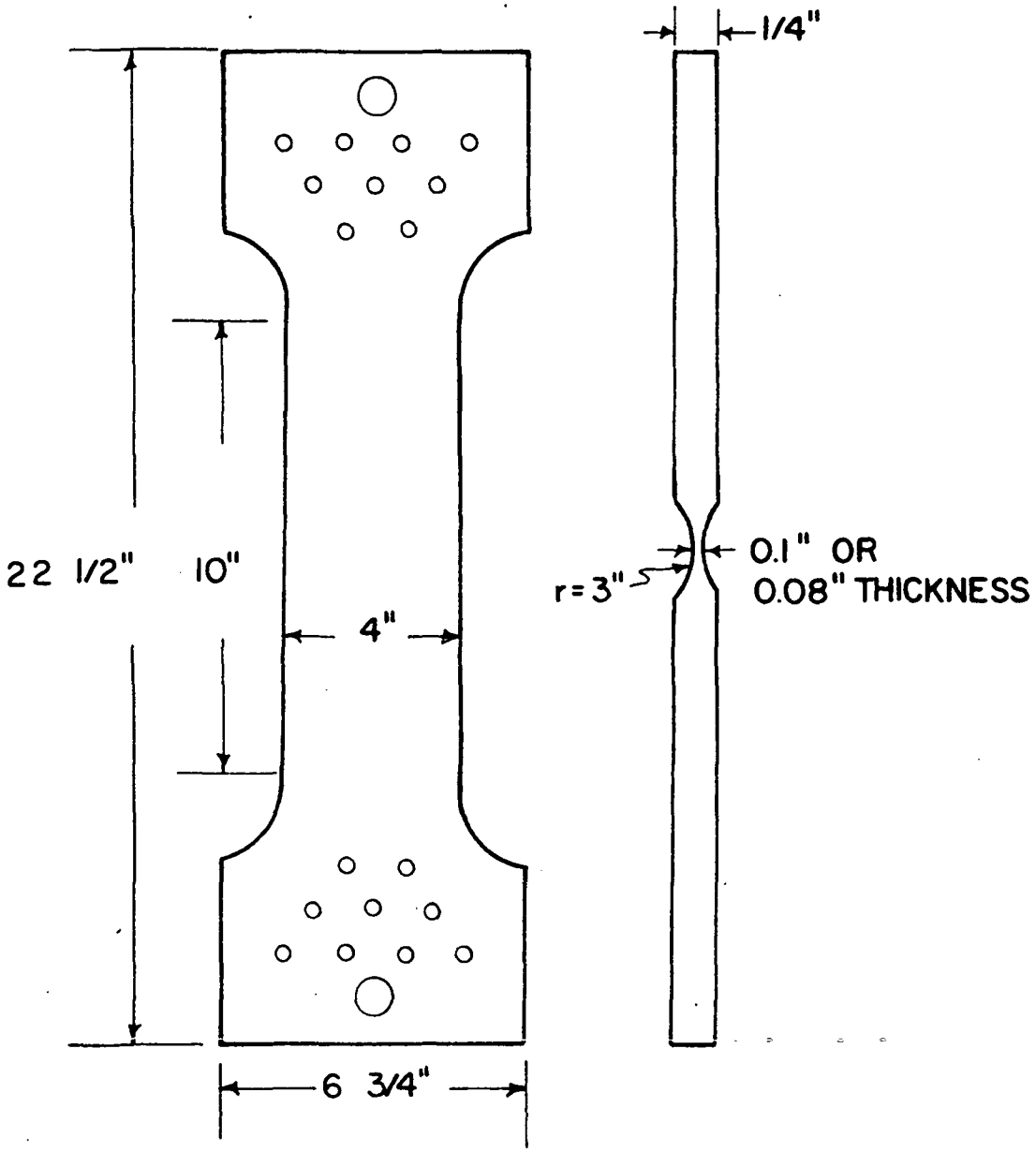

FIGURE 3a. SPECIMEN GEOMETRY FOR PRESTRESS TESTS

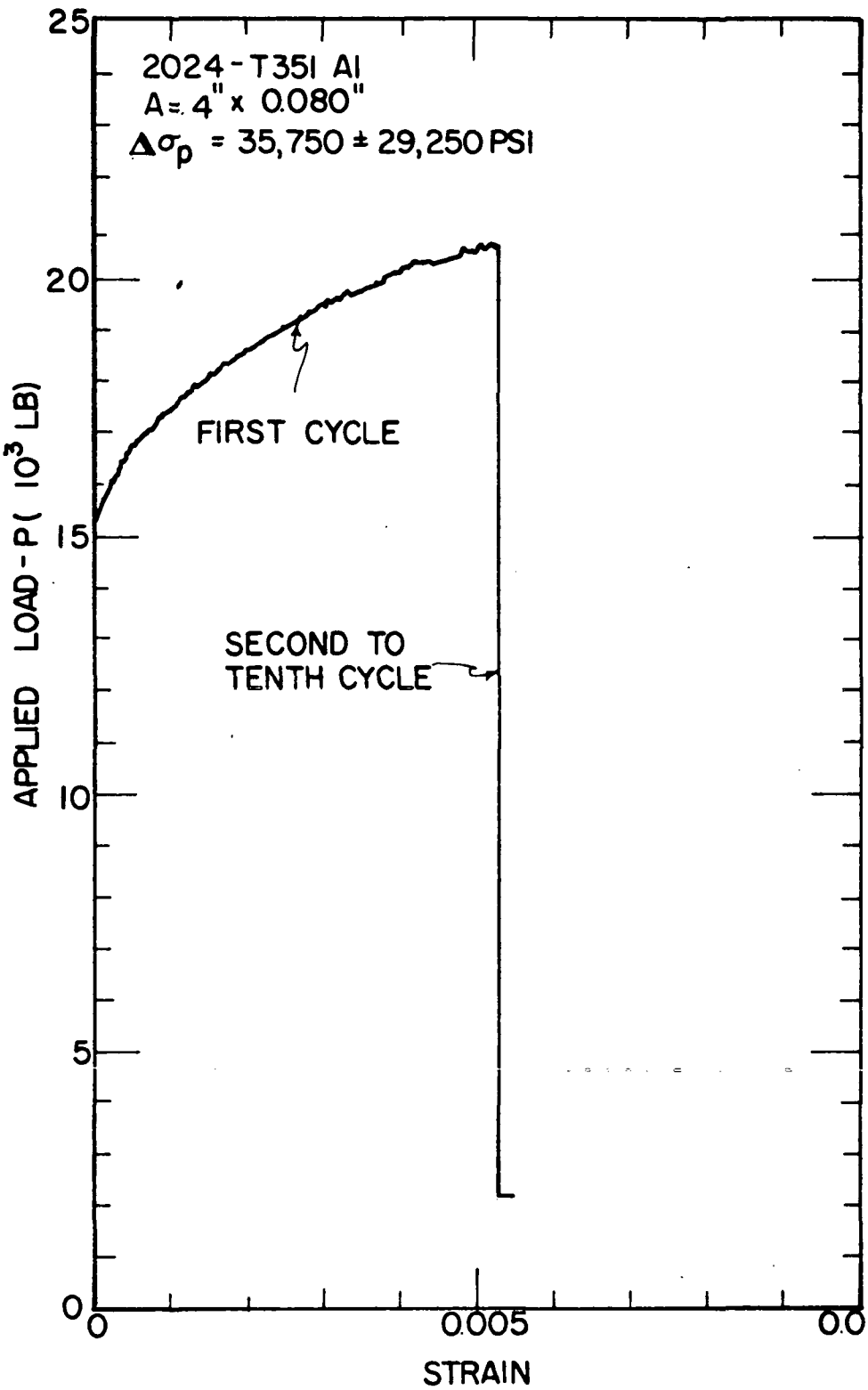

FIGURE 3b. LOAD-STRAIN TRACING FOR PRESTRESS CYCLES

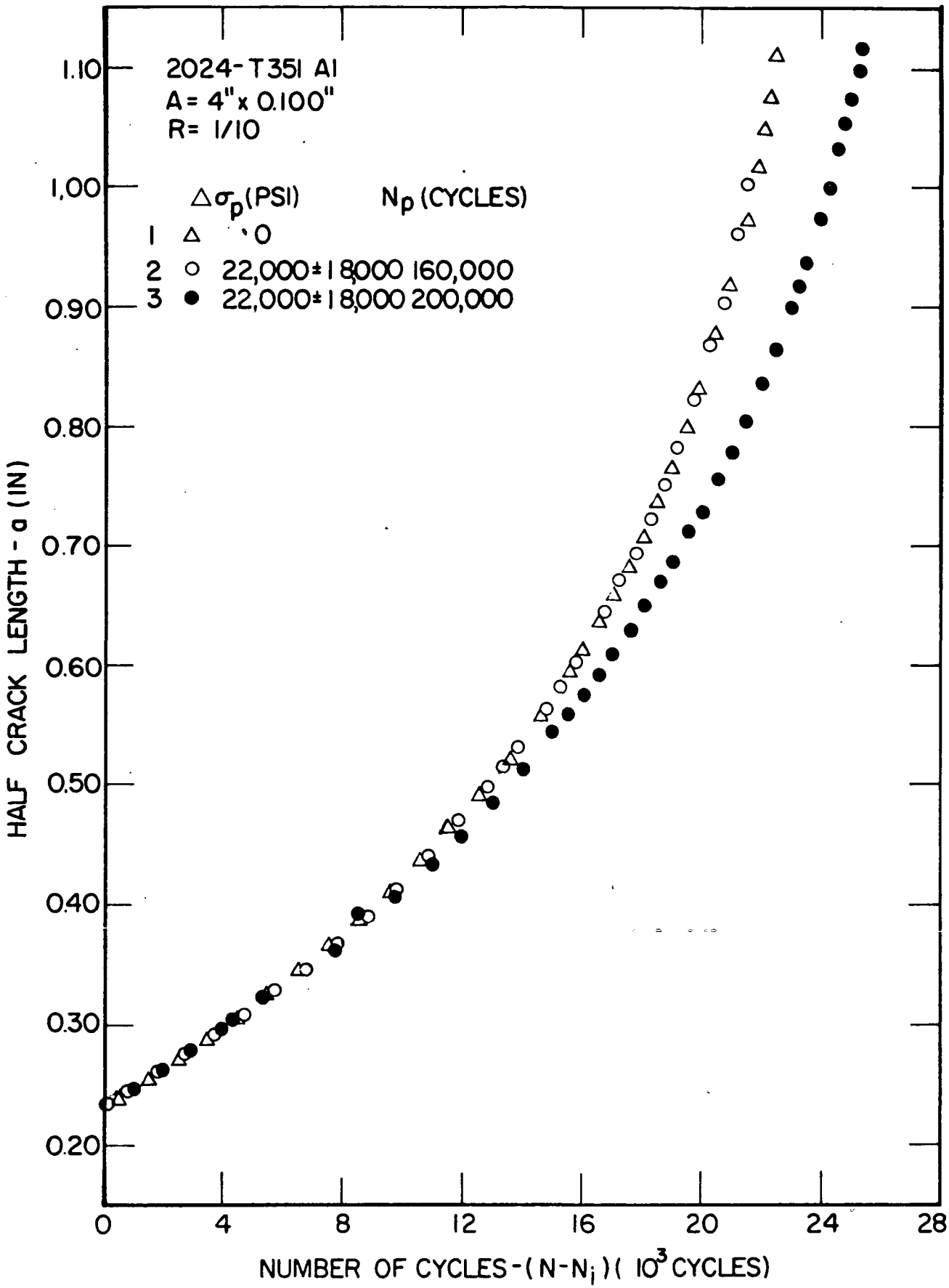

FIGURE 4a. EFFECT OF PRESTRESS CYCLES ON FATIGUE CRACK PROPAGATION, 0.100 INCHES THICK 2024-T351 ALUMINUM ALLOY

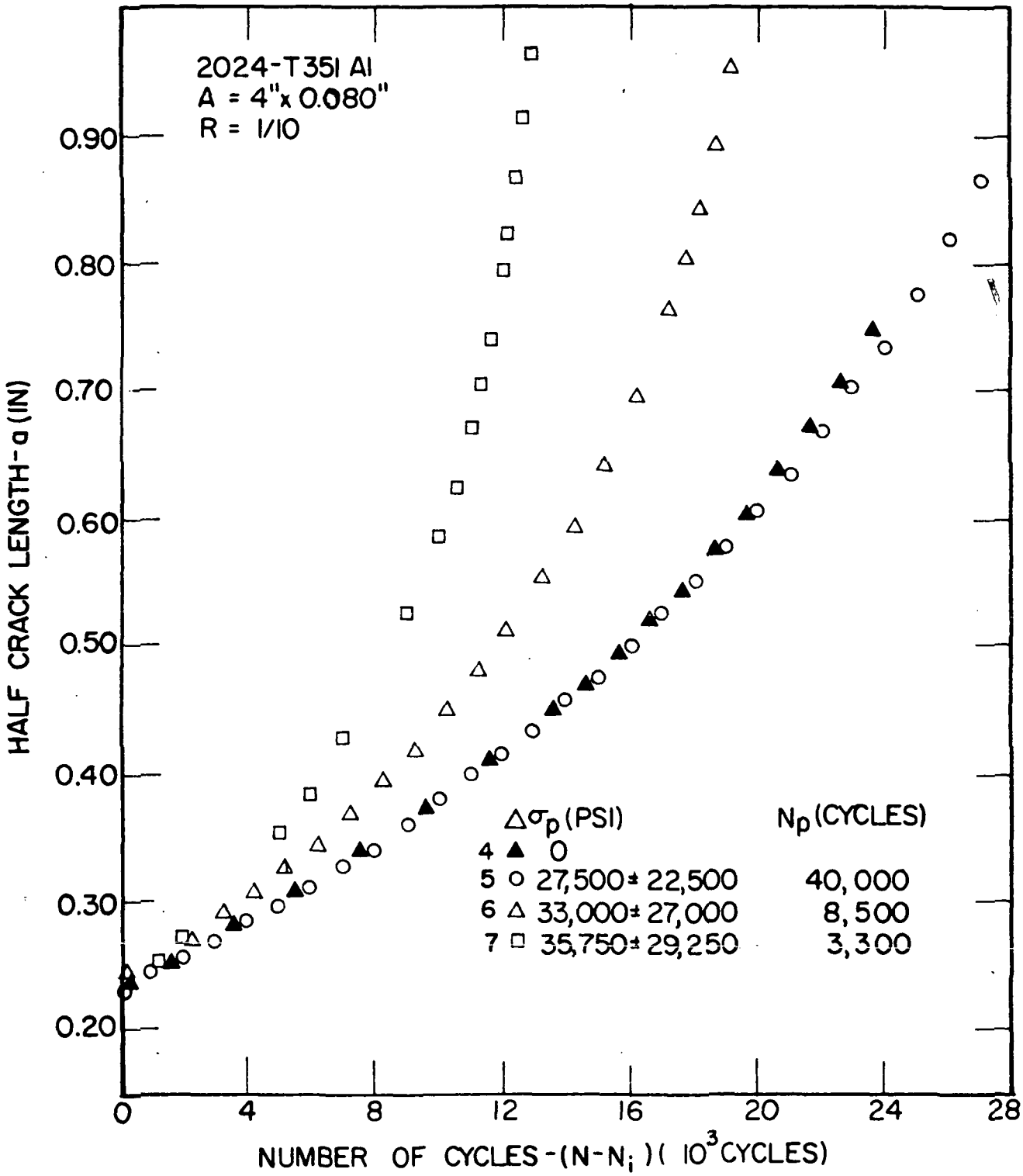

FIGURE 4b. EFFECT OF PRESTRESS CYCLES ON FATIGUE CRACK PROPAGATION, 0.080 INCHES THICK 2024-T351 ALUMINUM ALLOY

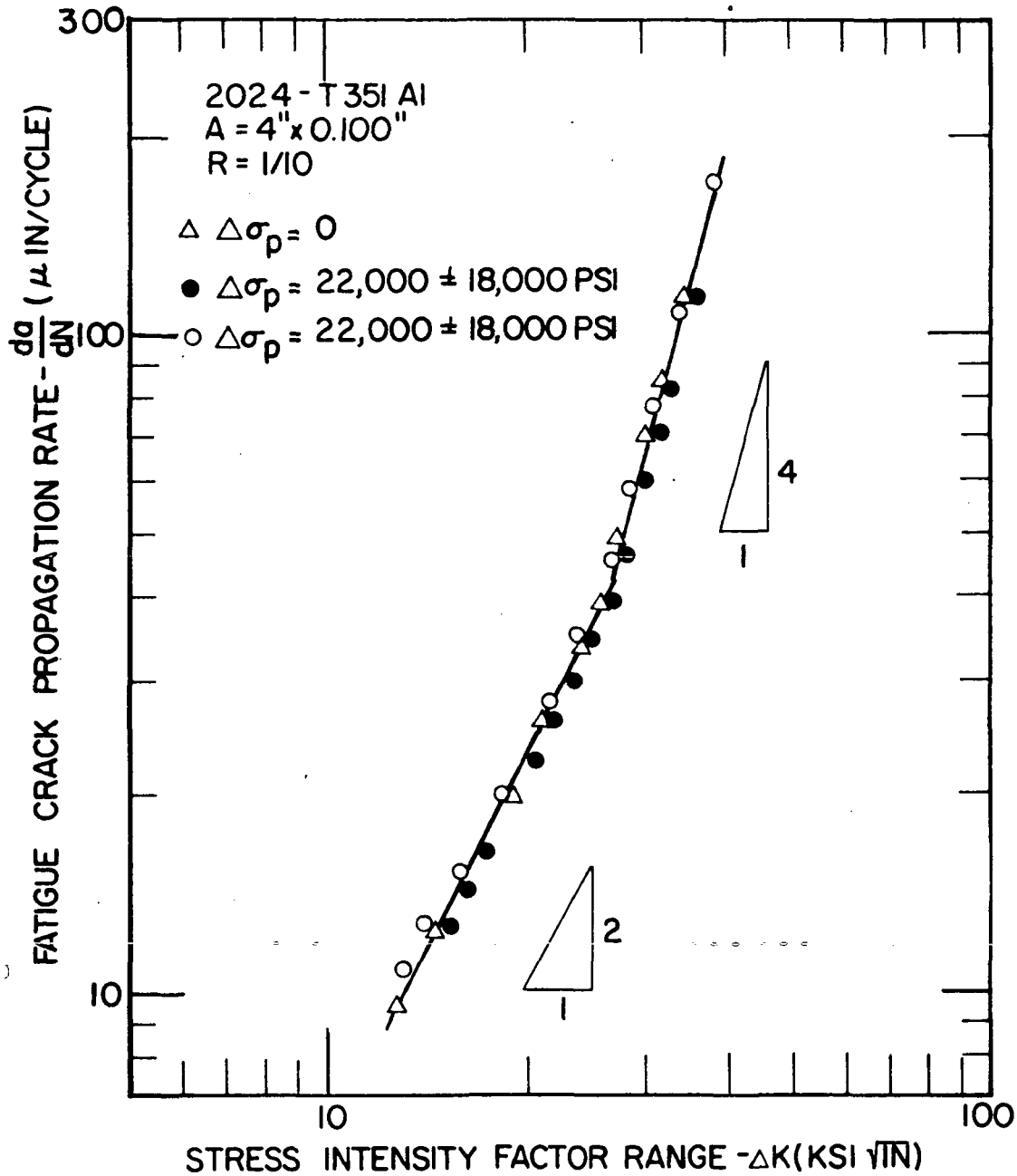

FIGURE 4c. EFFECT OF PRESTRESS CYCLES ON FATIGUE CRACK PROPAGATION RATE FOR 0.100 INCHES THICK 2024-T351 ALUMINUM ALLOY

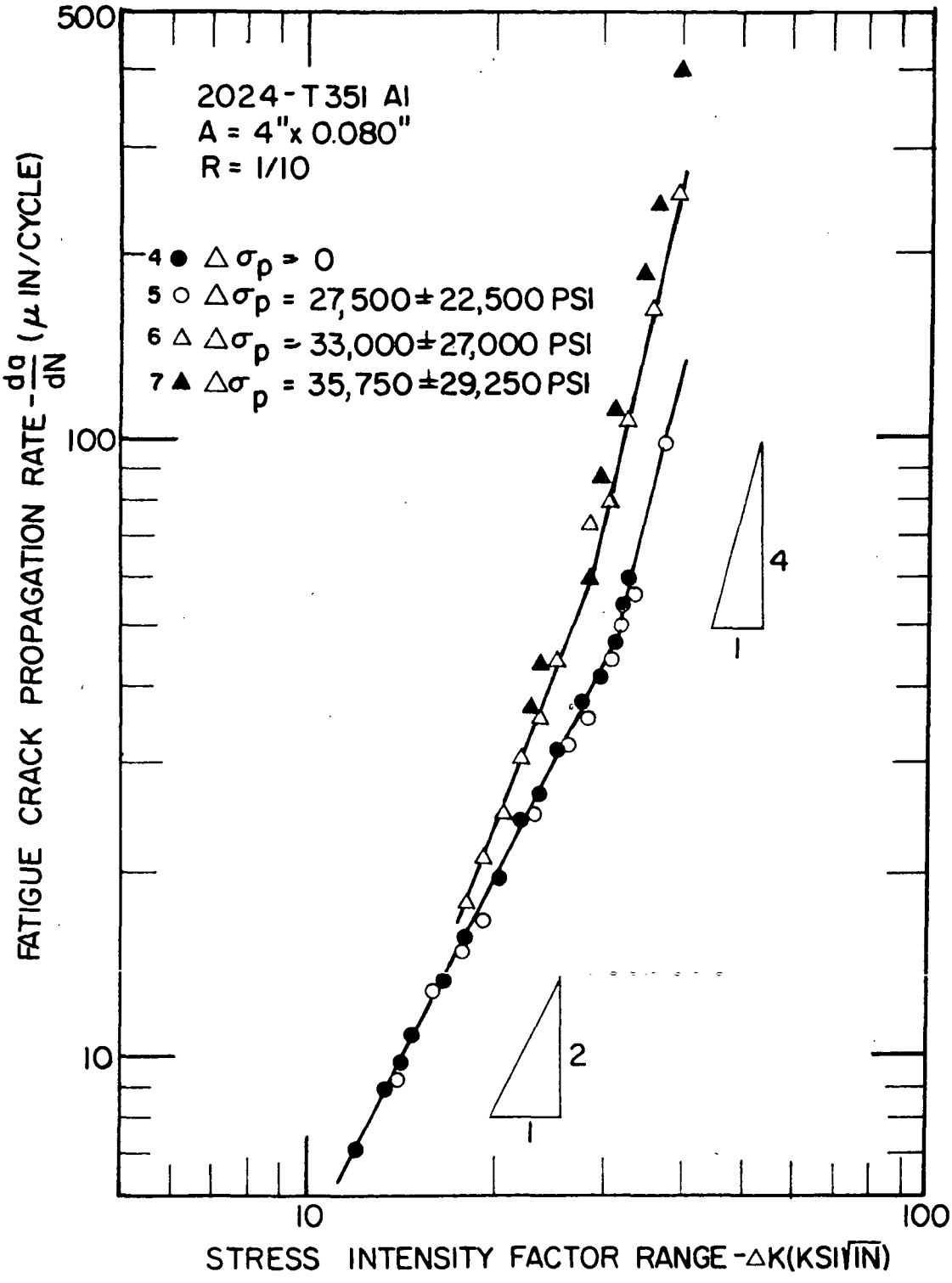

FIGURE 4d. EFFECT OF PRESTRESS CYCLES ON FATIGUE CRACK PROPAGATION RATE FOR 0.080 INCHES THICK 2024-T351 ALUMINUM ALLOY

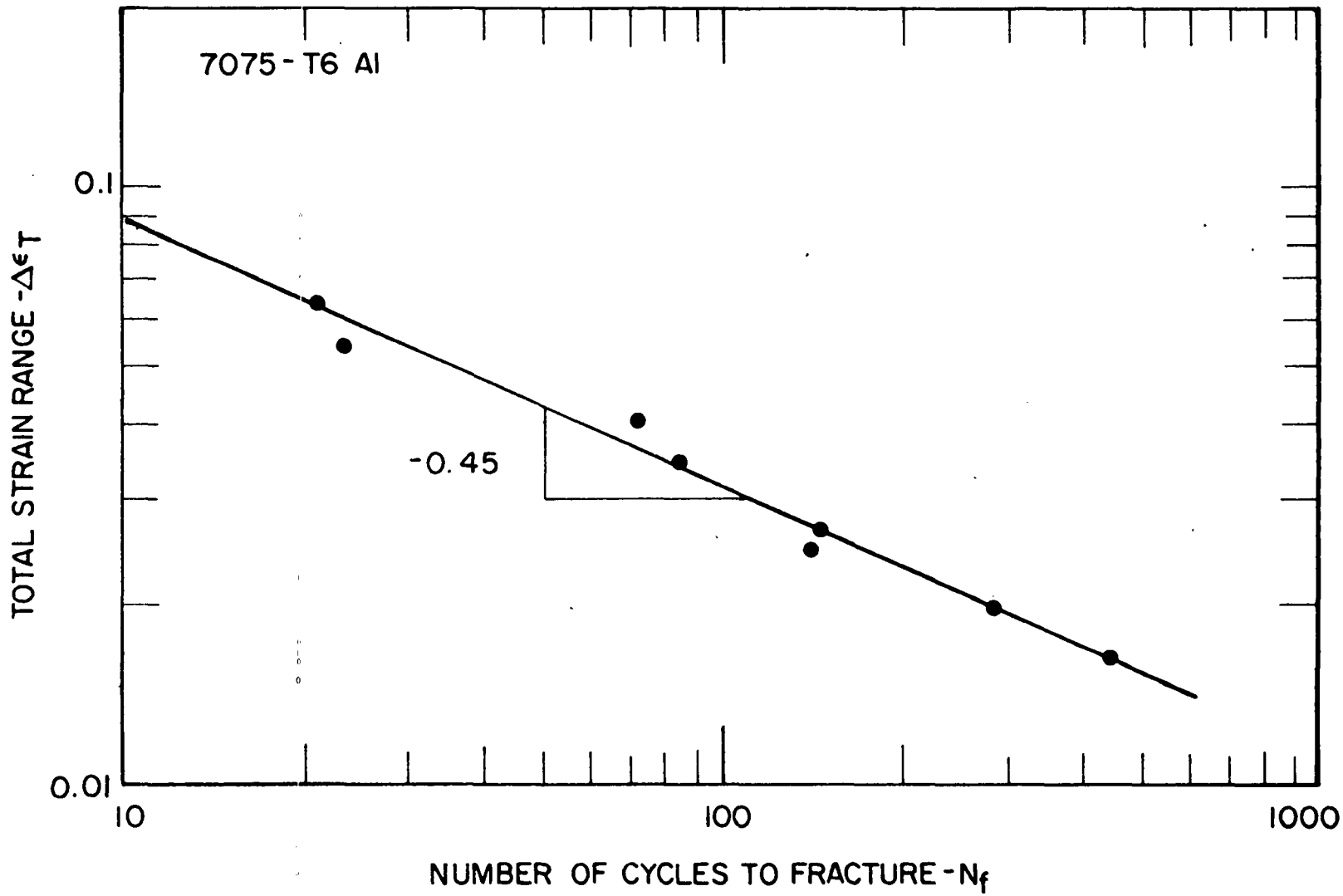

FIGURE 5a. FATIGUE BEHAVIOR OF 7075-T6 ALUMINUM ALLOY AT HIGH STRAIN RANGE

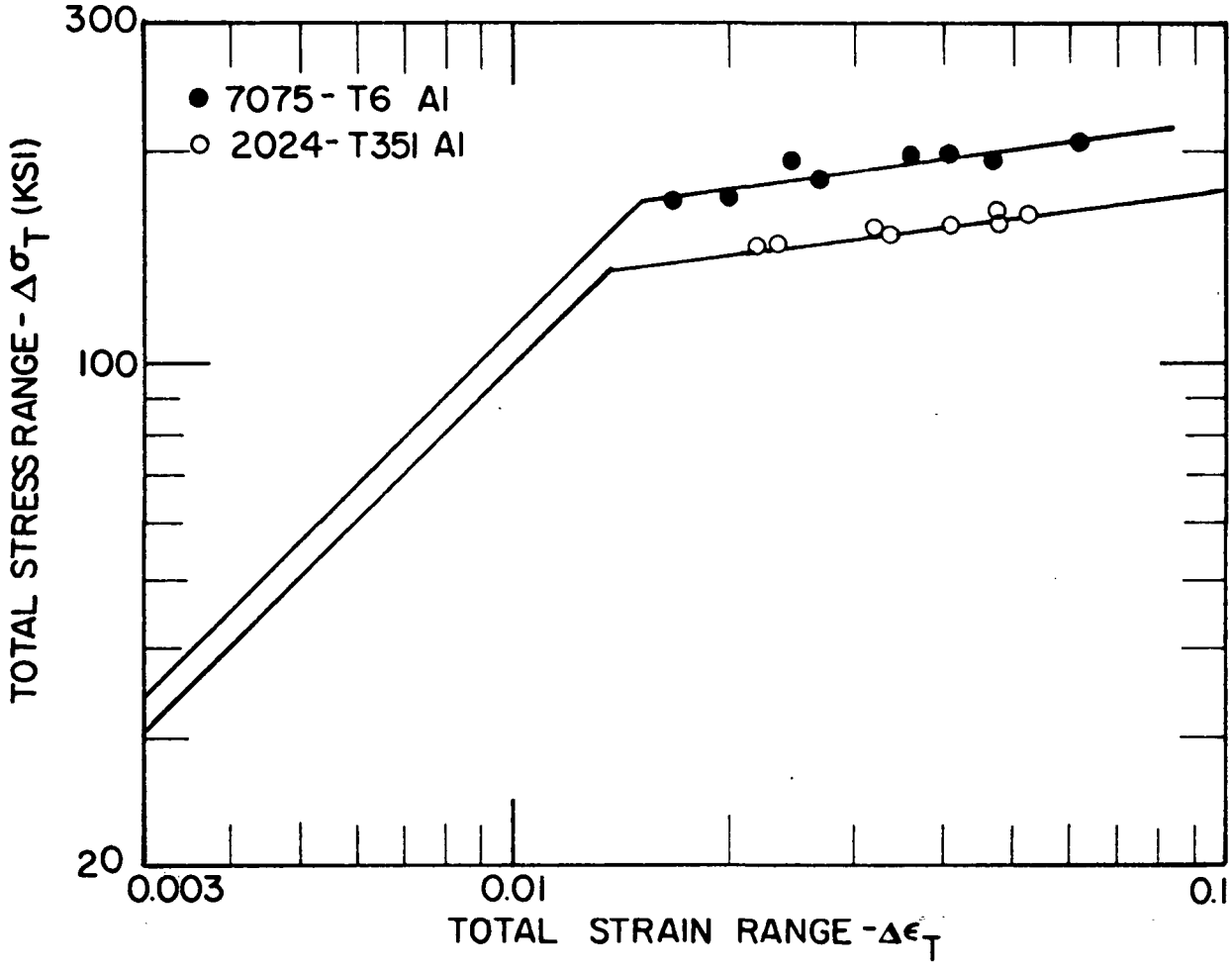

FIGURE 5b. CYCLIC STRESS-STRAIN CURVE FOR 7075-T6 AND 2024-T351 ALUMINUM ALLOYS

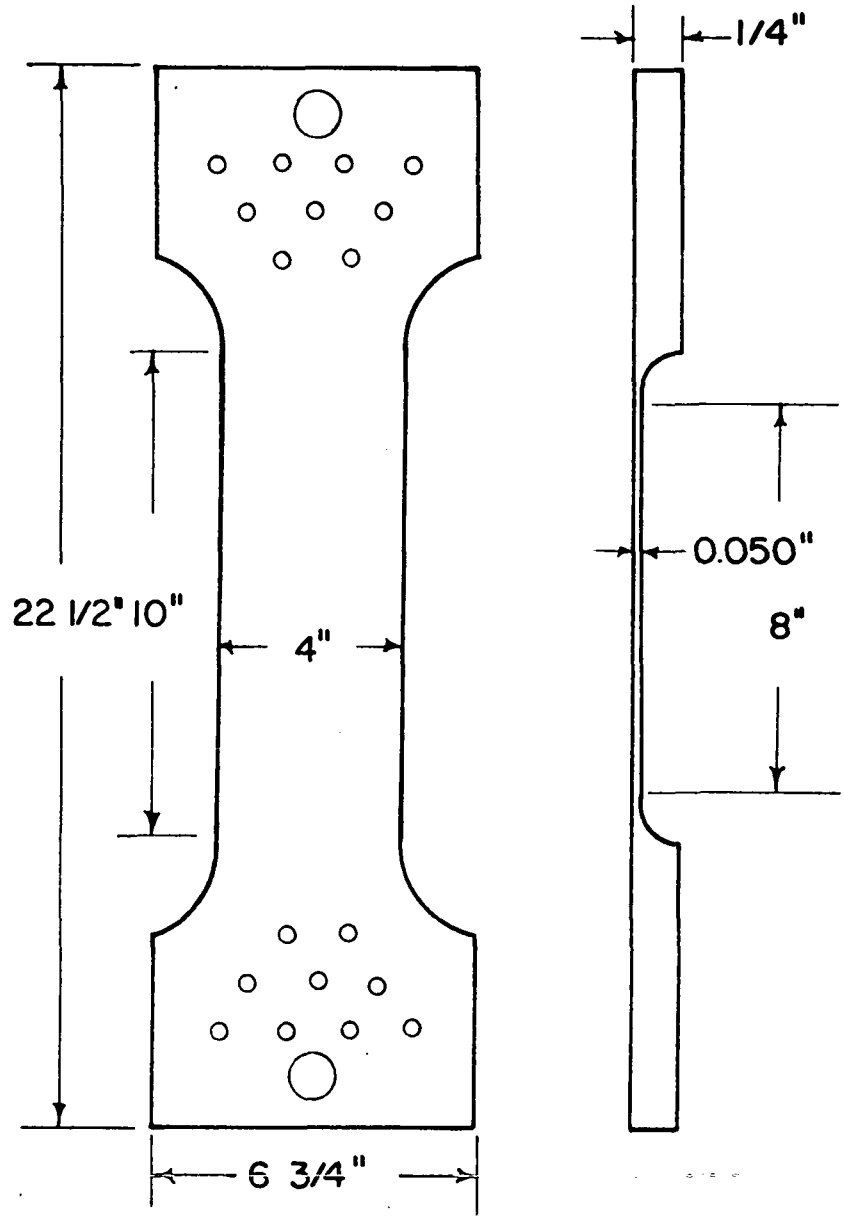

FIGURE 6. SPECIMEN GEOMETRY FOR 0.050 INCHES THICK 2024-T351 ALUMINUM ALLOY

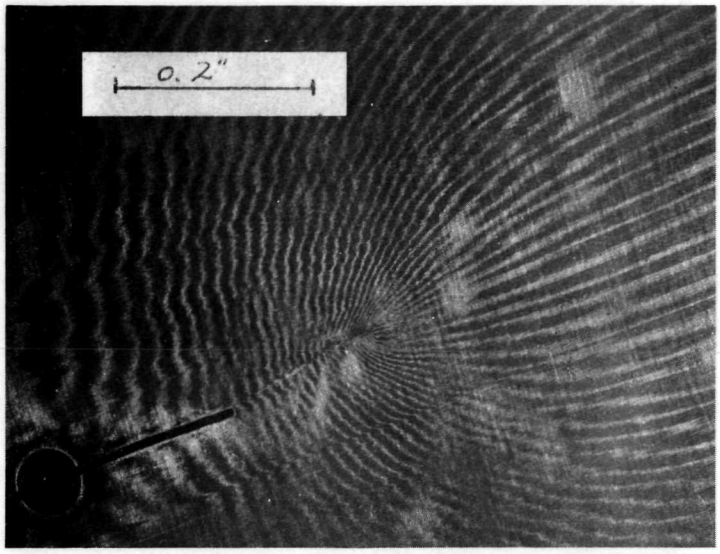

(a) ACCUMULATED DEFORMATION

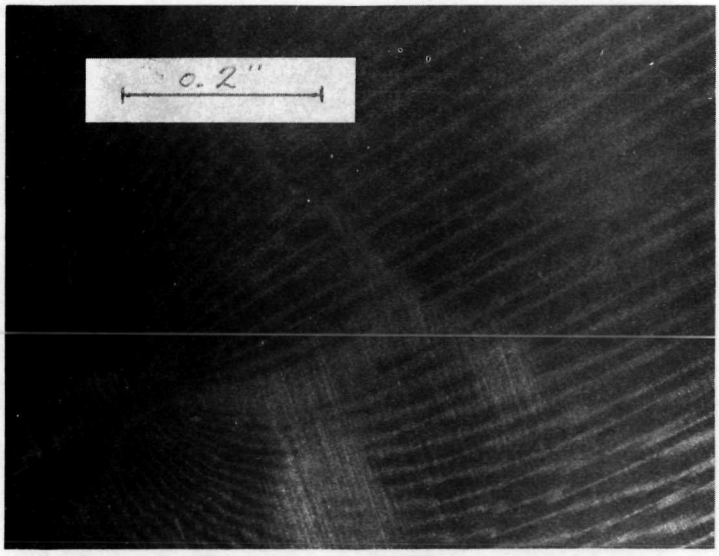

(b) CYCLIC DEFORMATION RANGE

FIG. (7a) MOIRE PATTERNS NEAR A CRACK TIP - 2024-T351 ALUMINUM ALLOY, ΔK=28.3 ksi $\sqrt{in.}$, K_{max}=32.3 ksi $\sqrt{in.}$

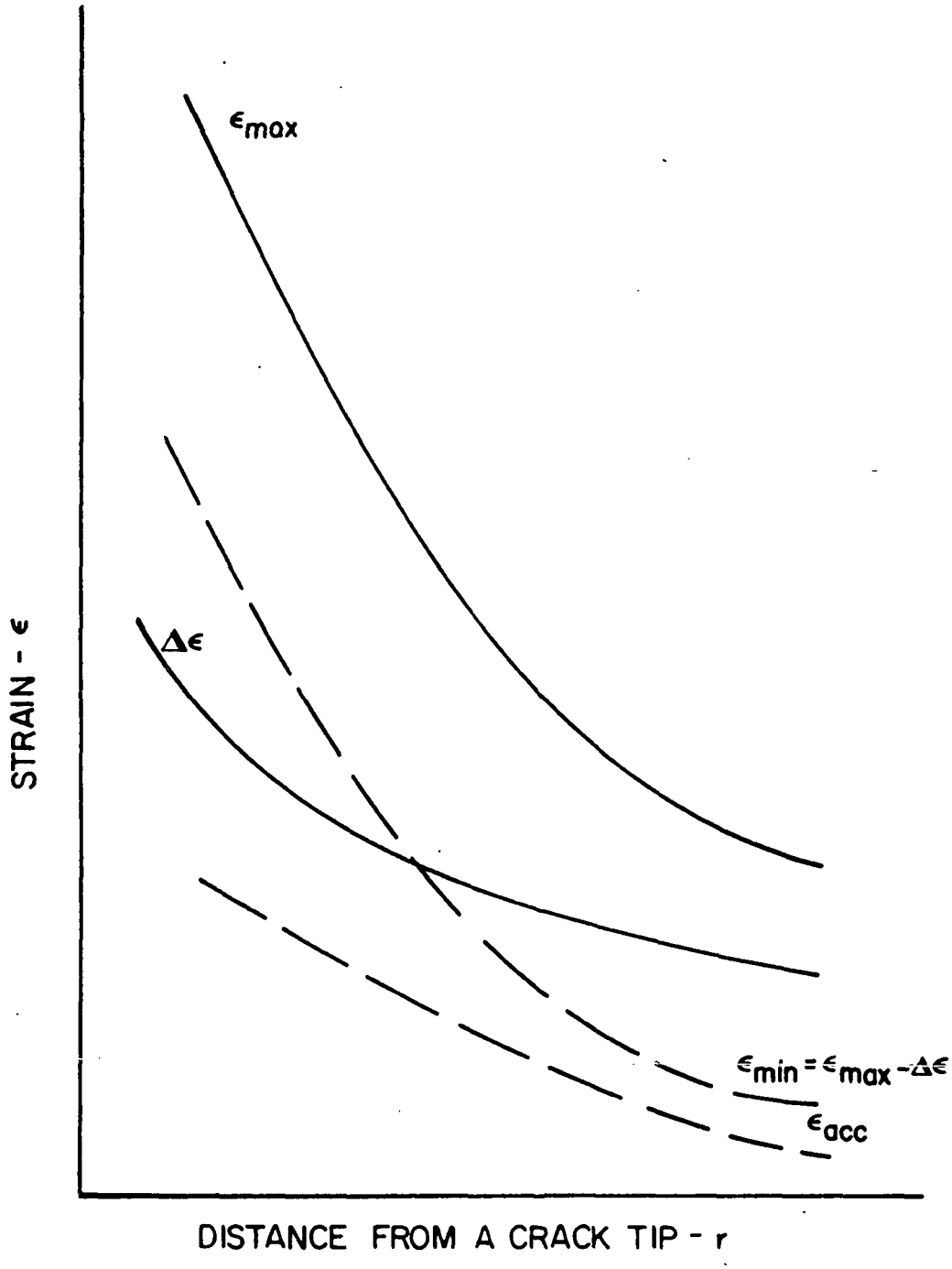

FIGURE 7b. SCHEMATIC DIAGRAM OF STRAIN QUANTITIES

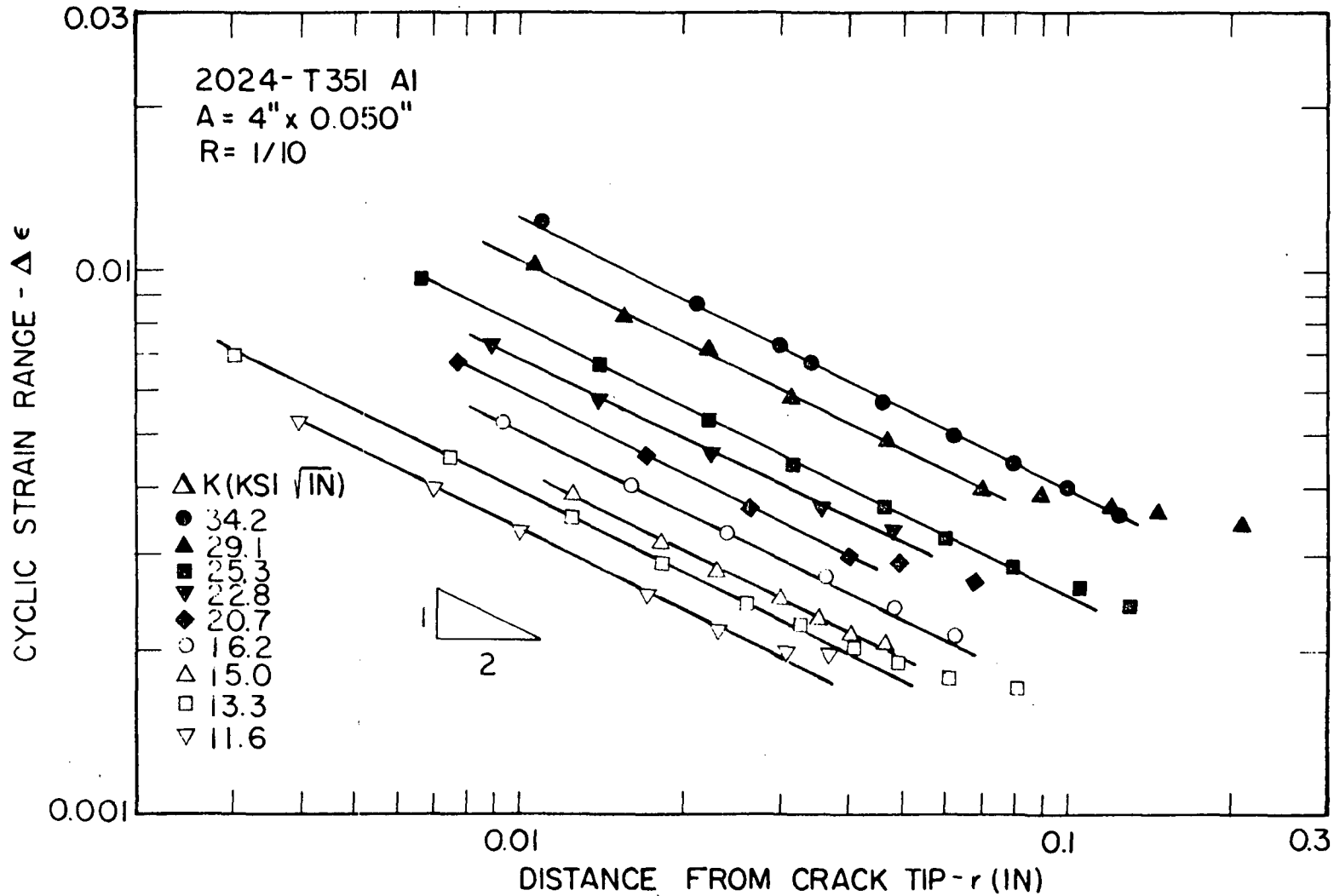

FIGURE 8a. STRAIN RANGE DISTRIBUTION AHEAD OF A CRACK TIP FOR 0.050 INCHES THICK 2024-T351 ALUMINUM ALLOY AT R=1/10

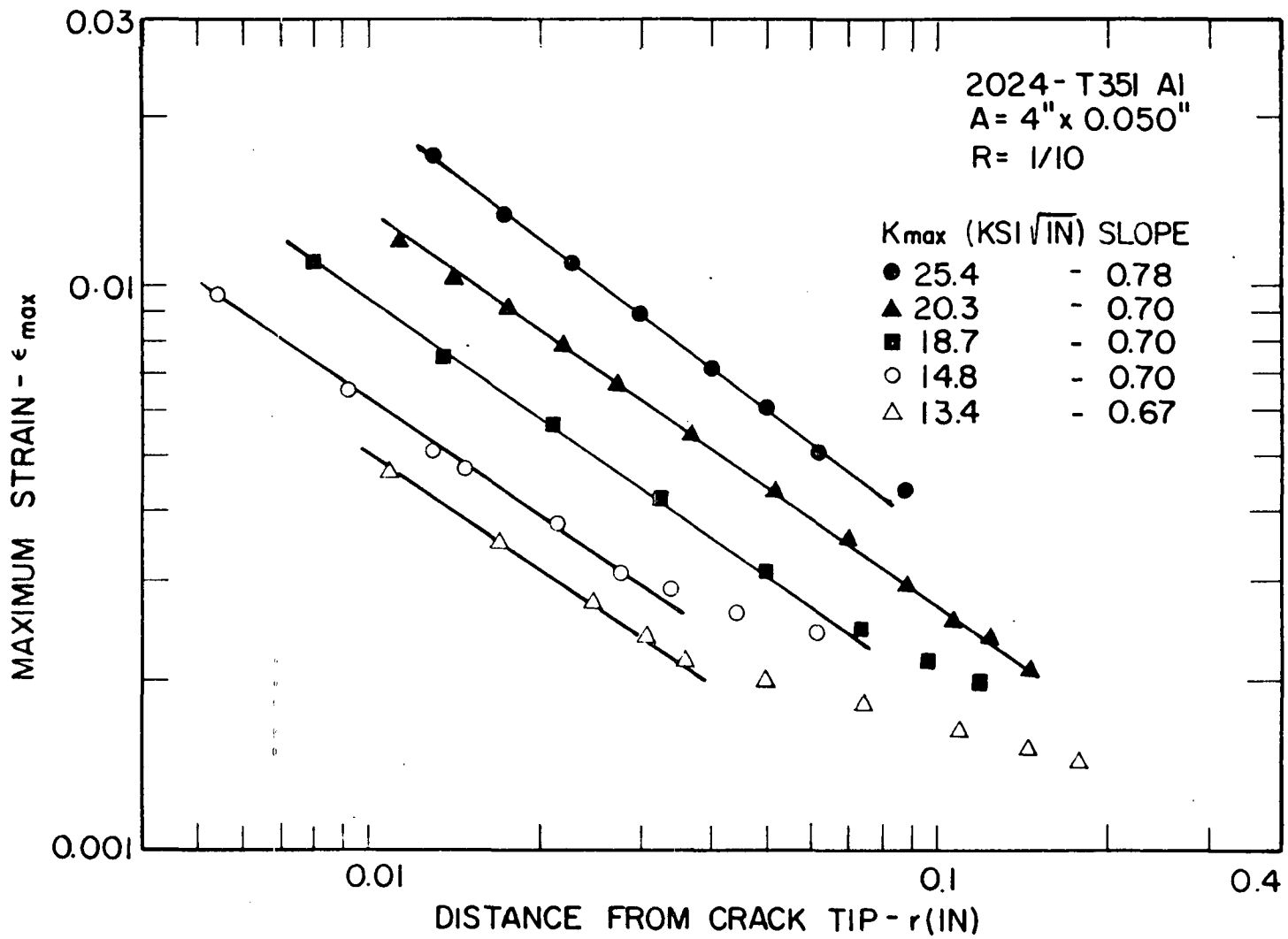

FIGURE 8b. MAXIMUM STRAIN DISTRIBUTION AHEAD OF A CRACK TIP FOR 0.050 INCHES THICK 2024-T351 ALUMINUM ALLOY AT R=1/10

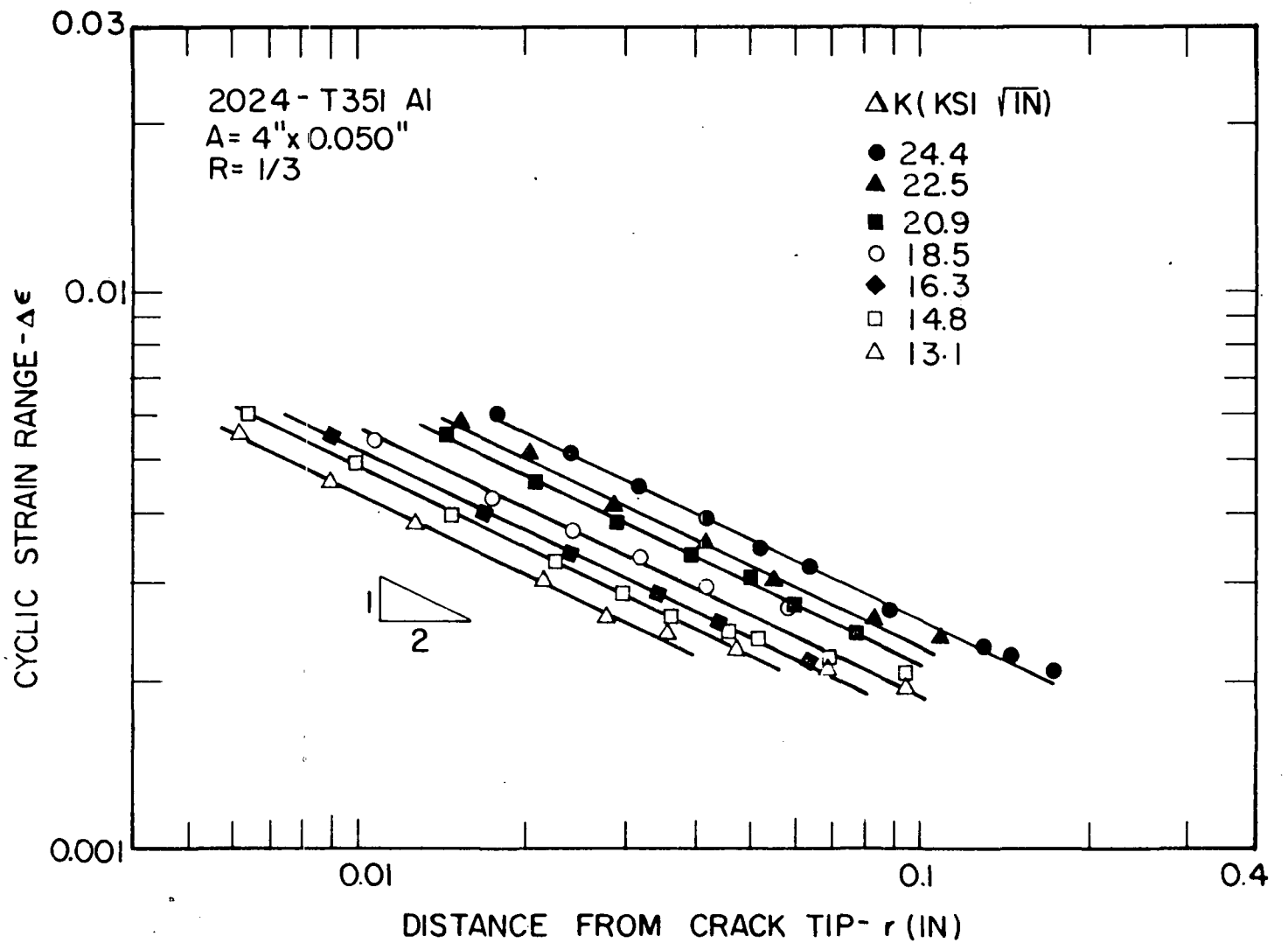

FIGURE 9a. STRAIN RANGE DISTRIBUTION AHEAD OF A CRACK TIP FOR 0.050 INCHES THICK 2024-T351 ALUMINUM ALLOY AT R=1/3

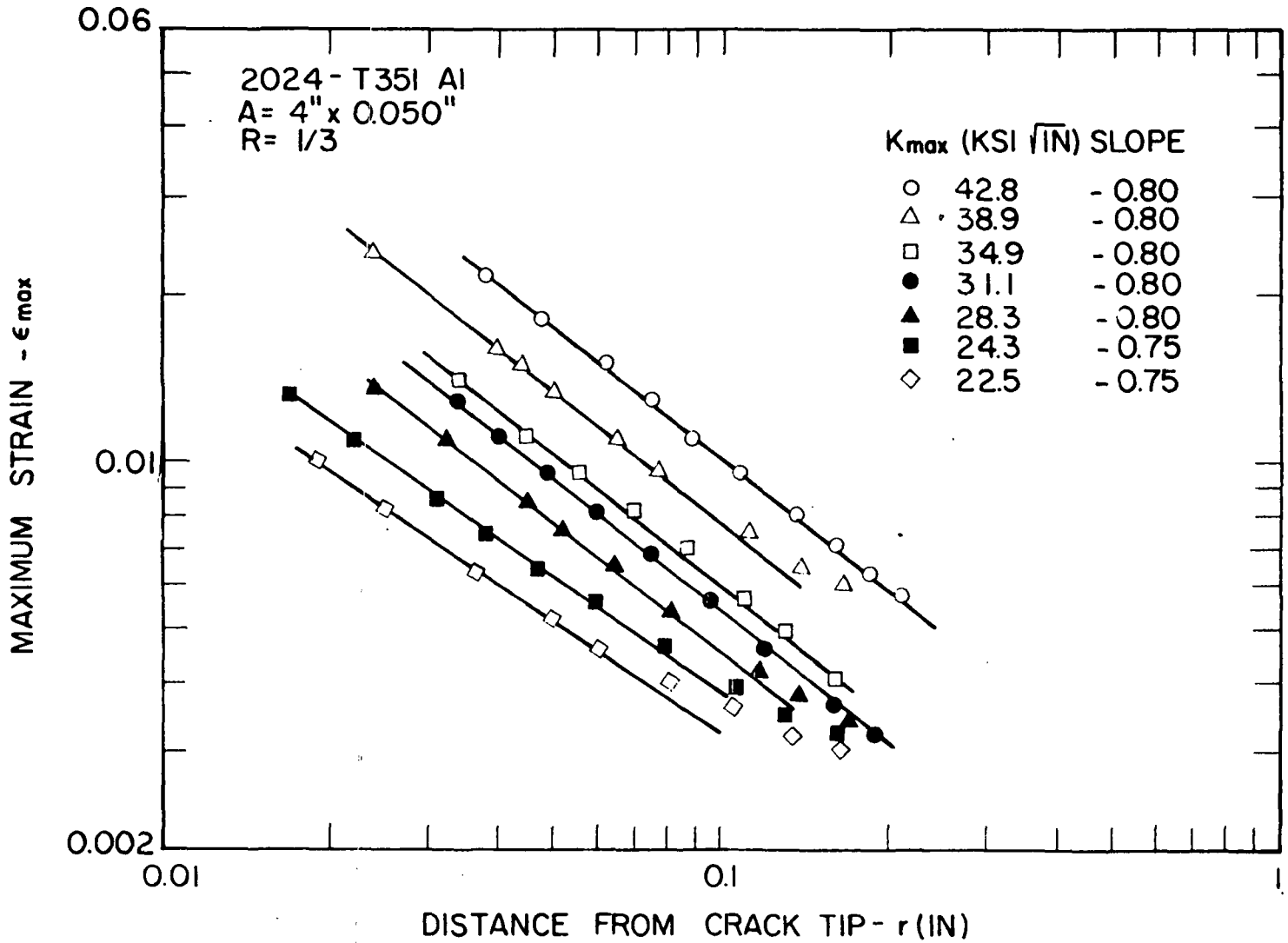

FIGURE 9b. MAXIMUM STRAIN DISTRIBUTION AHEAD OF A CRACK TIP FOR 0.050 INCHES THICK 2024-T351 ALUMINUM ALLOY AT R=1/3

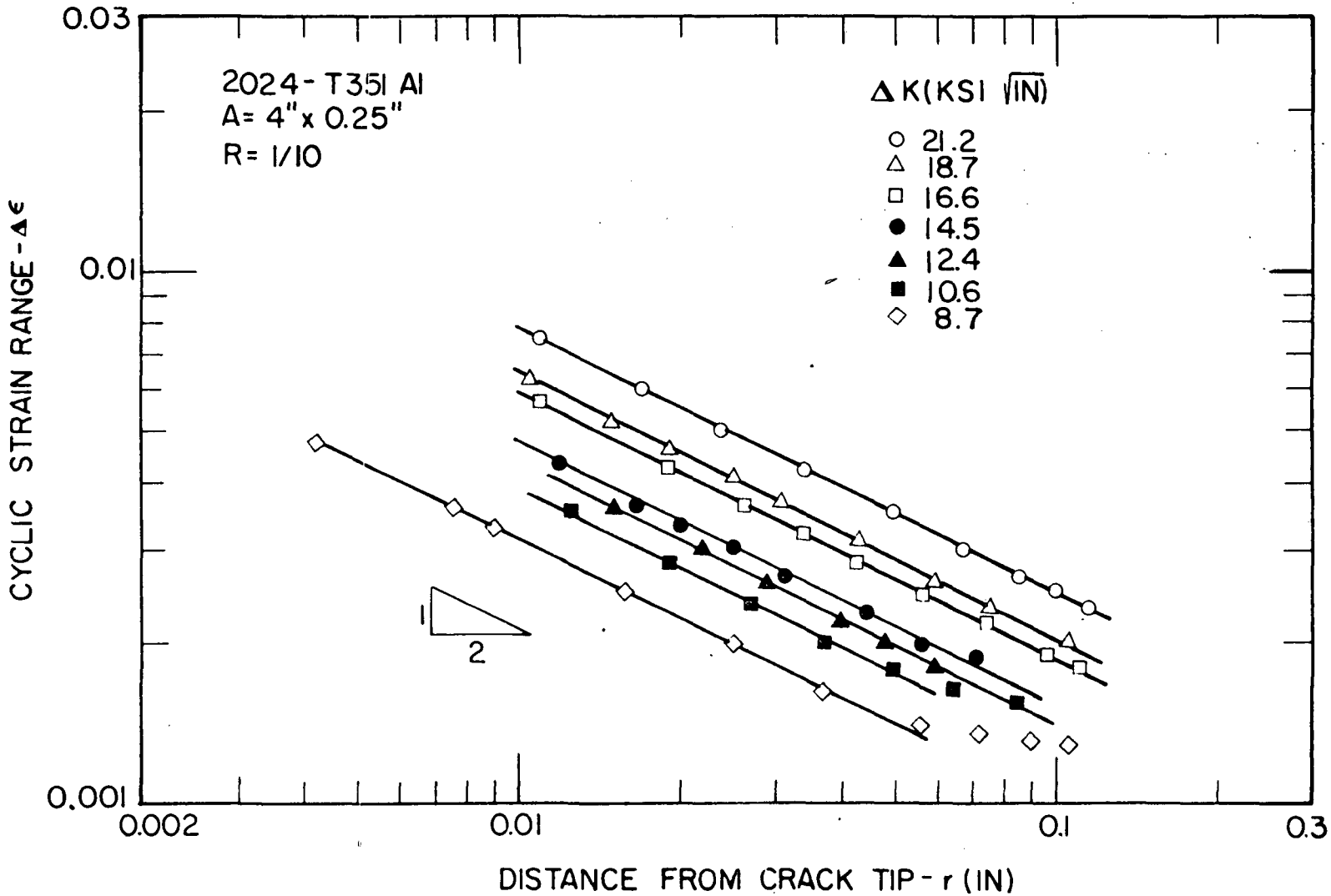

FIGURE 10a. STRAIN RANGE DISTRIBUTION AHEAD OF A CRACK TIP FOR 0.25 INCHES THICK 2024-T351 ALUMINUM ALLOY AT R=1/10

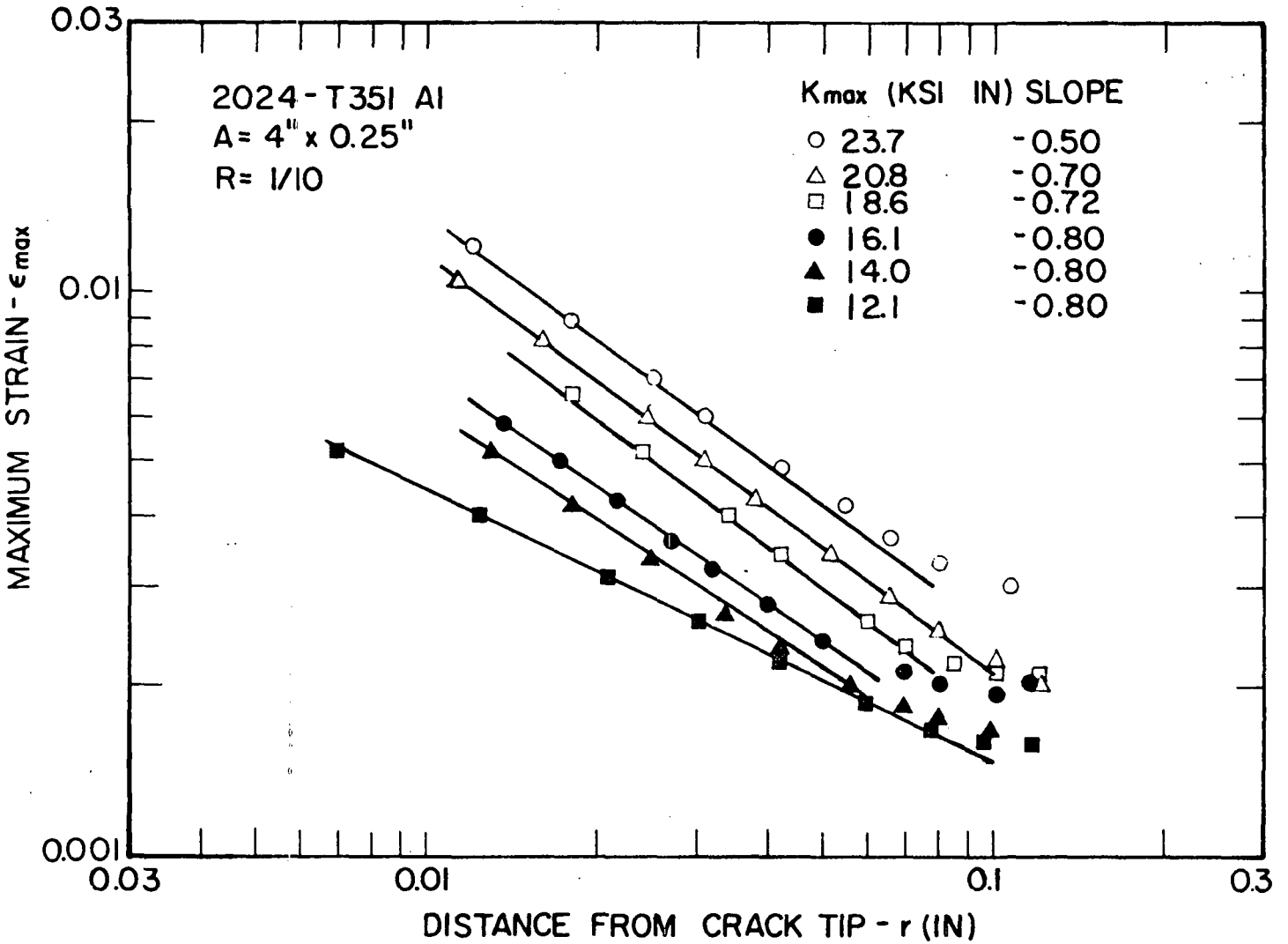

FIGURE 10b. MAXIMUM STRAIN DISTRIBUTION AHEAD OF A CRACK TIP FOR 0.25 INCHES THICK 2024-T351 ALUMINUM ALLOY AT R=1/10

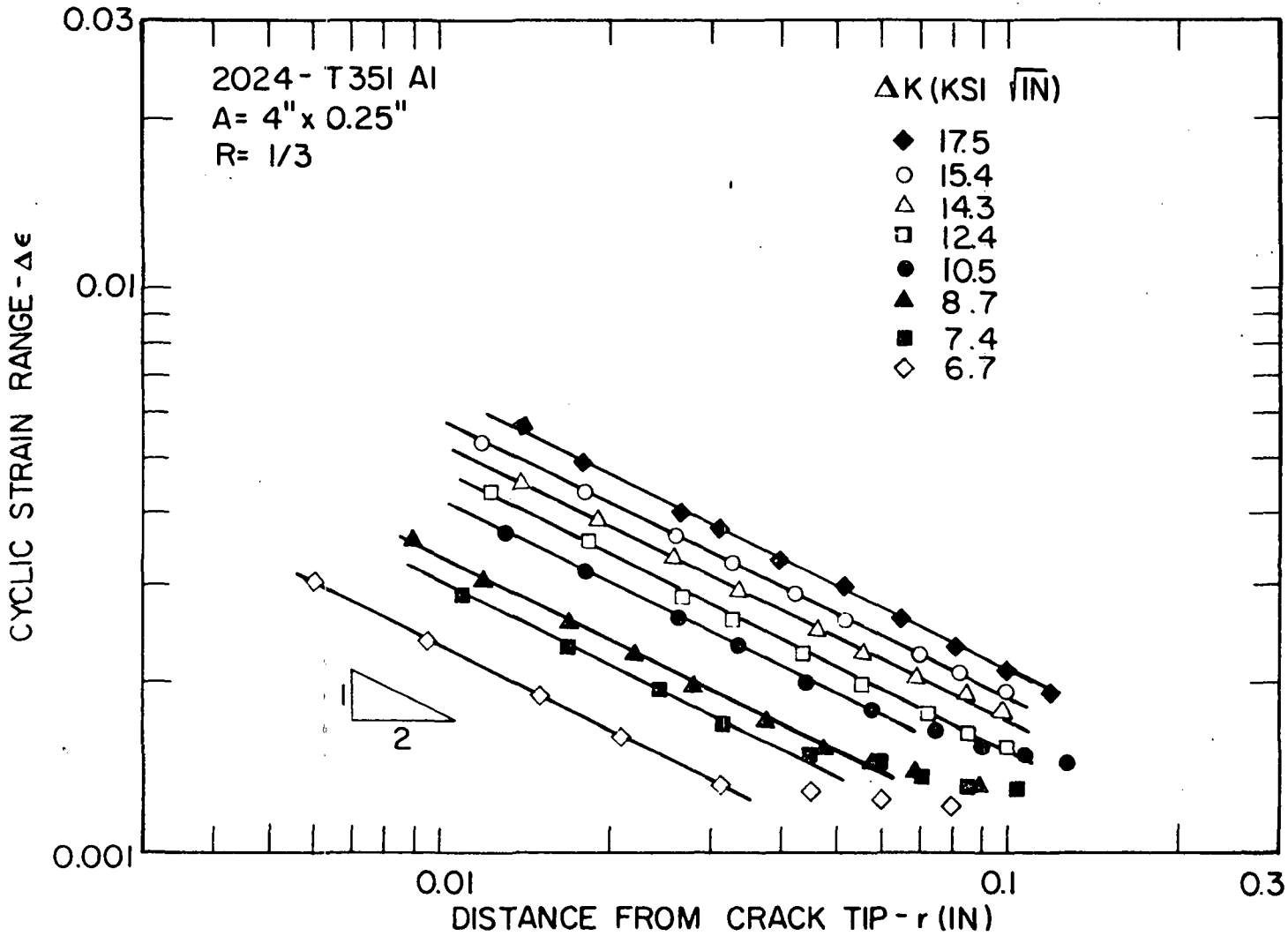

FIGURE 11a. STRAIN RANGE DISTRIBUTION AHEAD OF A CRACK TIP FOR 0.25 INCHES THICK 2024-T351 ALUMINUM ALLOY AT R=1/3

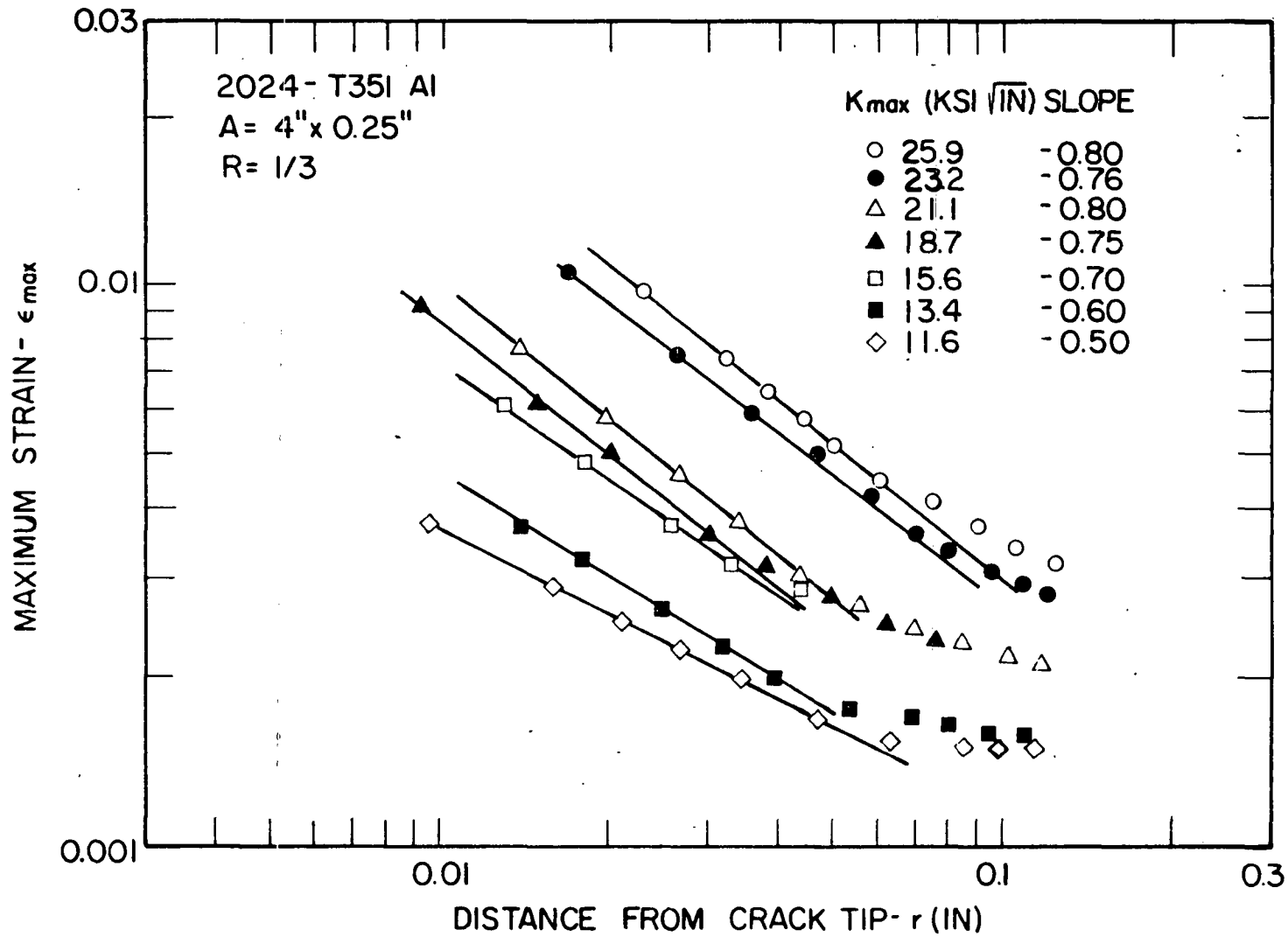

FIGURE 11b. MAXIMUM STRAIN DISTRIBUTION AHEAD OF A CRACK TIP FOR 0.25 INCHES THICK 2024-T351 ALUMINUM ALLOY AT R=1/3

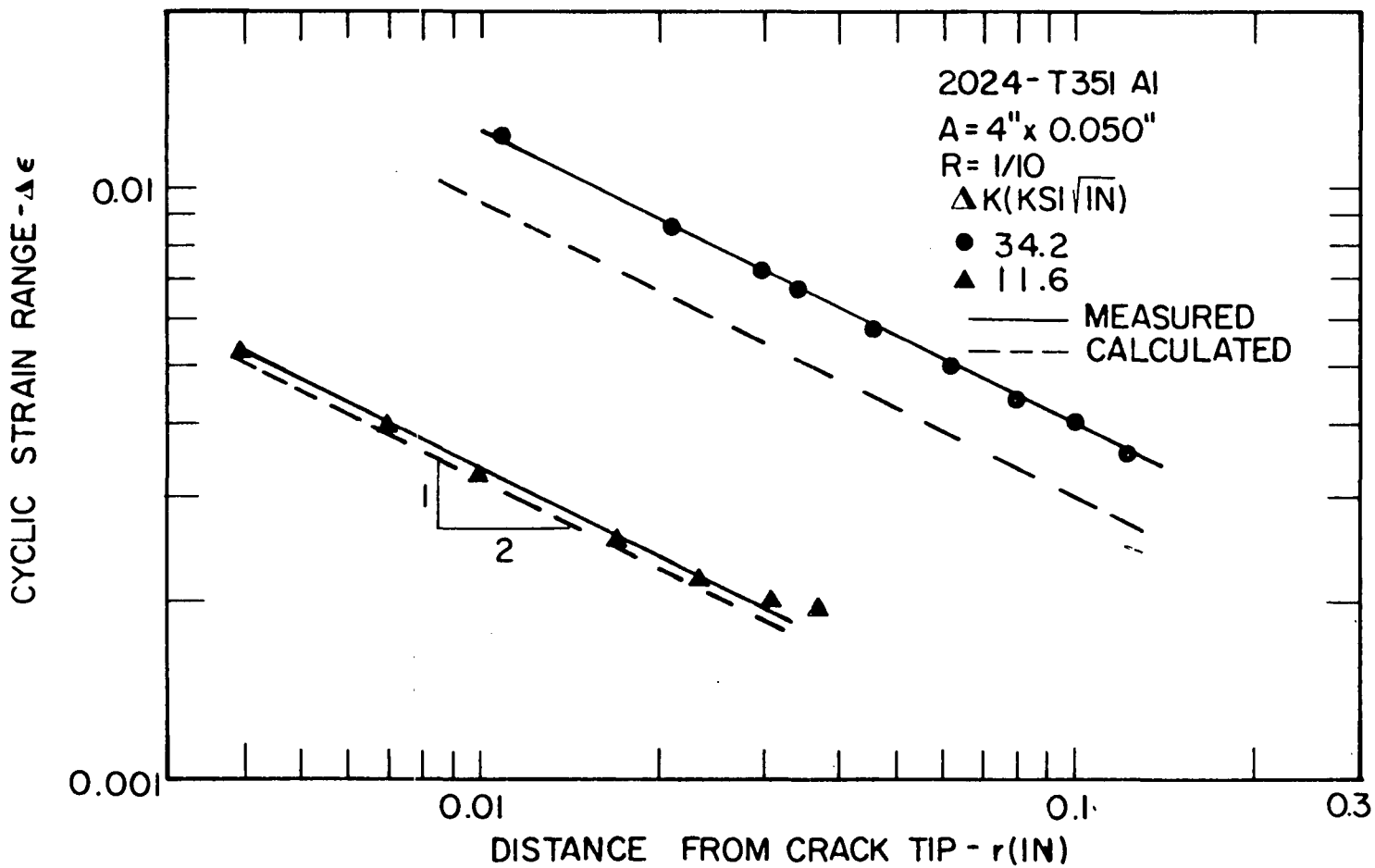

FIGURE 12. COMPARISON OF THE CALCULATED AND MEASURED STRAIN RANGE DISTRIBUTION AHEAD OF A CRACK TIP FOR 0.050 INCHES THICK 2024-T351 ALUMINUM ALLOY AT R=1/10

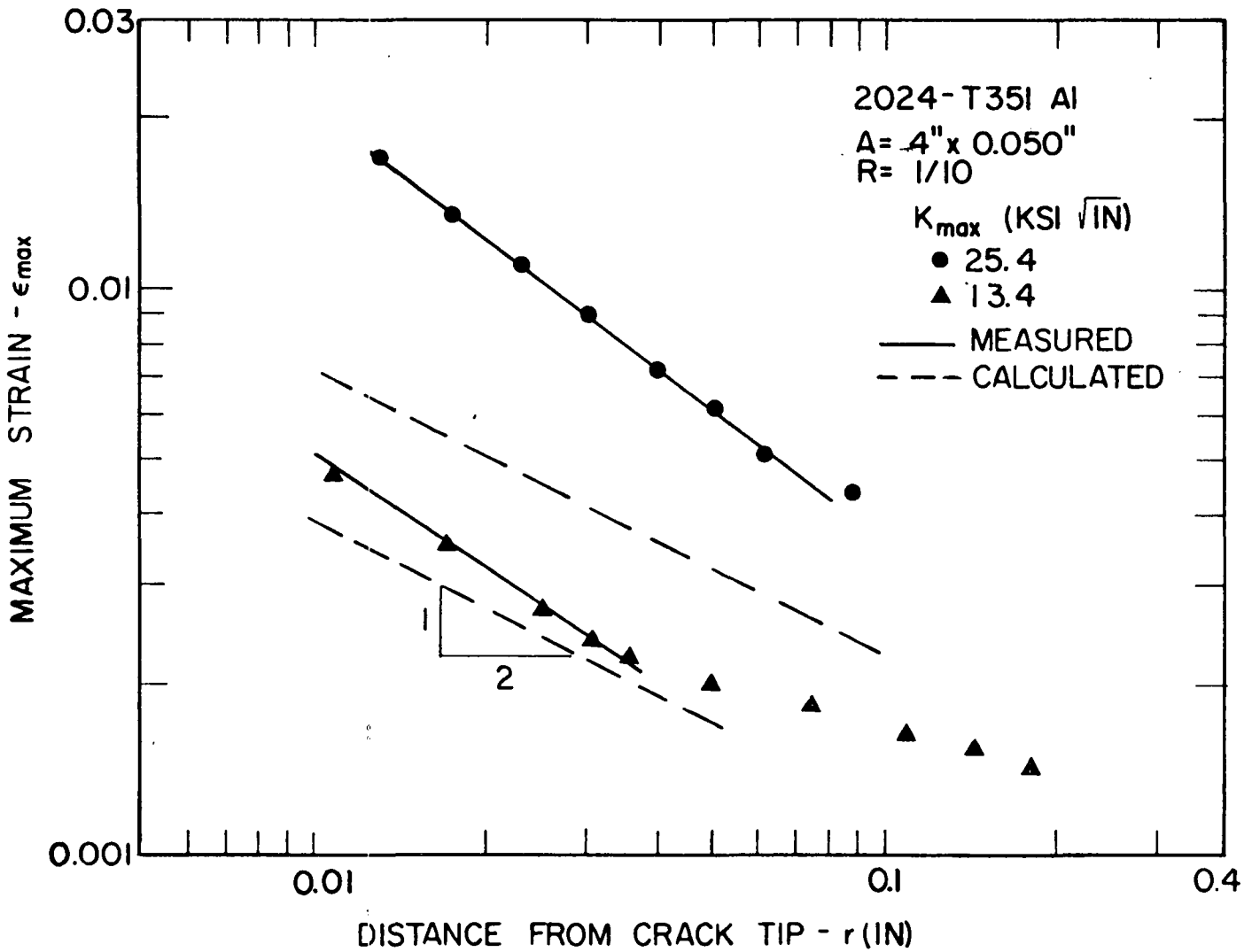

FIGURE 13. COMPARISON OF THE CALCULATED AND MEASURED MAXIMUM STRAIN DISTRIBUTION AHEAD OF A CRACK TIP FOR 0.050 INCHES THICK 2024-T351 ALUMINUM ALLOY AT R=1/10

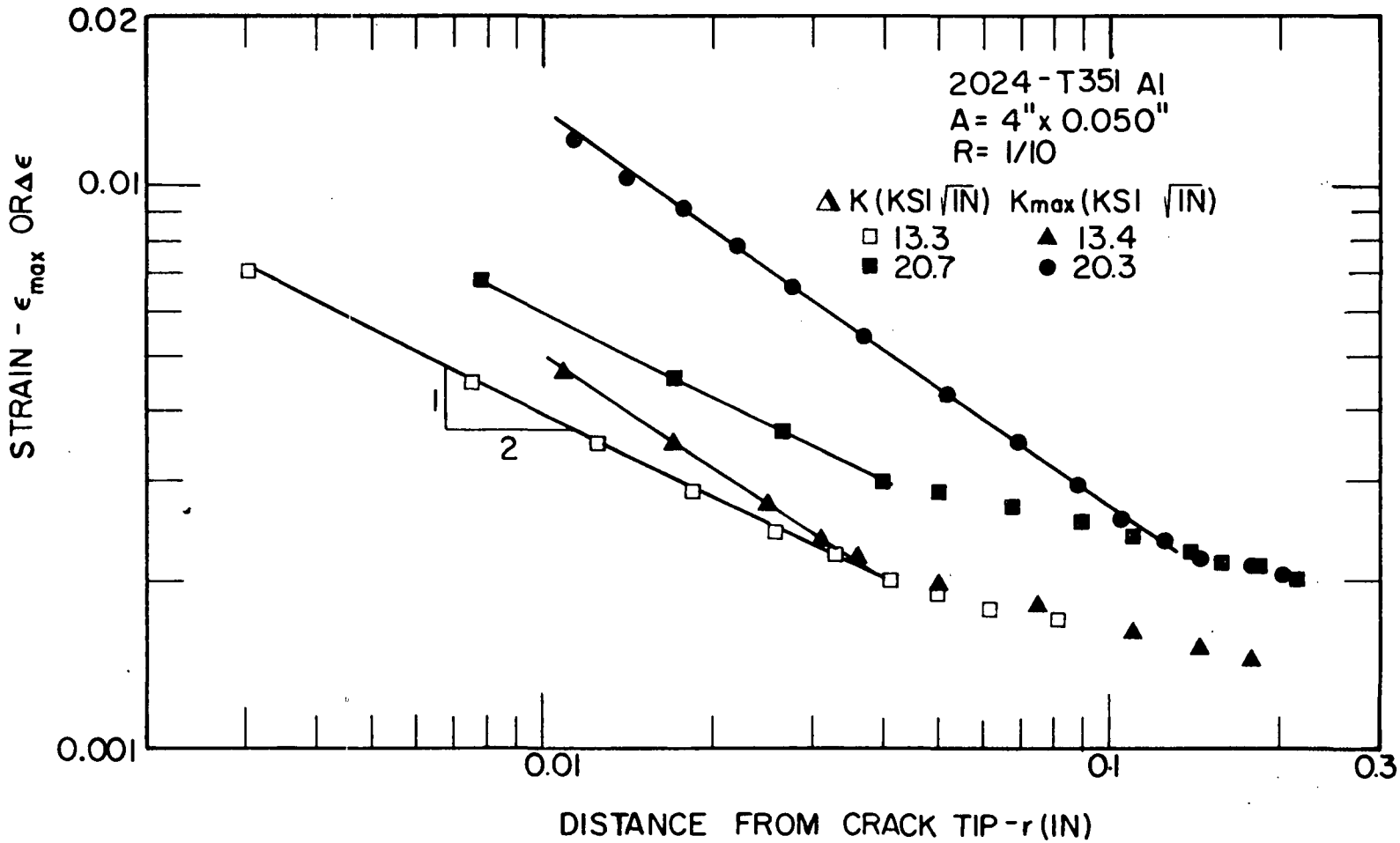

FIGURE 14. COMPARISON OF $\Delta\epsilon$ and ϵ_{max} DISTRIBUTION AHEAD OF A CRACK TIP FOR 0.050 INCHES THICK 2024-T351 ALUMINUM ALLOY AT R=1/10 FOR A SAME K VALUE

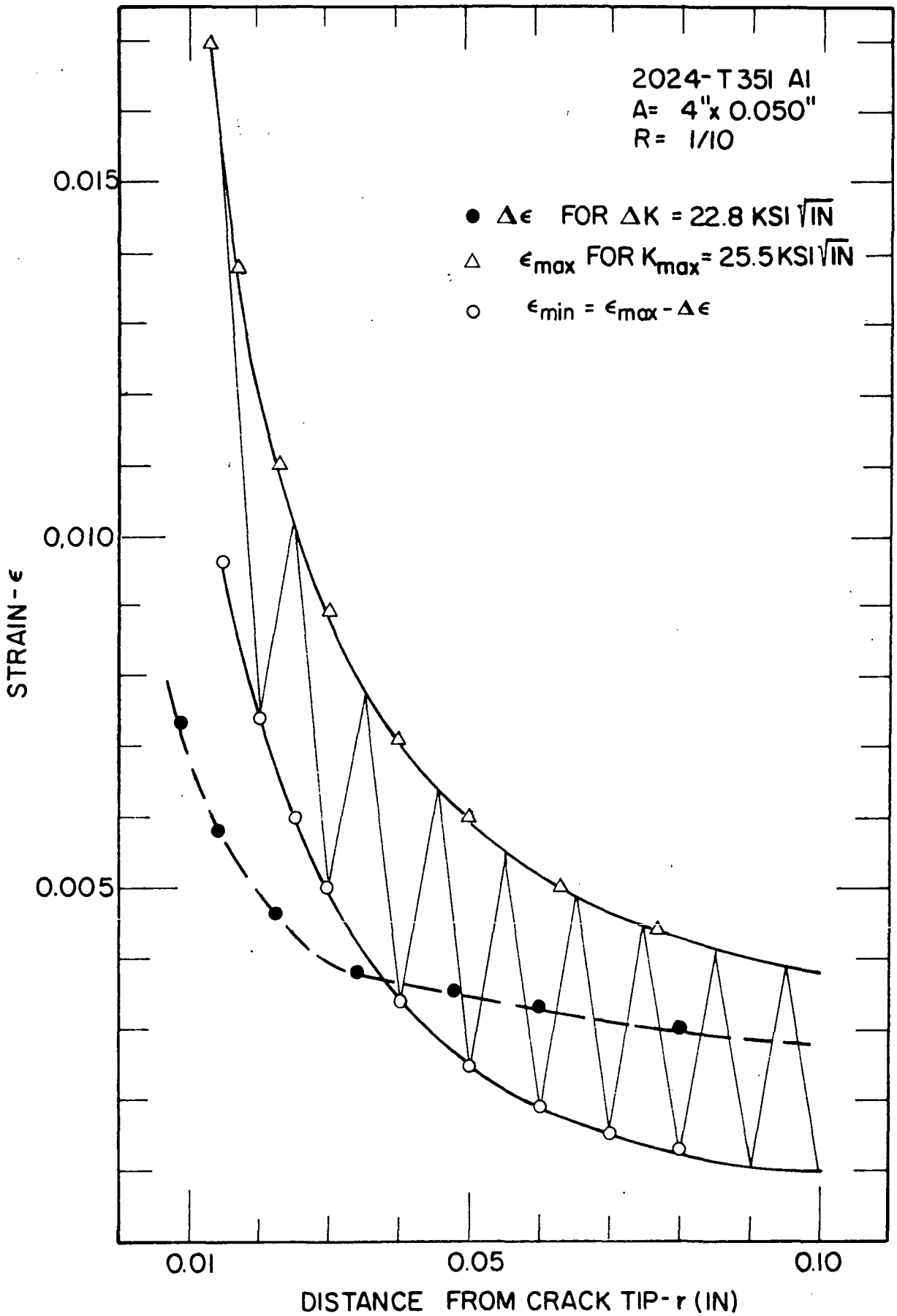

FIGURE 15. ϵ_{max}, ϵ_{min} and $\Delta\epsilon$ AHEAD OF A CRACK TIP FOR 0.050 INCHES THICK 2024-T351 ALUMINUM ALLOY AT R=1/10

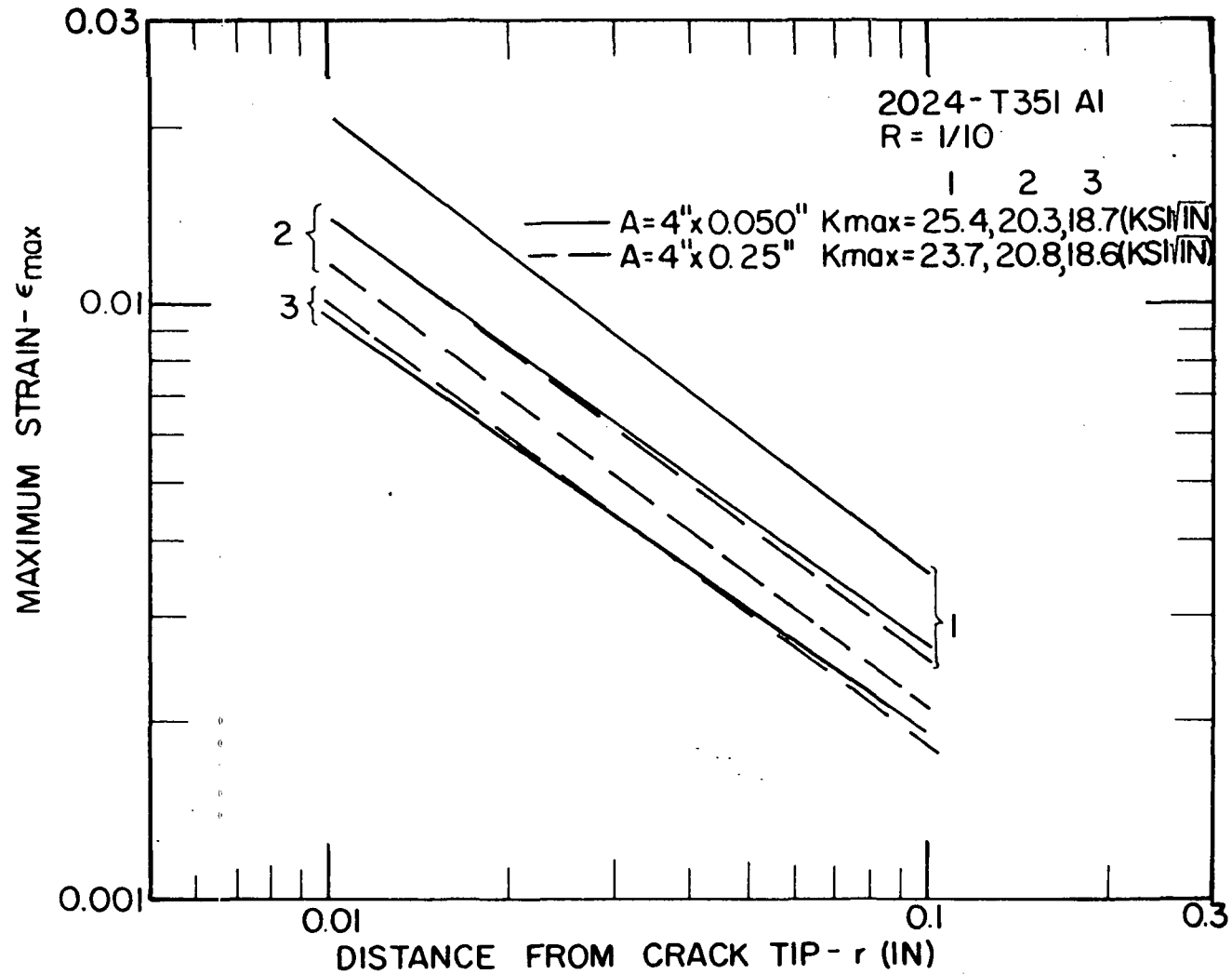

FIGURE 16. COMPARISON OF ϵ_{max} DISTRIBUTION AHEAD OF A CRACK TIP FOR 0.25 INCHES AND 0.050 INCHES THICK 2024-T351 ALUMINUM ALLOY AT R=1/10

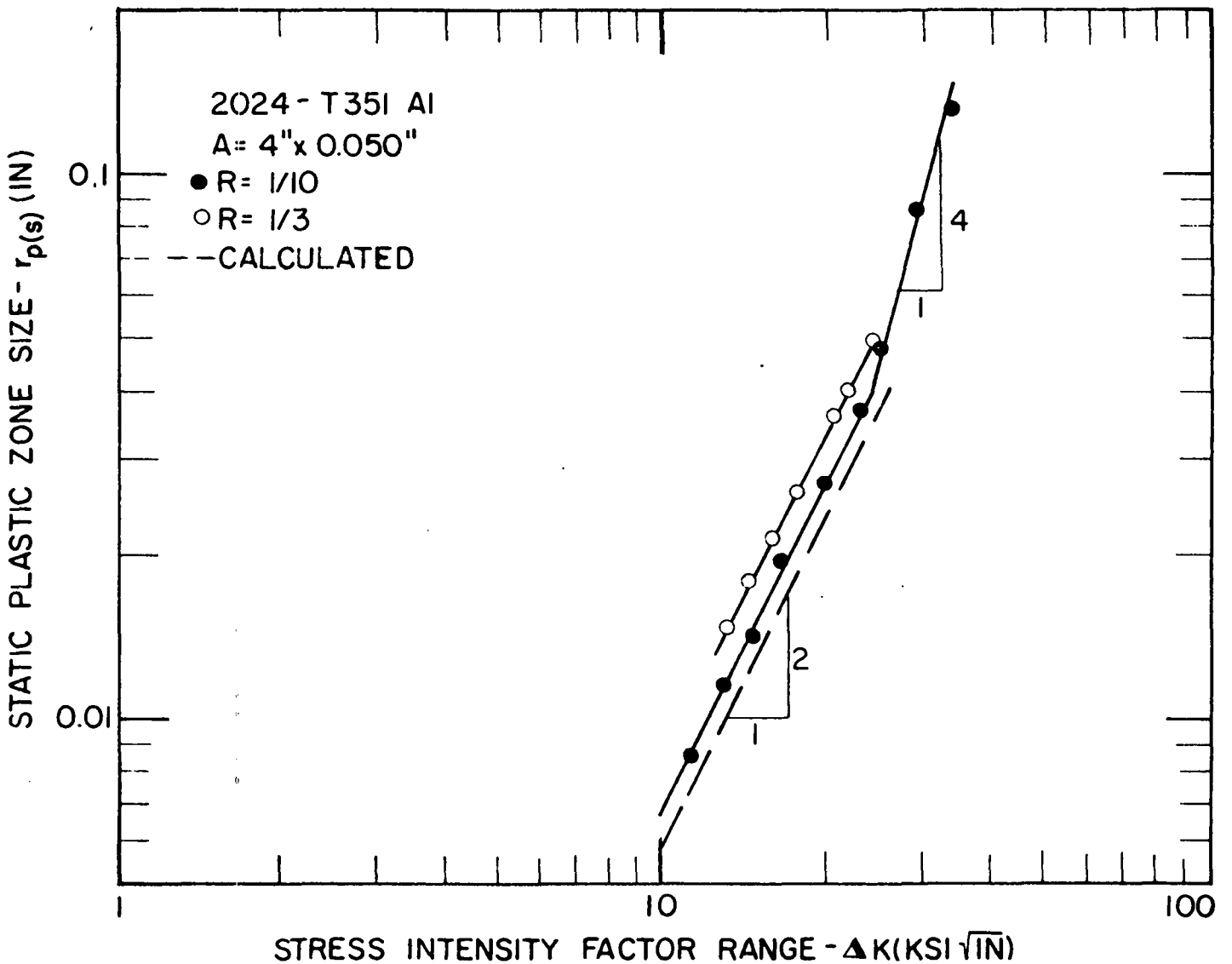

FIGURE 17a. STATIC PLASTIC ZONE SIZE VERSUS STRESS INTENSITY FACTOR RANGE FOR 0.050 INCHES THICK 2024-T351 ALUMINUM ALLOY

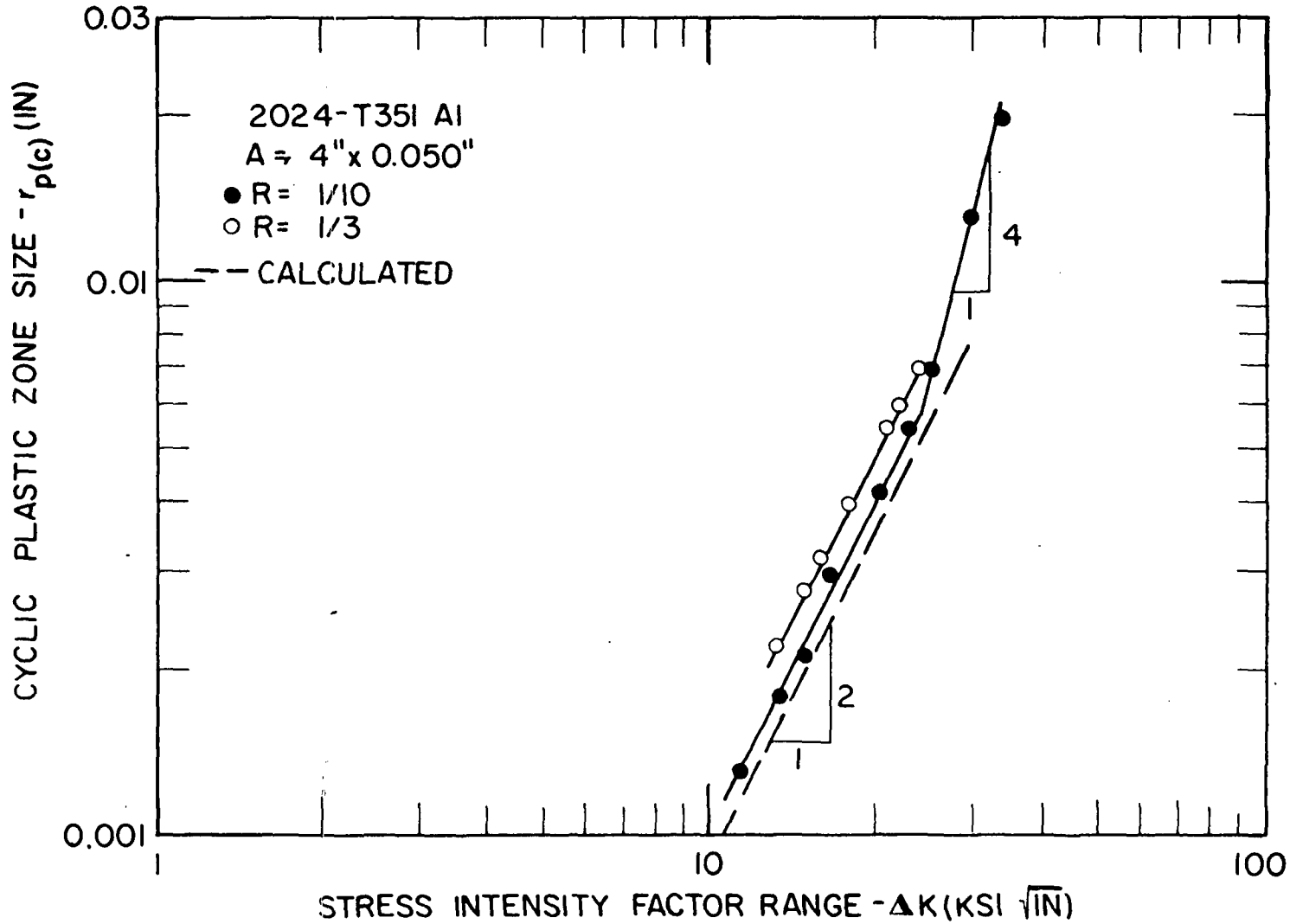

FIGURE 17b. CYCLIC PLASTIC ZONE SIZE VERSUS STRESS INTENSITY FACTOR RANGE FOR 0.050 INCHES THICK 2024-T351 ALUMINUM ALLOY

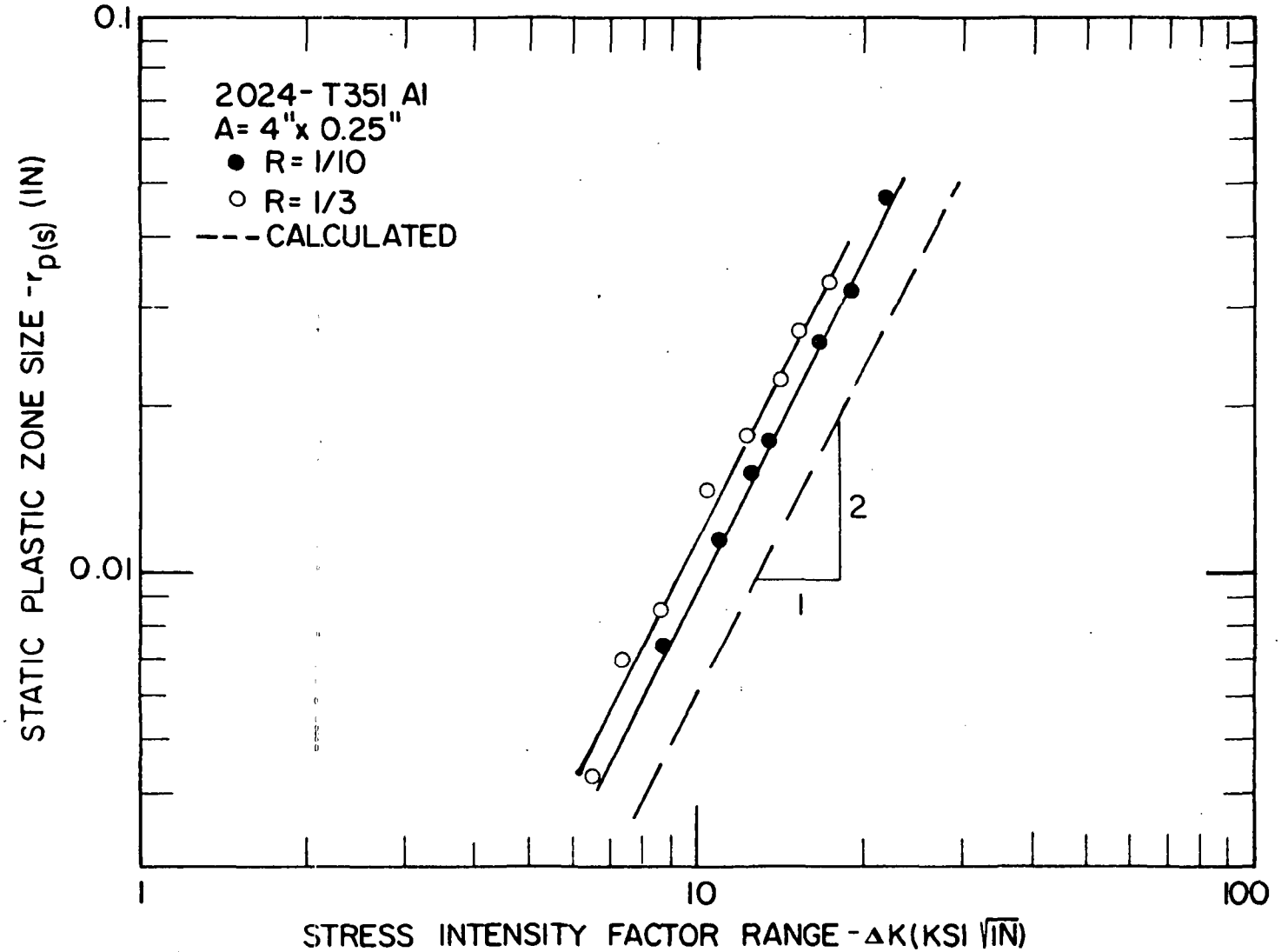

FIGURE 18. STATIC PLASTIC ZONE SIZE VERSUS STRESS INTENSITY FACTOR RANGE FOR 0.25 INCHES THICK 2024-T351 ALUMINUM ALLOY

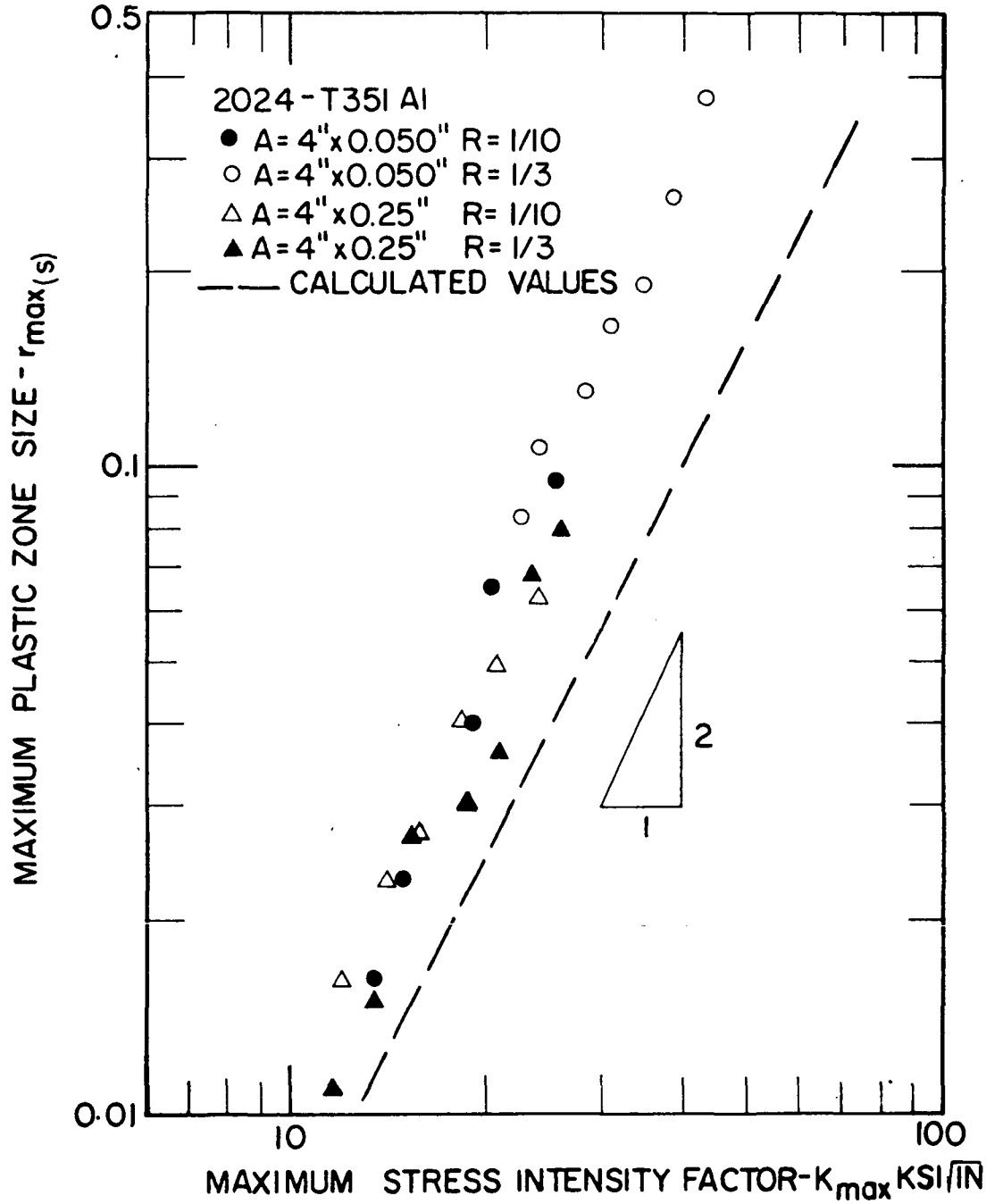

FIGURE 19. MAXIMUM STATIC PLASTIC ZONE SIZE VERSUS THE MAXIMUM STRESS INTENSITY FACTOR FOR 2024-T351 ALUMINUM ALLOY

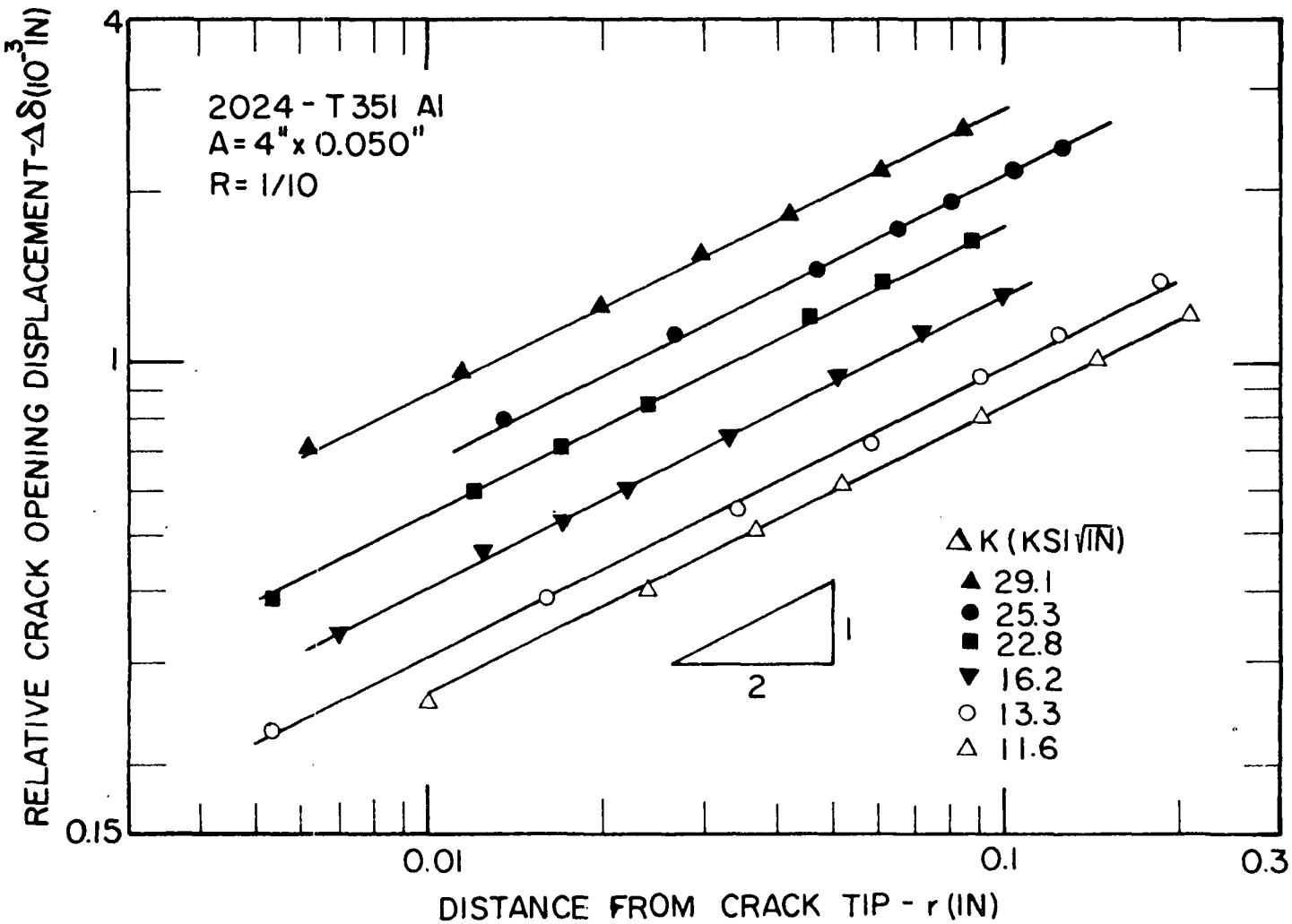

FIGURE 20a. RELATIVE CRACK OPENING DISPLACEMENT RANGE VERSUS THE DISTANCE FROM A CRACK TIP FOR 0.050 INCHES THICK 2024-T351 ALUMINUM ALLOY AT R=1/10

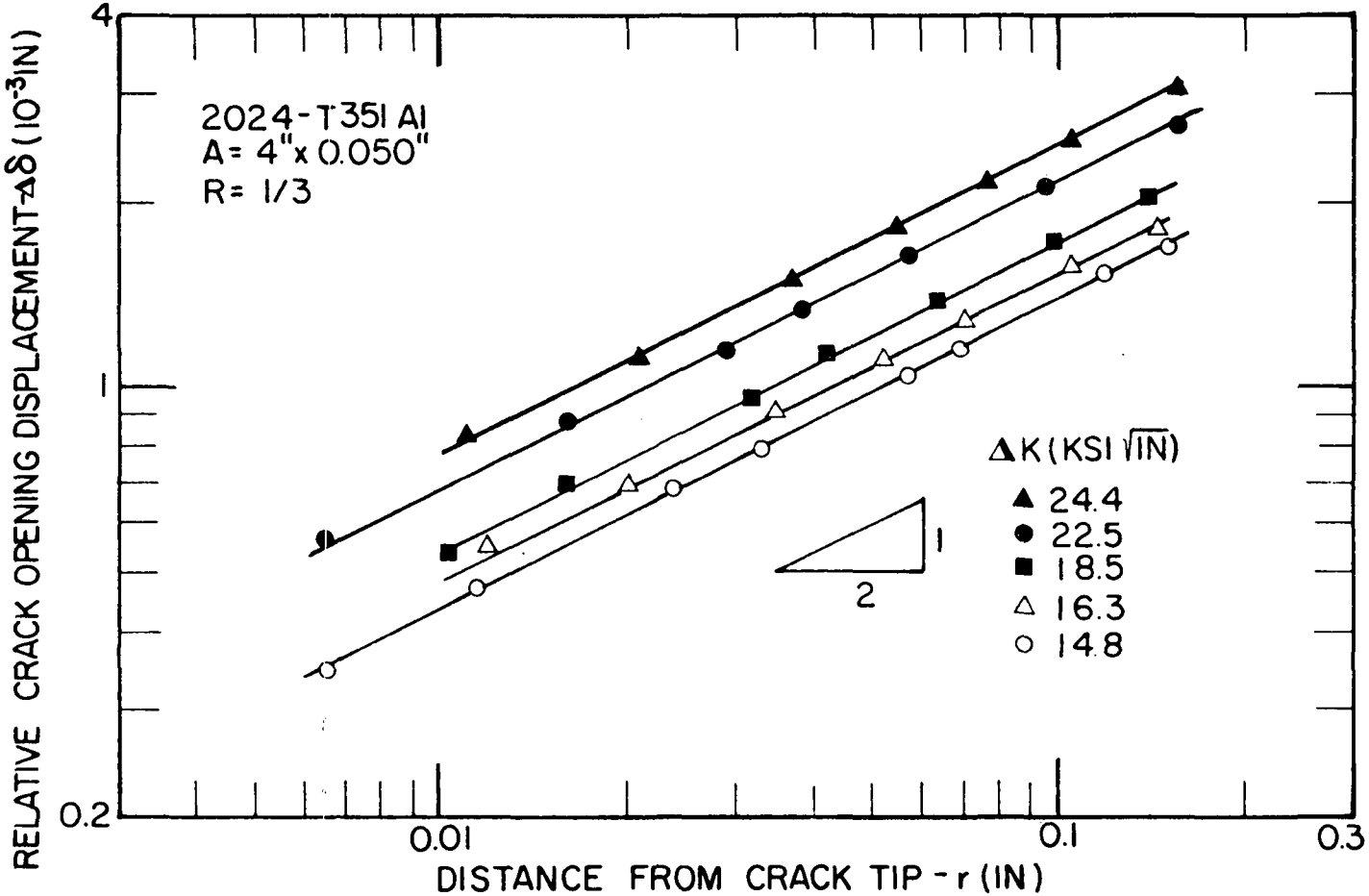

FIGURE 20b. RELATIVE CRACK OPENING DISPLACEMENT RANGE VERSUS THE DISTANCE FROM A CRACK TIP FOR 0.050 INCHES THICK 2024-T351 ALUMIMUM ALLOY AT R=1/3

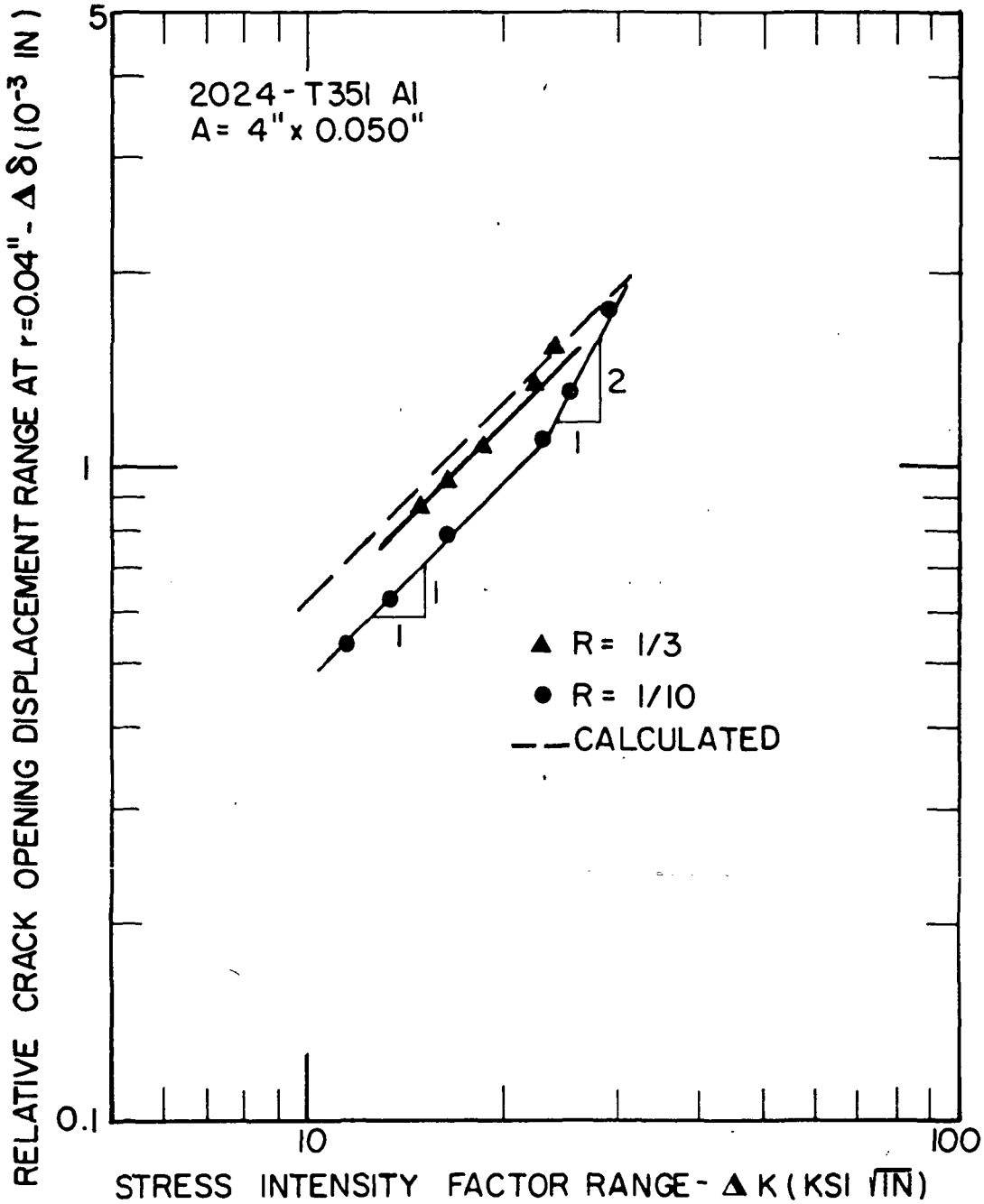

FIGURE 20c. RELATIVE CRACK OPENING DISPLACEMENT RANGE AT r=0.04 INCHES VERSUS STRESS INTENSITY FACTOR RANGE FOR 0.050 INCHES THICK 2024-T351 ALUMINUM ALLOY

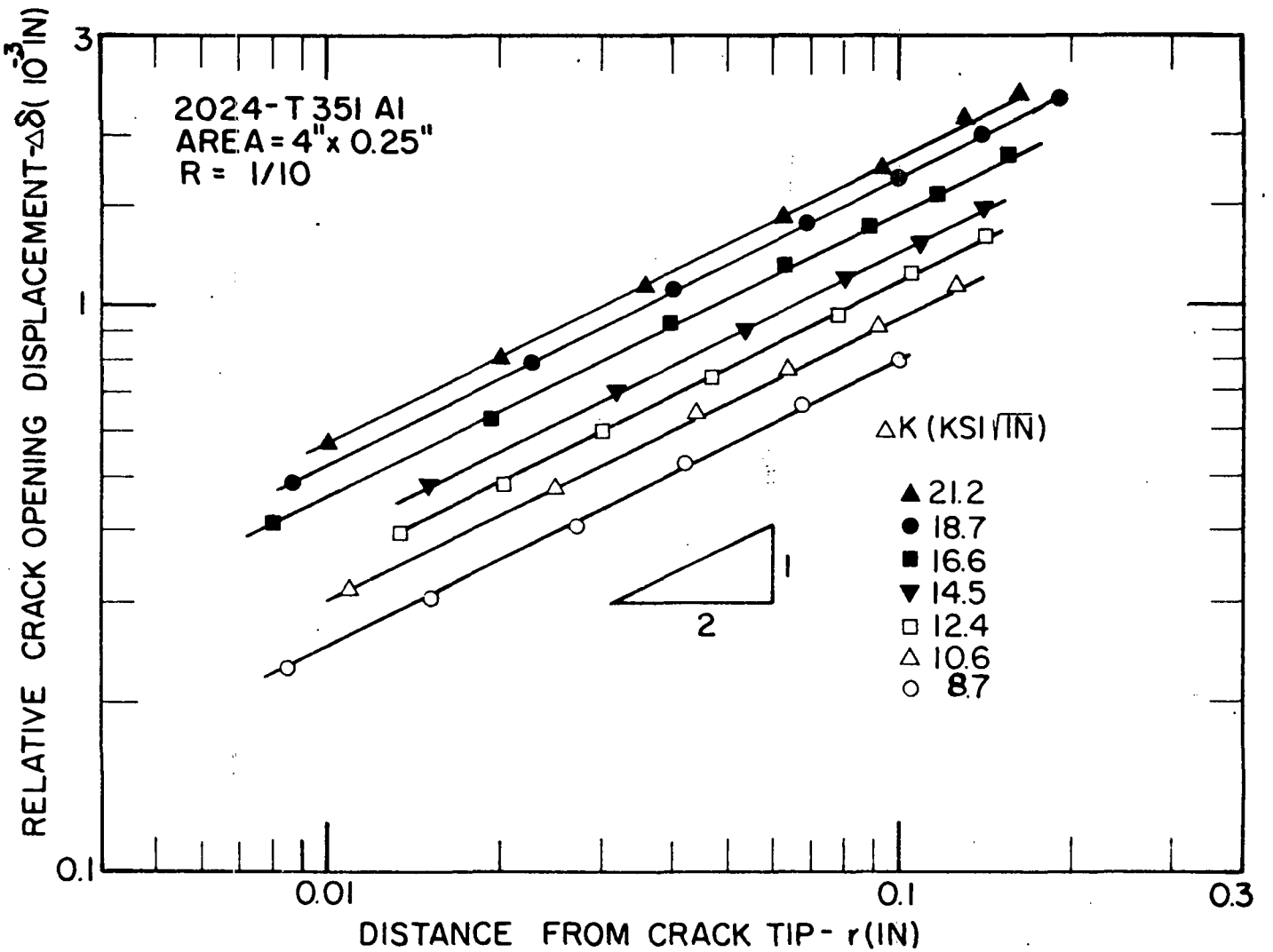

FIGURE 20d. RELATIVE CRACK OPENING DISPLACEMENT RANGE VERSUS THE DISTANCE FROM A CRACK TIP FOR 0.25 INCHES THICK 2024-T351 ALUMINUM ALLOY AT R=1/10

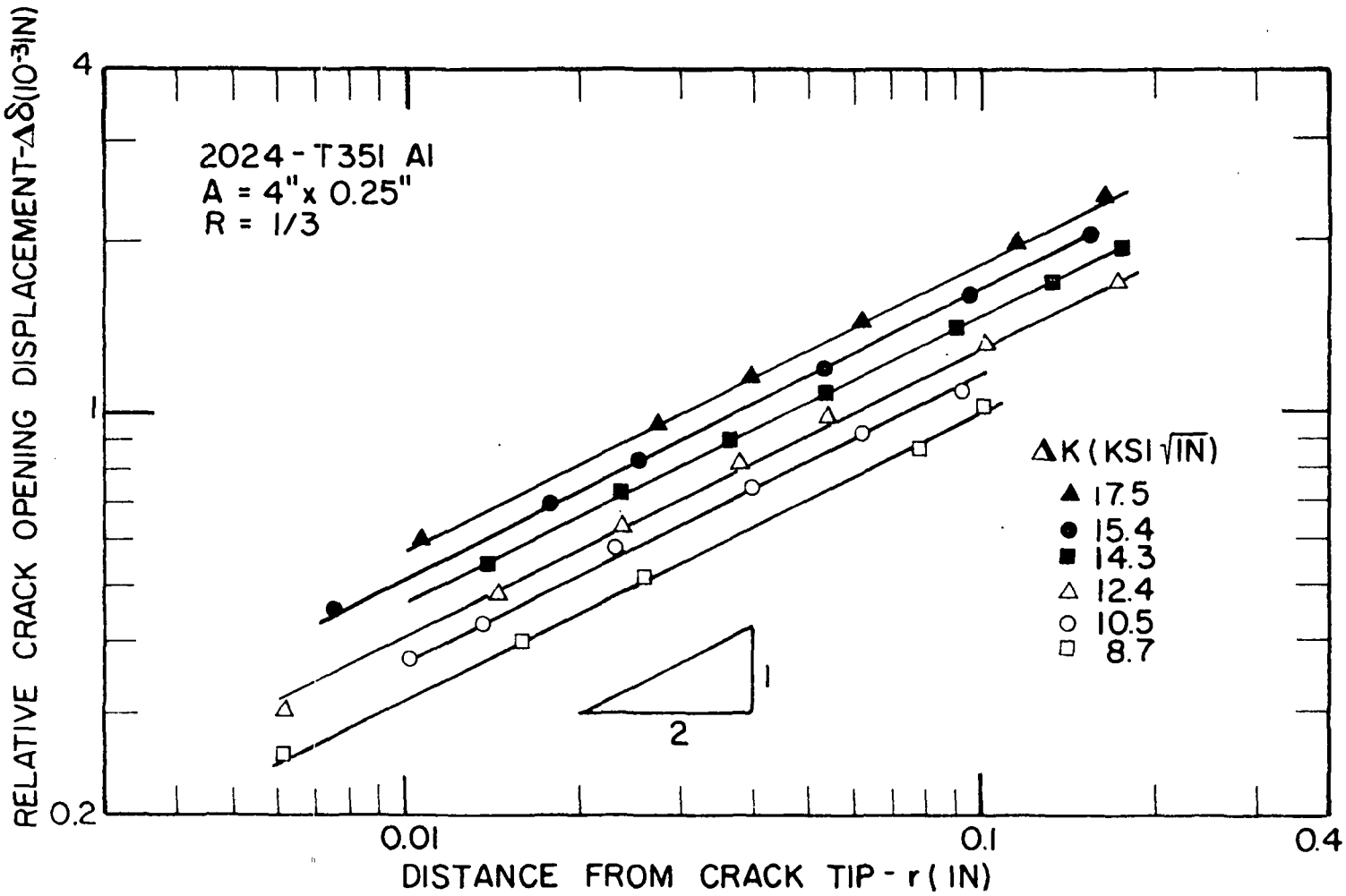

FIGURE 20e. RELATIVE CRACK OPENING DISPLACEMENT RANGE VERSUS THE DISTANCE FROM A CRACK TIP FOR 0.25 INCHES THICK 2024-T351 ALUMINUM ALLOY AT R=1/3

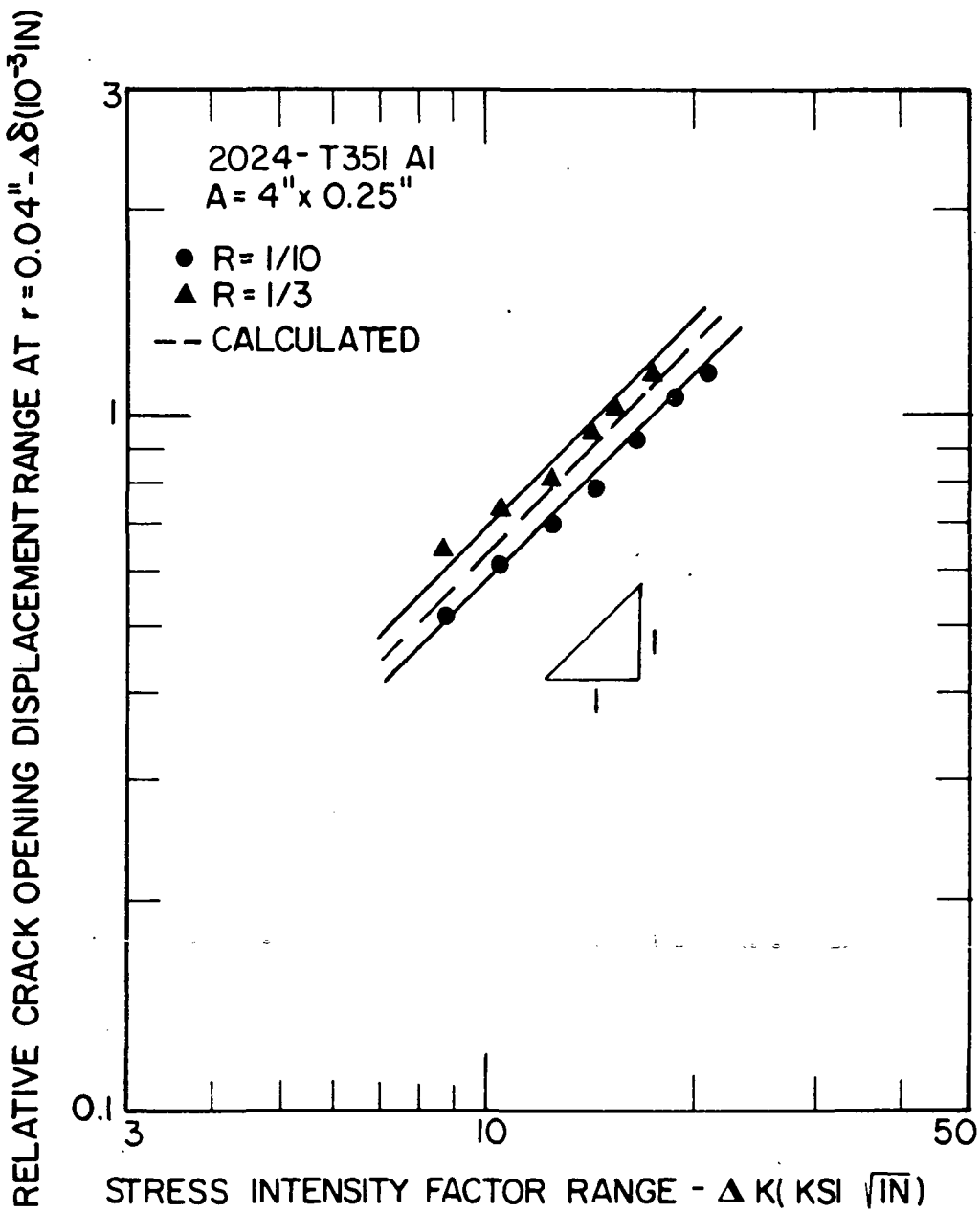

FIGURE 20f. RELATIVE CRACK OPENING DISPLACEMENT RANGE AT r=0.04 INCHES VERSUS THE STRESS INTENSITY FACTOR RANGE FOR 0.25 INCHES THICK 2024-T351 ALUMINUM ALLOY

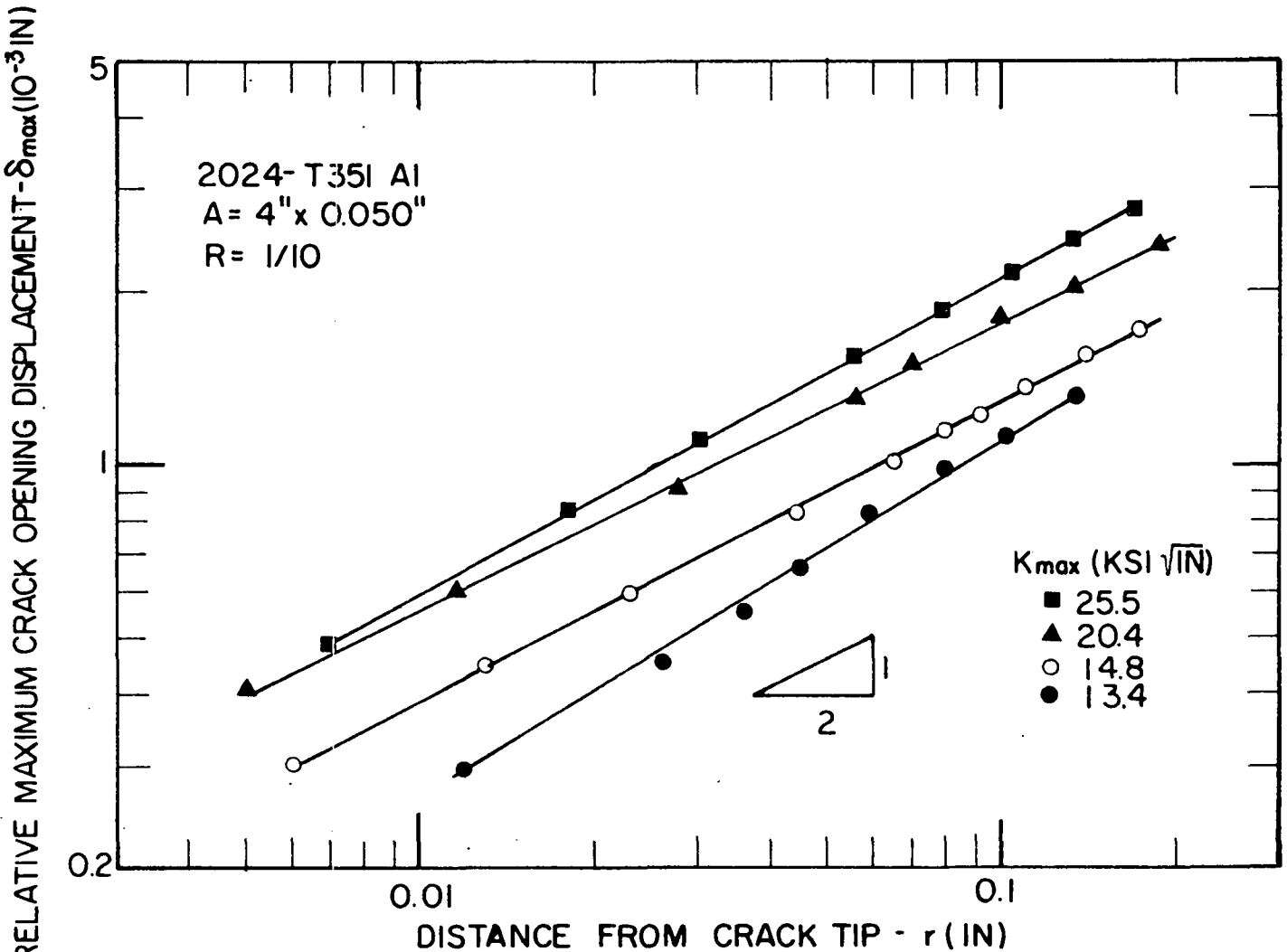

FIGURE 21a. RELATIVE MAXIMUM CRACK OPENING DISPLACEMENT VERSUS THE DISTANCE FROM A CRACK TIP FOR 0.050 INCHES THICK 2024-T351 ALUMINUM ALLOY AT R=1/10

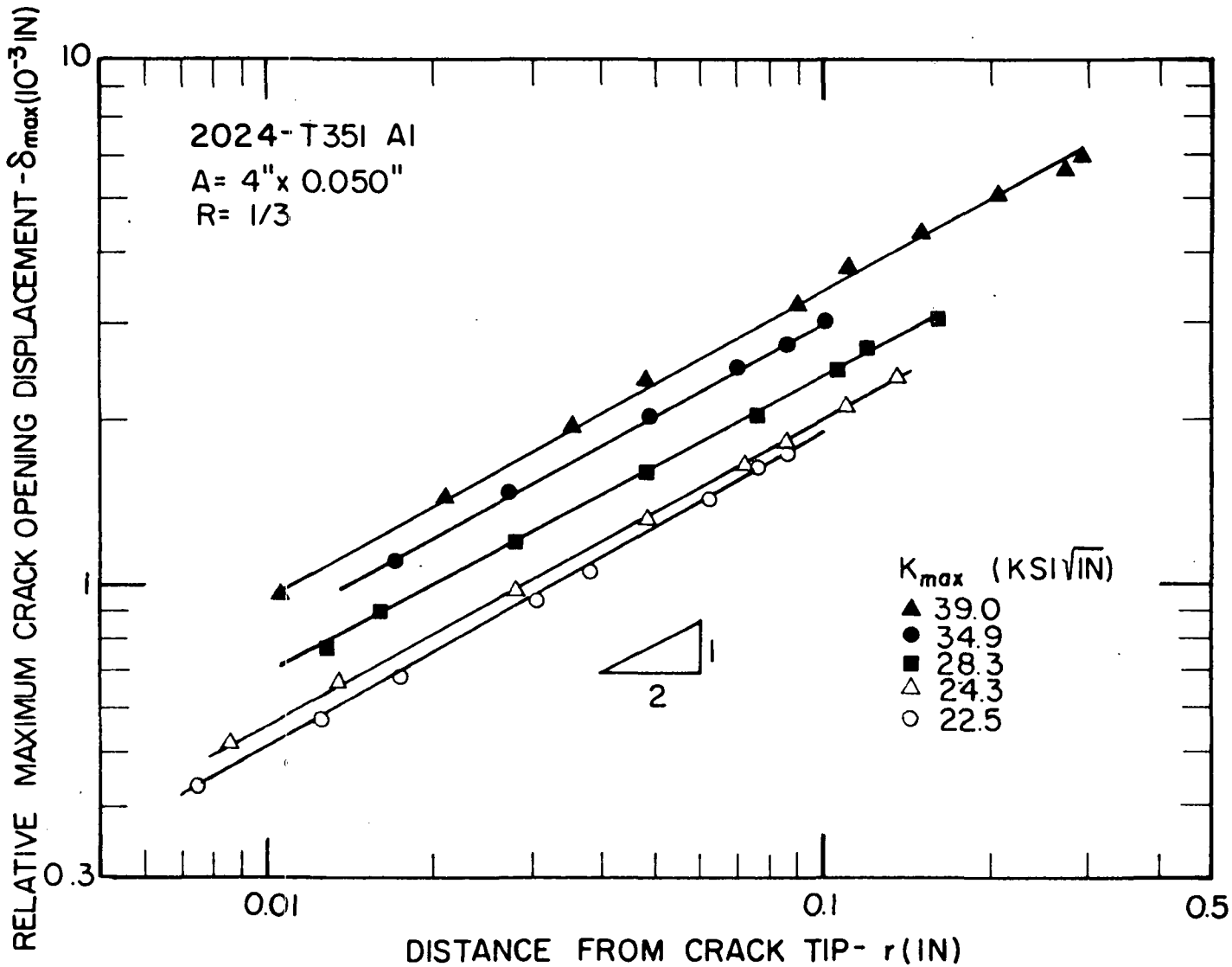

FIGURE 21b. RELATIVE MAXIMUM CRACK OPENING DISPLACEMENT VERSUS THE DISTANCE FROM A CRACK TIP FOR 0.050 INCHES THICK 2024-T351 ALUMINUM ALLOY AT R=1/3

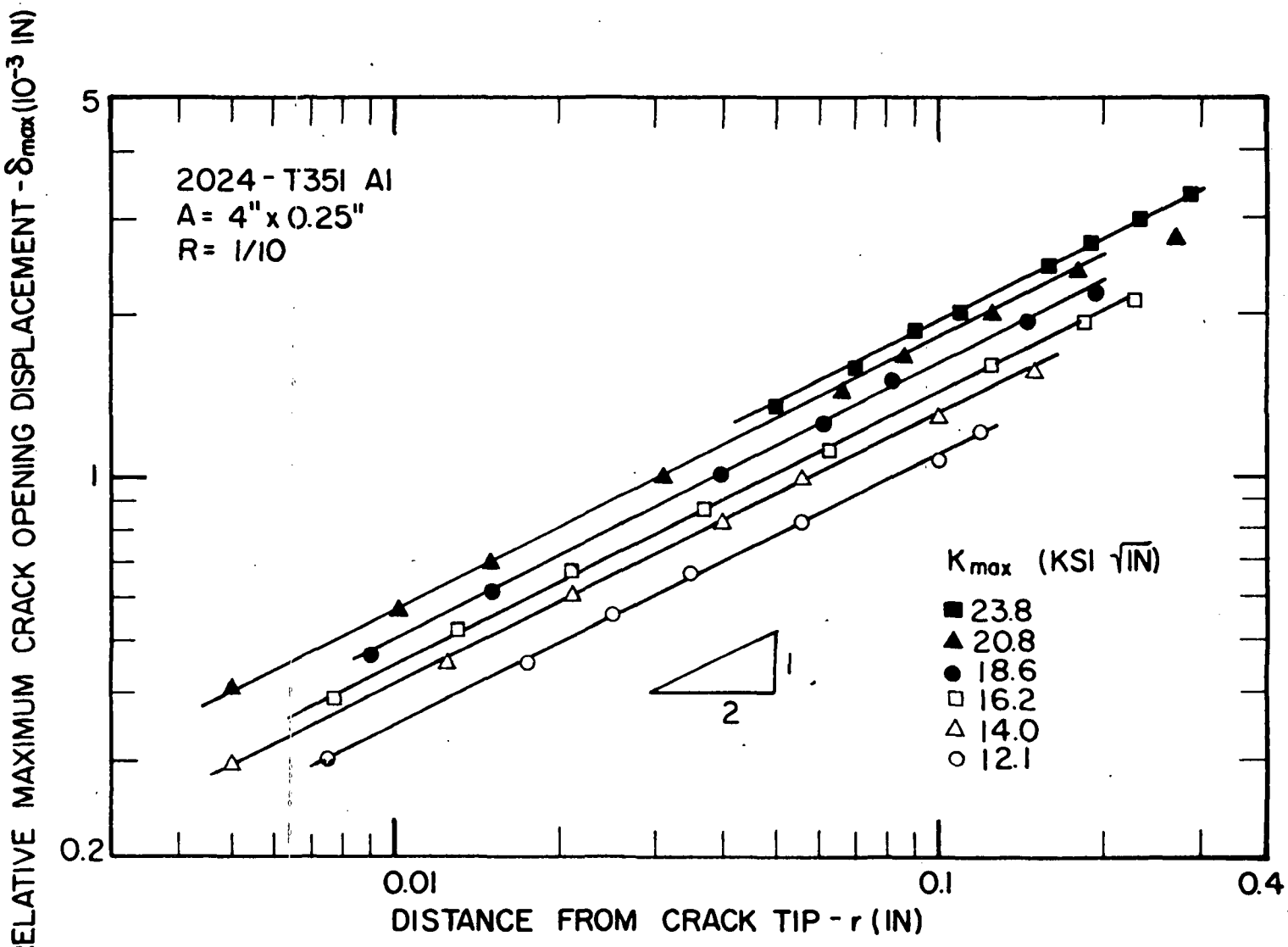

FIGURE 22a. RELATIVE MAXIMUM CRACK OPENING DISPLACEMENT VERSUS THE DISTANCE FROM A CRACK TIP FOR 0.25 INCHES THICK 2024-T351 ALUMINUM ALLOY AT R=1/10

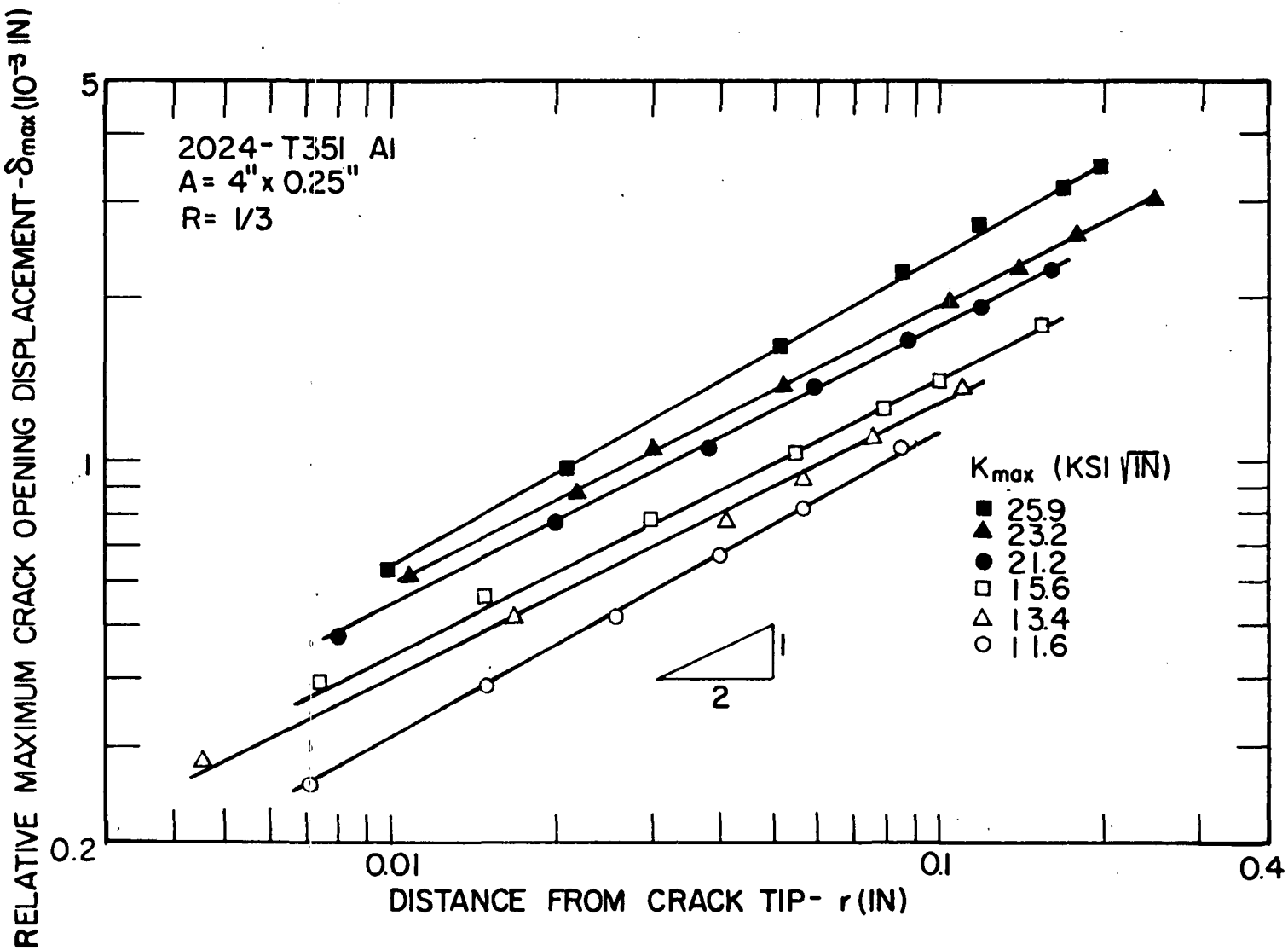

FIGURE 22b. RELATIVE MAXIMUM CRACK OPENING DISPLACEMENT VERSUS THE DISTANCE FROM A CRACK TIP FOR 0.25 INCHES THICK 2024-T351 ALUMINUM ALLOY AT R=1/3

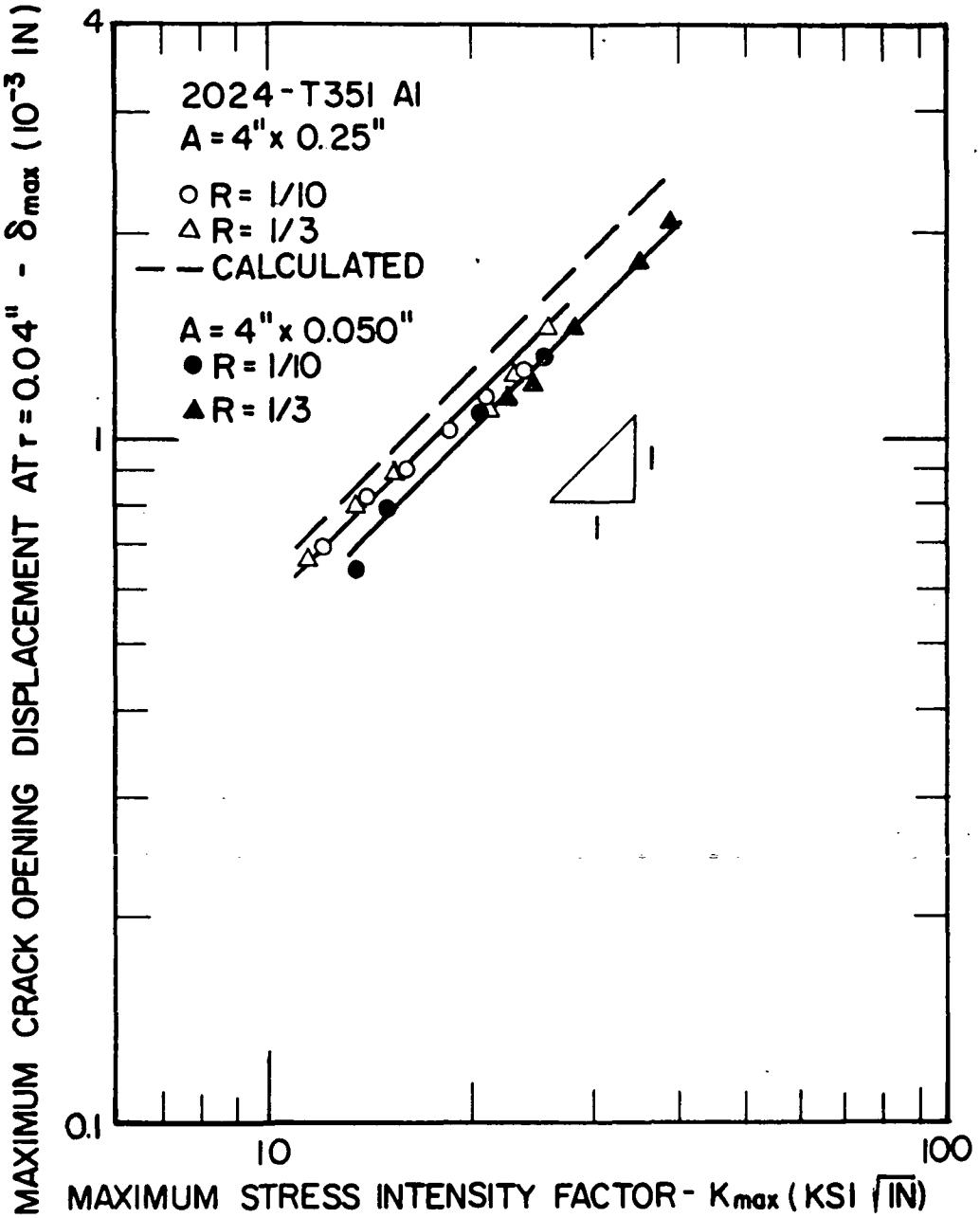

FIGURE 22c. RELATIVE MAXIMUM CRACK OPENING DISPLACEMENT VERSUS MAXIMUM STRESS INTENSITY FACTOR FOR 2024-T351 ALUMINUM ALLOY

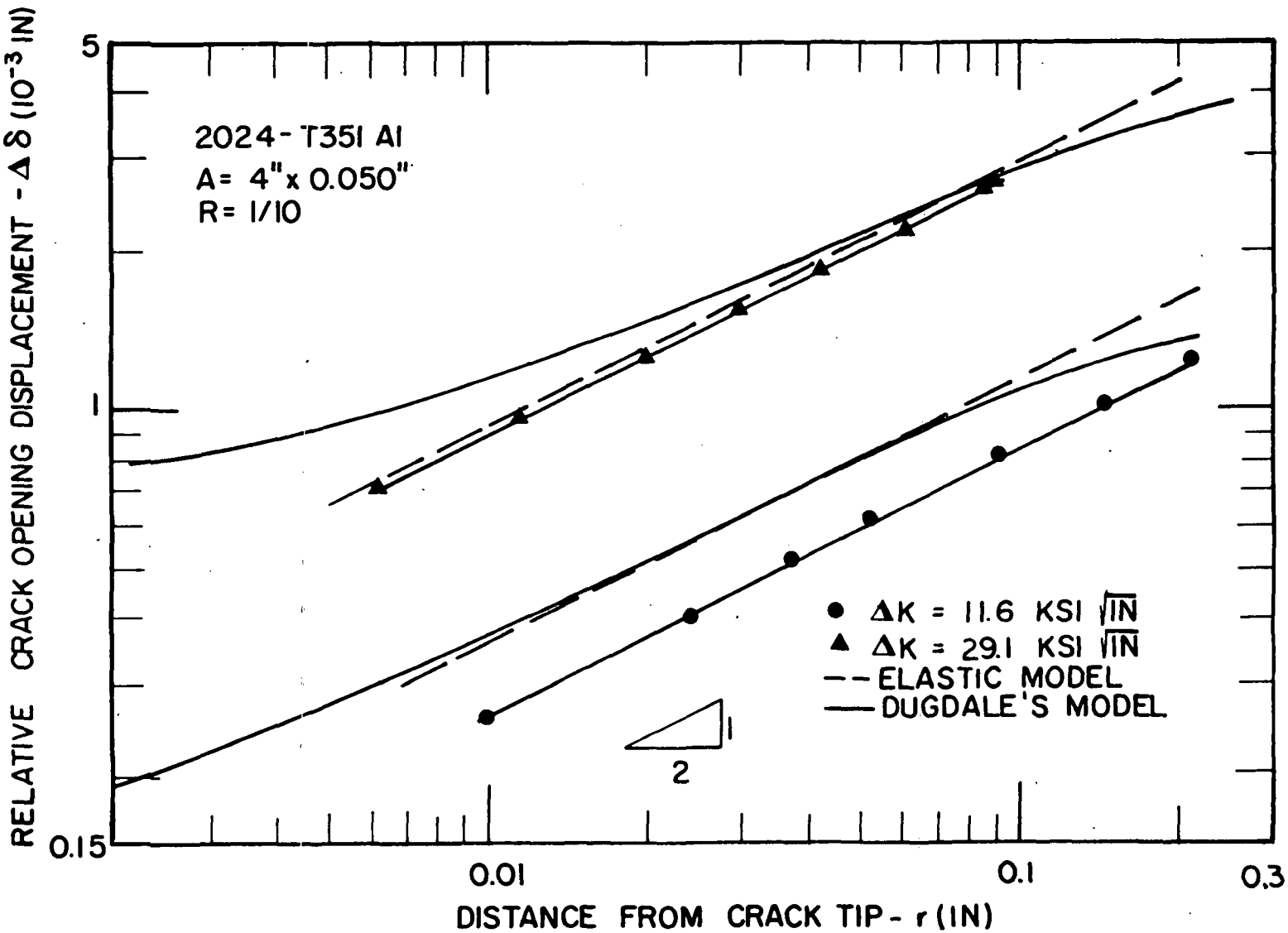

FIGURE 22d. COMPARISON OF THE CRACK OPENING DISPLACEMENT RANGE PREDICTED BY ELASTIC CALCULATION AND THE DUGDALE'S MODEL WITH THE MEASURED VALUES FOR 0.050 INCHES THICK 2024-T351 ALUMINUM ALLOY

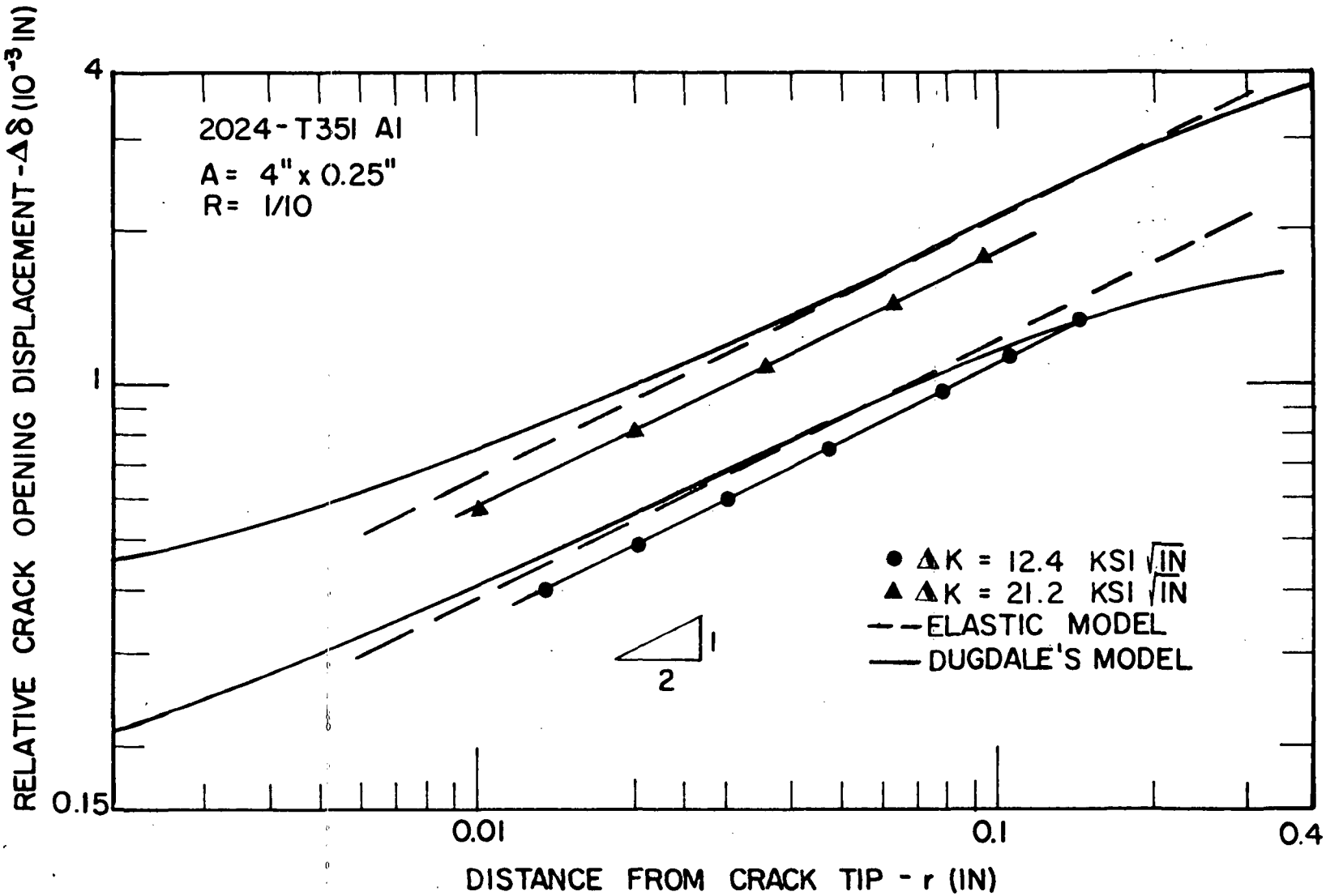

FIGURE 22e. COMPARISON OF THE CRACK OPENING DISPLACEMENT RANGE, PREDICTED BY ELASTIC CALCULATION AND THE DUGDALE'S MODEL, WITH THE MEASURED VALUES FOR 0.25 INCHES THICK 2024-T351 ALUMINUM ALLOY

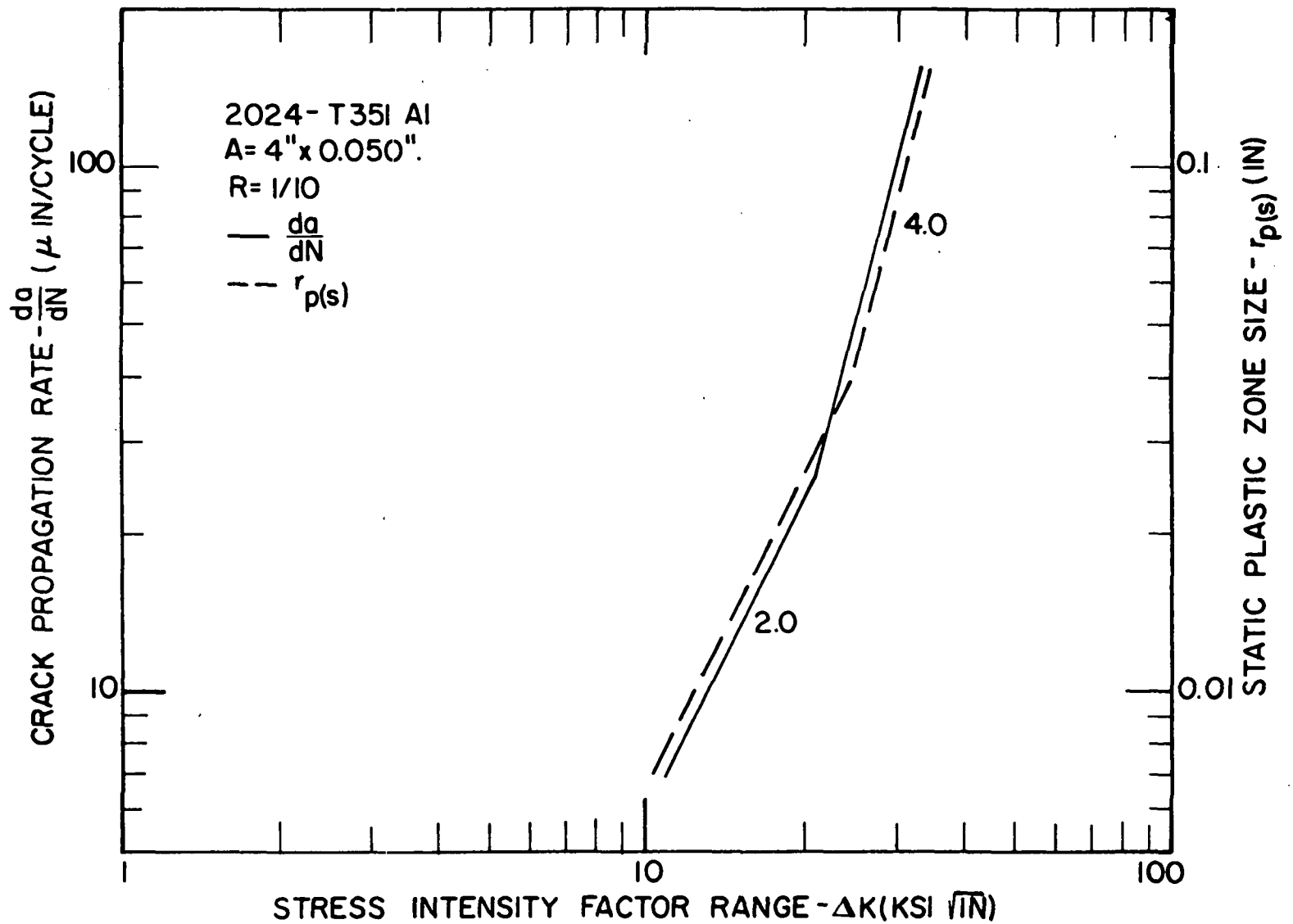

FIGURE 23a. FATIGUE CRACK PROPAGATION RATE AND STATIC PLASTIC ZONE SIZE VERSUS STRESS INTENSITY FACTOR RANGE FOR 0.050 INCHES THICK 2024-T351 ALUMINUM ALLOY AT R=1/10

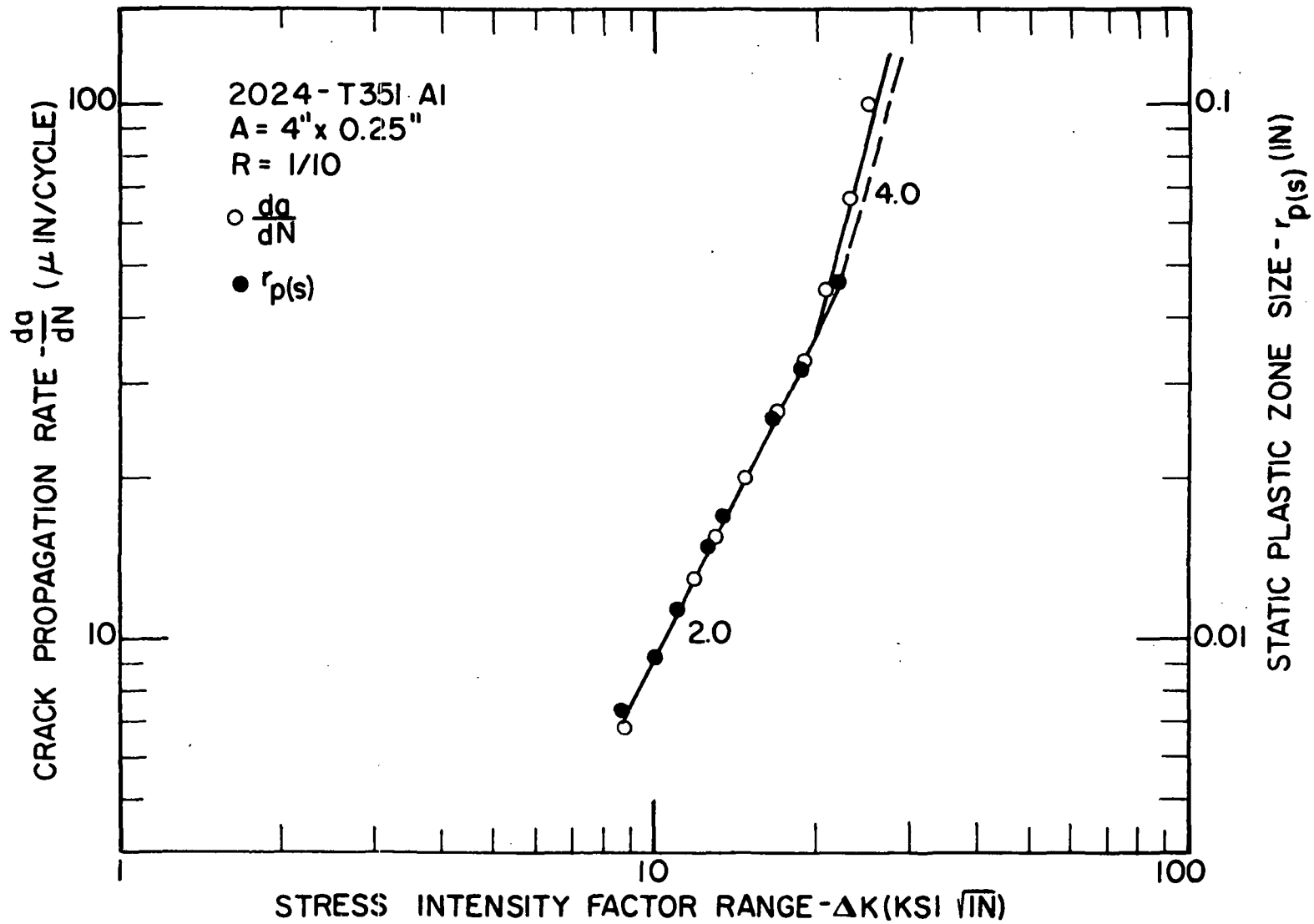

FIGURE 23b. FATIGUE CRACK PROPAGATION RATE AND STATIC PLASTIC ZONE SIZE VERSUS STRESS INTENSITY FACTOR RANGE FOR 0.25 INCHES THICK 2024-T351 ALUMINUM ALLOY AT R=1/10

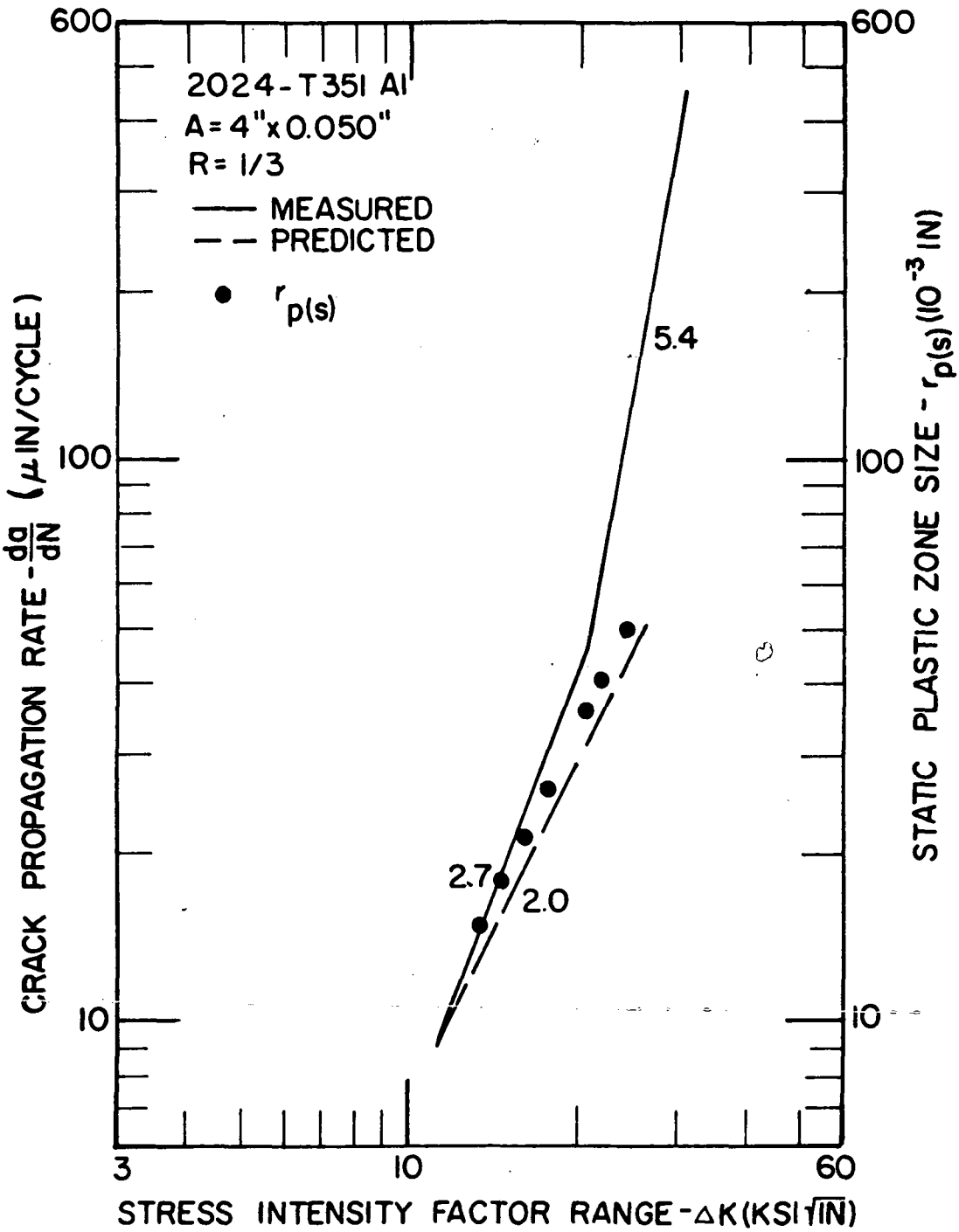

FIGURE 24a. FATIGUE CRACK PROPAGATION RATE AND STATIC PLASTIC ZONE SIZE VERSUS STRESS INTENSITY FACTOR RANGE FOR 0.050 INCHES THICK 2024-T351 ALUMINUM ALLOY AT R=1/3

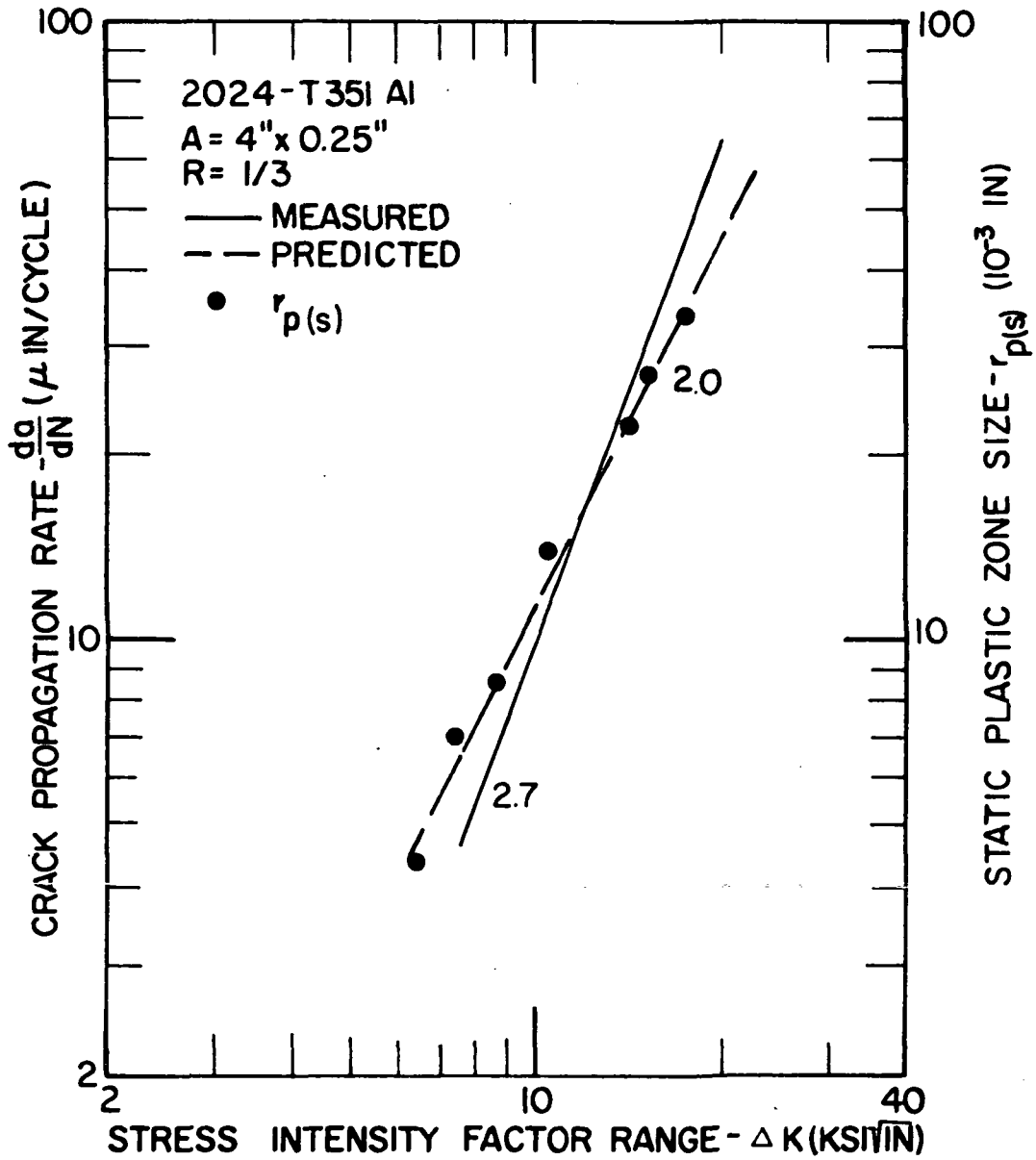

FIGURE 24b. FATIGUE CRACK PROPAGATION RATE AND STATIC PLASTIC ZONE SIZE VERSUS STRESS INTENSITY FACTOR RANGE FOR 0.25 INCHES THICK 2024-T351 ALUMINUM ALLOY AT R=1/3

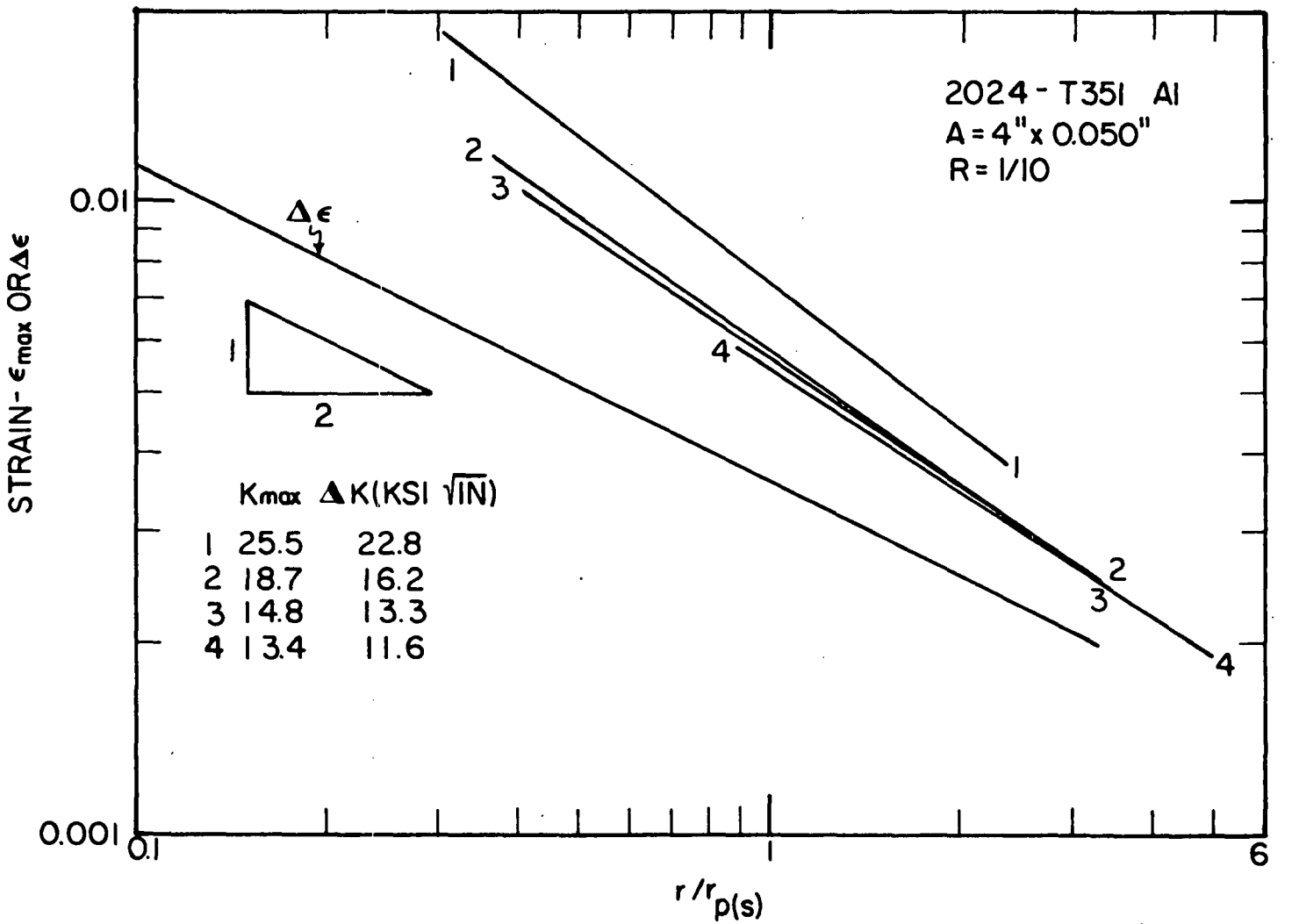

FIGURE 25a. STRAINS VERSUS $r/r_{p(s)}$ FOR 0.050 INCHES THICK 2024-T351 ALUMINUM ALLOY AT R=1/10

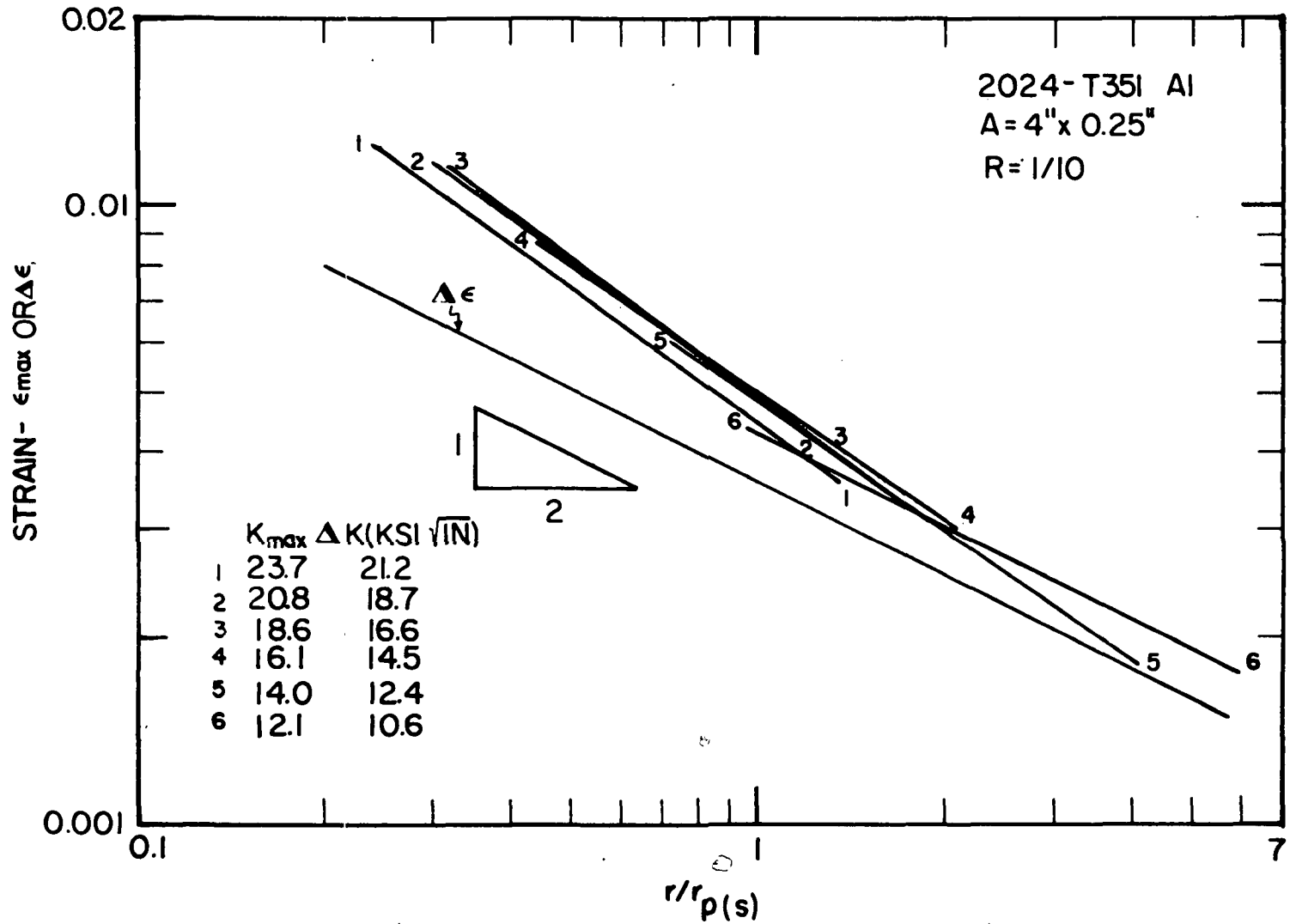

FIGURE 25b. STRAINS VERSUS $r/r_{p(s)}$ FOR 0.25 INCHES THICK 2024-T351 ALUMINUM ALLOY AT R=1/10

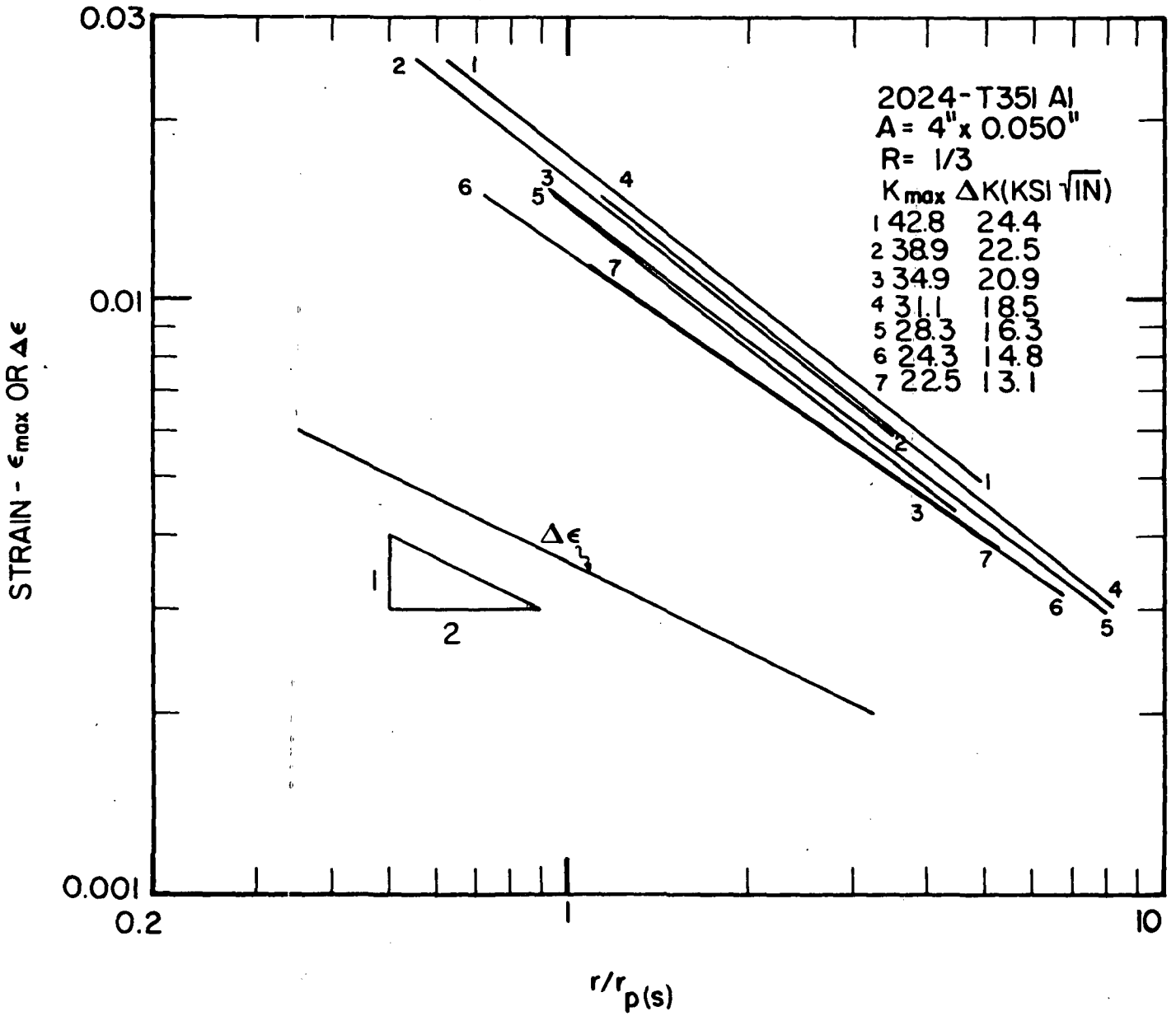

FIGURE 25c. STRAINS VERSUS $r/r_{p(s)}$ FOR 0.050 INCHES THICK 2024-T351 ALUMINUM ALLOY AT R=1/3

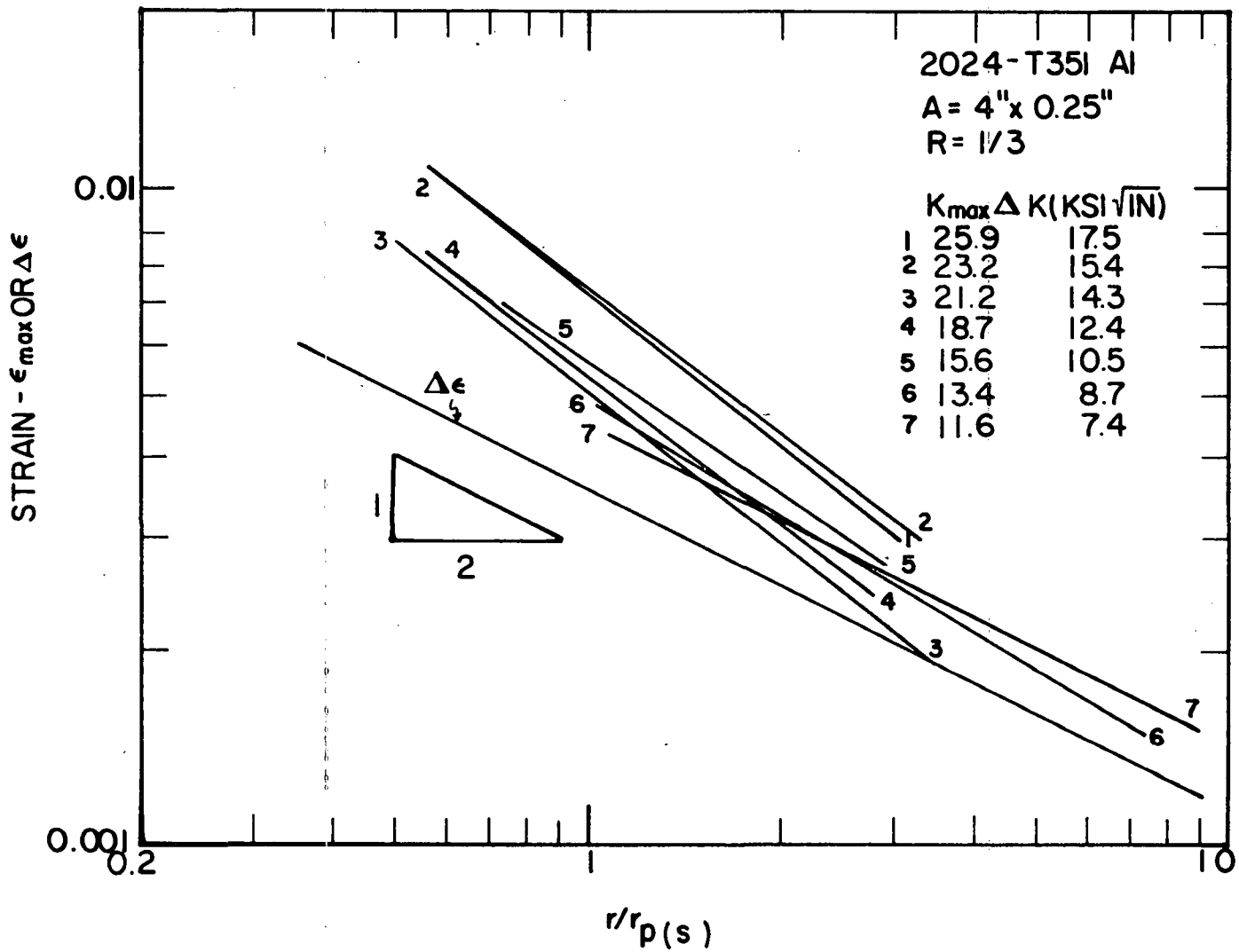

FIGURE 25d. STRAINS VERSUS $r/r_{p(s)}$ FOR 0.25 INCHES THICK 2024-T351 ALUMINUM ALLOY AT R=1/3

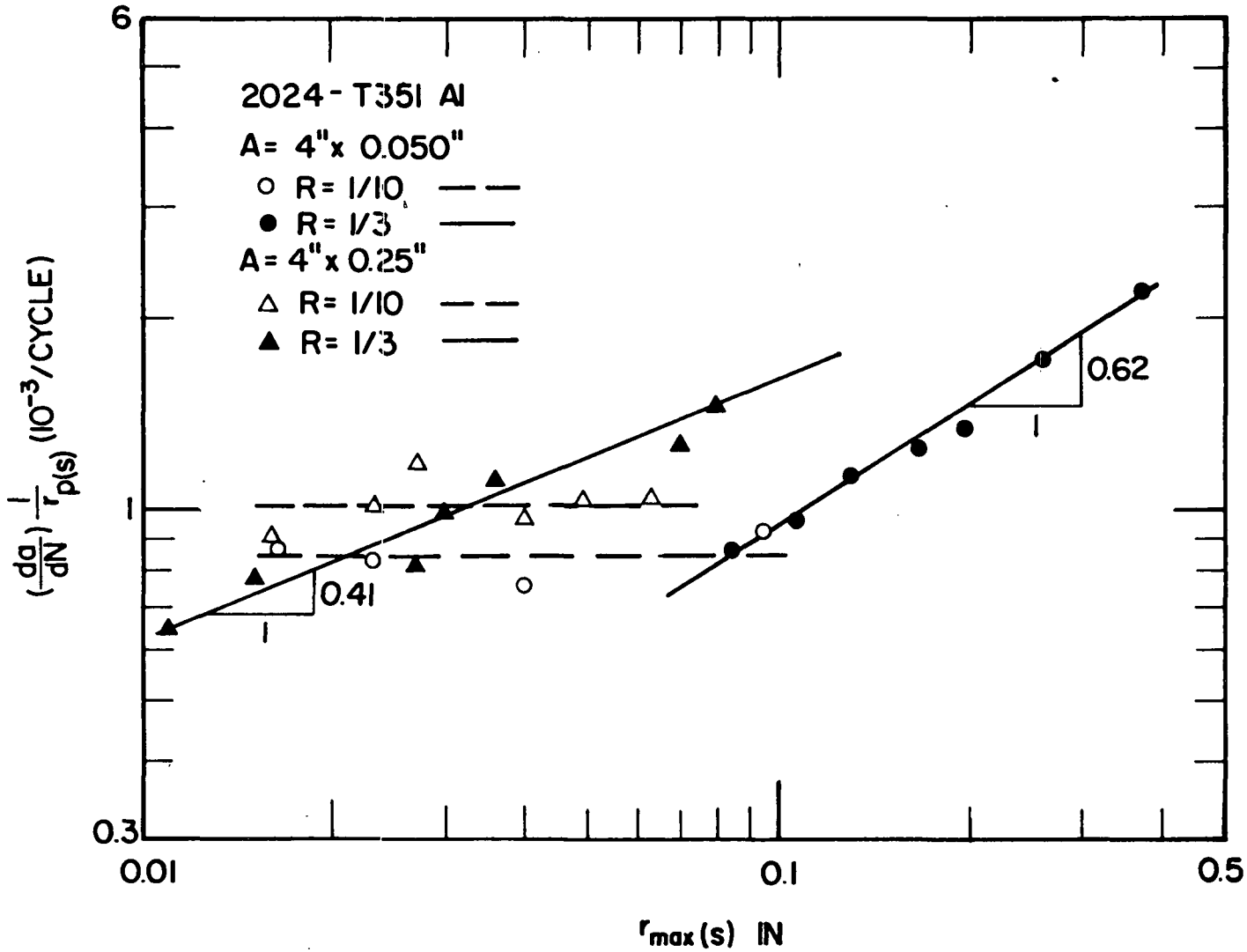

FIGURE 25e. $(da/dN)/r_{p(s)}$ VERSUS $r_{max(s)}$ FOR 2024-T351 ALUMINUM ALLOY